SOME CHARACTERISTICS OF LATERAL FLOW

Benito Luis Carballada

A Thesis

in

The Faculty

of

Engineering

Presented in Partial Fulfillment of the Requirements
for the degree of Doctor of Engineering at
Concordia University
Montréal, Québec, Canada

October 1978

ABSTRACT

ABSTRACT

SOME CHARACTERISTICS OF LATERAL FLOW

Benito Luis Carballada, D.Eng.
Concordia University, 1978

The well-known Schwarz-Christoffel transformation and the free streamline theory are used to solve the problem of flow past a lateral outlet housed in a two-dimensional conduit. The solution presented can be applied to lateral outlets which are fitted with a barrier that can be set at arbitrary inclinations. For particular cases such as the free outlet and the outlet fitted with a barrier normal to the conduit, closed form solutions were obtained. For the more general case, where the barrier inclination is arbitrary, numerical techniques were used to obtain the solution. The contraction coefficient and the jet inclination of the flow issuing out of the outlet are obtained as functions of the jet velocity ratio.

The theory of flow through a lateral outlet housed in a two-dimensional conduit has been adopted to develop a hydrodynamic model related to the flow through a lateral weir set in the side of a rectangular channel. The proposed relationships are valid when the flow in the channel upstream of the weir is subcritical. The experimental data obtained in a test flume provides a verification of the theoretical relationships between the geometric and fluid

dynamic parameters of the weir flow. The proposed expressions are valid for flow through lateral weirs which can be as wide as the parent channel.

In certain applications such as automated irrigation systems, multiple lateral weirs are housed in open channels in which spatially decreasing flow occurs. When the channel bed slope and the friction slope are very small, spatially decreasing subcritical channel flow results in a rising profile in the reach containing the multiple lateral weirs. This causes non-uniform distribution of weir outflows. For purposes of analysis, a single equivalent weir is considered and it is shown that uniform water surface profile ensuring uniform outflow can be obtained by modifying the weir system geometry. The proposed methods to obtain uniformly discharging outlets are simple and easy to construct, even in existing channels. A number of tests were conducted to verify the proposed methods. The modifications suggested are simple and easy to construct. The present study is limited to rectangular open channels.

ACKNOWLEDGEMENT

ACKNOWLEDGEMENT

The author wishes to express his appreciation to Dr. A.S. Ramamurthy for his guidance in the course of the investigation.

Assistance of the Québec Government which was provided in the form of a scholarship funding during the years 1974-75, and 1975-76, is greatly appreciated. The research projected was funded by the NRC under Grant No. 040-204 and the FCAC Grant No. 042-128.

TABLE OF CONTENTS

TABLE OF CONTENTS

LIST OF FIGURES

LIST OF FIGURES

LIST OF TABLES

LIST OF TABLES

NOTATIONS

NOTATIONS

a	Outlet width
b	Conduit width
b_1	Side contraction
B_x, B_y	Abbreviations for integrals
B	Channel width
B_1	Channel width at entry
B_2	Channel width at exit
c_1, c_2, c_3	Coefficients for polynomial fit
C	Barrier length
C_c	Contraction coefficient
C_{co}	Contraction coefficient when $\eta \to o$
C_d	Contraction coefficient of lateral conduit
$\bar{C}_{d..e}$	Mean discharge coefficient of the weir (theoretical)
$\bar{C}_{dw}$	Mean discharge coefficient of the weir (actual)
C_w	Weir coefficient
$\bar{C}_d(F_o, L/B)$	Function represented in Figure 28
C_x, C_y	Abbreviations for integrals
$f(\eta_o, L/B)$	Intermediate function
$f(\gamma)$	Defined by Equation (2.29)
F_1	Froude number of the flow upstream of the weir
F_o	Weir parameter
F_x, F_y	Abbreviations for integrals

g	Acceleration due to gravity
h	Depth (Figure 1)
h_o	Head over weir sill
i	Imaginary number ($=\sqrt{-1}$)
K	Barrier inclination parameter
L	Weir length
p_1	Upstream pressure
p_2	Downstream pressure
p_{atm}	Atmospheric pressure
Q_1	Discharge in the channel upstream of weir
Q_t	Theoretical discharge of weir
Q_2	Discharge in the downstream channel
Q_t	Theoretical discharge of weir
Q_t'	Modified discharge of weir
Q_w	Actual discharge of the weir
R_H	Water profile indicator (bed contouring)
R_b	Water profile indicator (side contouring)
s	Distance measured along the free streamline
S	Sill height of the weir
S_y	Layer depth ratio, h/Y_1
S_{y_1}	Sill height ratio, h_0/Y_1
t	Complex variable plane
t_B	Real axis coordinates of the source point
t_{B_1}, t_{B_2}	Abbreviations for intermediate steps
t_C	Real axis coordinate of the sink point
t_{C_1}, t_{C_2}	Abbreviations for intermediate steps

t_F	Real axis coordinate of the sink point
t_{F_1}, t_{F_2}	Abbreviations for intermediate steps
V_1	Mean velocity in the upstream channel
V_2	Mean velocity in the downstream channel
V_j	Velocity of the jet
$\bar{V}_j$	Mean velocity of the weir outflow
w	Complex potential
x	x-axis
x_{AE}, y_{AE}	Variables defined in Equations (2.19) and (2.18) respectively
X_{AE}, Y_{AE}	General expression to indicate the value of the free streamline projection on the x,y-axis, respectively
y	y-axis
Y_1	Flow depth in the upstream channel
Z	Physical plane
Z_1	Hump height
η	Jet velocity ratio ($=V_1/V_j$)
η_o	Jet velocity ratio at $h = h_o$
ε	Infinitesimal increment
α	Jet angle
β	Exit velocity ratio ($=V_2/V_1$)
γ	Velocity angle defined by Figs. 2a and 2b
$\Delta F_x, \Delta F_y$	Increment of the projection of the F.S. in the x,y-axis respectively, as one moves from the upper to the lower surface of the free streamline
$\gamma_A, \gamma_E, \gamma_F$	Angles defined by Equation (2.32)
ξ'	Log-plane

ξ	Inverse hodograph-plane
ϕ	Potential function
ψ	Stream function

SUBSCRIPTS

AE	Indicates integral path (Equations (2.13) and (2.14))
A,E,F	Refers to the same point in the physical plane
B	Coordinate of the point B of the physical plane
B_1, C_1, F_1	Abbreviations for intermediate steps
B_2, C_2, F_2	Abbreviations for intermediate steps
c	Value of the contraction coefficient as Equation (2.5)
co	Value of contraction coefficient when $\eta \to 0$
C	Coordinate of the point C of the physical plane
d	Discharge coefficient
F	Coordinate of the point F of the physical plane
j	Jet velocity
o	Value at $h = h_o$
t	Theoretical discharge
w	At the weir
y	Depth
x,y	Refers to y and x projections respectively
1	Upstream of weir
2	downstream of weir
1,2,3	Polynomial fitting

CHAPTER I

INTRODUCTION

CHAPTER I

INTRODUCTION

1.1 GENERAL REMARKS

The following section deals very briefly with the previous work done related to flow-past lateral outlets housed in conduits and open channels.

1.2 LATERAL OUTLET IN A TWO-DIMENSIONAL CONDUIT

The division of flow from a lateral outlet housed in a canal or a conduit constitutes a common feature in many hydraulic systems. Familiar examples of such systems include the flow through side weirs and multiport diffusers. Often barriers are fitted to the outlets as in curb outlets, branch channels and pipe manifolds. The characteristics of lateral flow past free outlets and outlets fitted with barriers set at right-angles to the main conduit have been studied in the past. These studies are based on the free streamline theory. However, the case where the barrier is set at arbitrary angles to the conduit has not been studied so far, although practical applications in irrigation systems and urban sewer systems include branch channels which are often set at arbitrary angles to the parent channel.

In Chapter II, numerical solutions based on the well-known Schwarz-Christoffel transformation [26] and the free streamline theory are presented for flow past a lateral outlet housed in two-dimensional conduit. For some special cases, closed form solutions are obtained and the results are verified using the solutions suggested earlier by other investigators. The approximate relationship proposed for the coefficient of discharge of a free outlet is shown to compare well with the empirical formula suggested by Rawn, et al [21], who conducted tests on flow through a lateral outlet of a pipe.

The jet contraction coefficient and the jet angle constitute the main characteristics of the outflow. To limit the number of variables in the general case, the analysis presented assumes the barrier length to be infinitely long. It should be noted that the contraction of the jet in a physical model occurs within a short length of the barrier. Consequently, the theoretical model is strictly not restrictive from the point of view of practical applications. Table 1 provides a summary of the studies made to obtain the characteristics of flow through a lateral conduit outlet.

1.3 LATERAL WEIR OUTLET IN AN OPEN CHANNEL

Lateral weirs are used extensively in irrigation and urban sewer systems. The mechanics of flow through such a weir has been studied by a number of investigators in

the past [6,7,8,11,19,23]. De Marchi [7] has presented an explicit solution to the problem of flow through a lateral weir which is housed in a rectangular channel, based on the assumption that the energy loss is negligible in the main channel section that spans the lateral weir and that the discharge coefficient C_w in the simple weir relationship given by equation (1.1) is constant.

$$q = C_w h_o^{3/2} \qquad (1.1)$$

In the above equation, q denotes the discharge per foot width of the weir due to the static head h_o. Application of equation (1.1) is appropriate to flow through a lateral weir, when the Froude number of the flow in the channel upstream of the weir is relatively low ($F_1 < 0.4$). Various versions of the De Marchi equation have been proposed by several investigators in the past. In particular, Frazer [11], Collinge [6] and Subramanya [23] considered the effect of V_1 and hence F_1 on the weir coefficient. Subramanya [23] assumed the nature of outflow in the weir plane to be critical and proposed a theoretical expression for the De Marchi coefficient for flow through lateral weirs whose sill heights were zero. His experimental data indicates that the proposed formula is valid in the low Froude number range ($F_1 < 0.4$). Nimmo [19] and El Khashab [8] have used the momentum principles to predict the nature of flow through lateral weirs.

Visual observations indicate that the outflow emerges as a jet which makes an oblique angle with the weir plane. The normal velocity component of the jet (outflow) corresponding to any infinitesimal layer is a function of the depth of the layer below the free surface (Figure 1). Consequently, this variation in the jet angle has to be accounted for in any lateral weir model. Based on the existing lateral conduit outflow models [14,17,18], a lateral weir flow model is developed in Chapter II. In the ensuing sections, this model will be referred to as the hydrodynamic weir model.

A brief summary of previous studies related to lateral weirs is provided in Table 2.

1.4 UNIFORMLY DISCHARGING LATERAL WEIR SYSTEM

Water is becoming universally accepted as a national resource. The increasing use of this resource suggests the need to adopt methods for its wise and efficient use. Intensification of agriculture in existing farmlands also points out the need to improve the existing methods of applying irrigation water. Conventional surface irrigation systems resulting in non-uniform application of water lead to increased runn-off and deep percolation. Recently, methods such as automated furrow irrigation [16], cutback systems [12], etc., have come into vogue.

Automated irrigation systems permit the use of less skilled labour besides allowing substantial reduction in the labour force required for farm work. Humphreys [16] provides a useful summary of existing automatic surface irrigation systems. Sweeten et al [24] studied the uniformity of discharge from a bank of siphons set in the side of an open channel under conditions of spatially varied flow. Sweeten and Garton [25] have conducted field experiments to find the non-uniformity of outflow from multiple lateral weir systems.

In Chapter V, test data related to uniformly discharging lateral weirs is presented. Uniform weir outflow conditions were obtained by altering the geometric parameters of the weir system. The outflow through the lateral weir model was obtained on the basis of the hydrodynamic model. Chapter II provides a brief outline of the theoretical model related to uniformly discharging lateral weir systems. A brief review of previous research is given in Table 3.

CHAPTER II

THEORETICAL ANALYSIS

CHAPTER II

THEORETICAL ANALYSIS

2.1 GENERAL REMARKS

An outline of the theoretical analysis related to the following problems is presented in this section.

(1) Lateral outlet in a two-dimensional conduit

(2) Lateral weir outlet in an open channel

(3) Uniformly discharging lateral weir system

The theoretical model of a lateral weir is compared with the experimental data in Chapter IV.

2.2 LATERAL OUTLET IN A TWO-DIMENSIONAL CONDUIT

A brief analysis of flow past a lateral outlet fitted with an infinitely long barrier set at arbitrary angles is presented below.

2.2.1 The Physical Plane

Consider the flow past a two-dimensional lateral outlet (Fig. 2a) which is fitted with a guide DE. For this outlet, the flow characteristics are obtained through conformal transformations. Figures 2 to 4 denote the mapping planes of

the transformations.

To begin with, the solution for the most generalized case is sought. To this end, let us consider the following physically realizable conditions.

(1) The barrier angle (π/K) is arbitrary in the range:

$$1 \leq K \leq \infty$$

(2) The dimensionless barrier length C/b and the outlet ratio a/b are variable:

$$0 \leq (C/b) \leq \infty \quad \text{and} \quad 0 < a/b < \infty$$

(3) The range of the velocity ratios $\beta\,(= V_2/V_1)$ and $\eta\,(= V_1/V_j)$ are as follows:

$$0 \leq \beta < 1 \quad \text{and} \quad 0 \leq \eta < 1$$

where

V_1 and V_2 = the velocities upstream and downstream of the outlet respectively

In conformity with familiar practice, the jet velocity V_j is assumed to be unity without any loss of generality. The liquid issues through the slot AD (Fig. 2a) and is guided by the outlet barrier DE. When the angle of the

free jet (unguided) is smaller than the angle of the guide, the guide forms the lower bounding streamline up to E, while the rest of the jet boundary is defined by the free-streamline pattern. Table 3a provides a summary of the basic transformations adopted. The same letter is used to denote the corresponding points in all planes. In the physical plane (Fig. 2a) D is assumed to be the stagnation point. When the value of K is unity, the barrier DE will be aligned with the conduit (Fig. 5a) and the stagnation point D is located in a region downstream of the outlet point E. Figure 5b shows the disposition in the Z and ξ' planes, when K has a value of 0.75.

2.2.2 The Inverse Hodograph Plane ($Z \rightarrow \xi \rightarrow \xi'$)

Figure 2b denotes the inverse hodograph plane $\xi (= |V| e^{i\gamma})$. Figure 3 denotes the logarithmic hodograph plane $\xi' (= \log \frac{1}{|V|} e^{i\gamma})$, where V denotes the velocity and γ is the angle of the velocity vector with respect to the x-axis.

2.2.3 The t-plane ($\xi' \rightarrow t$)

The semi-infinite strip in the ξ'-plane (Fig. 3) is opened at the D_1D_2 vertex and the points D_1, E, F, A, B, C_1 and D_2 are located along the real axis of the t-plane (Fig. 4) in order, at $-\infty$, -1, t_E, 1, t_B, t_C, ∞, with the following relations:

$$t_B = \cosh \ln \left(\frac{V_j}{V_1}\right)^K \qquad (2.1)$$

$$t_C = \cosh \ln \left(\frac{V_j}{V_2}\right)^K \qquad (2.2)$$

$$t_F = \cos K\alpha \qquad (2.3)$$

The transformation that provides the above correspondence is:

$$t = \cos\left[\frac{2\xi' i - \pi}{(2/K)}\right] \qquad (2.4)$$

2.2.4 The w-plane (t → w)

By continuity, we get

$$V_1 b = V_2 b + C_c a V_j \qquad (2.5)$$

Noting that C and F are sinks and B is a source, the transformations from the t-plane to the w-plane can be obtained as:

$$w = \frac{b}{\pi}\left[V_1 \ln(t-t_B) - \frac{C_c a V_j}{b} \ln(t-t_F) - V_2 \ln(t-t_C)\right] \qquad (2.6)$$

2.3 THE JET CONTRACTION COEFFICIENT C_c

2.3.1 Free Streamline Development

Along the free streamlines AFE, the magnitude of the velocity is unity and ψ the stream function is constant. Hence $d\psi = 0$.

Further,

$$\xi' = \ln \left|\frac{1}{V}\right| + i\gamma = i\gamma \qquad (2.7)$$

Accordingly,

$$dw = d\phi = \frac{d\phi}{ds}\, ds = V ds \qquad (2.8)$$

so that,

$$dw = ds \qquad (2.9)$$

where

ϕ = the velocity potential

and

ds = the differential length along the streamline

From Equation (2.6), one notes that,

$$dw = \frac{b}{\pi}\left\{V_1\left(\frac{1}{t-t_B}\right) - \frac{C_c a V_j}{b}\left(\frac{1}{t-t_F}\right) - V_2\left(\frac{1}{t-t_C}\right)\right\} dt \qquad (2.10)$$

On the free streamline, the following relations hold:

$$dy = ds \sin\gamma \tag{2.11}$$

$$dx = ds \cos\gamma \tag{2.12}$$

Hence, the expressions for the projections of the free-streamline on the coordinate axes are:

$$Y_{AE} = \int_A^E dy = \int_A^E ds \sin\gamma = \int_A^E dw \sin\gamma \tag{2.13}$$

$$X_{AE} = \int_A^E dx = \int_A^E ds \cos\gamma = \int_A^E dw \cos\gamma \tag{2.14}$$

From Geometry (Figs.6a and 6b) one gets

$$a = -Y_{AE} + \Delta F_y - C \cos\frac{\pi}{K} \tag{2.15}$$

$$X_{AE} = C \sin\frac{\pi}{K} + \Delta F_x \tag{2.16}$$

$$\Delta F_y = C_c a \sin\alpha, \quad F_y = C_c a \cos\alpha \tag{2.17}$$

Let

$$Y_{AE} = \frac{b}{\pi} y_{AE} \tag{2.18}$$

$$X_{AE} = \frac{b}{\pi} x_{AE} \tag{2.19}$$

Using equations (2.18) and (2.19), equations (2.15) and (2.16)

can be written as

$$a = \frac{-Y_{AE}}{\pi} b + C_c a \sin\alpha - C \cos\frac{\pi}{K} \qquad (2.20)$$

$$x_{AE}\frac{b}{\pi} = C \sin\frac{\pi}{K} + C_c a \cos\alpha \qquad (2.21)$$

Since $V_j = 1$, from equation (2.5)

$$C_c = (V_1 - V_2)/(a/b) \qquad (2.22)$$

Hence Eqs. (2.20) and (2.16) can be reduced to the following form:

$$C/b = \{(x_{AE})/\pi\} - (V_1 - V_2) \cos\alpha/\sin(\pi/K) \qquad (2.23)$$

$$a/b = \{-(Y_{AE})/\pi\} + (V_1 - V_2) \sin\alpha - (C/b) \cos(\pi/K) \qquad (2.24)$$

Consequently, equation (2.22) yields C_c in terms of known quantities.

The expressions for x_{AE} and Y_{AE} are obtained as follows:

From equations (2.4) and (2.7), the following relations can be obtained;

$$t = \cos K\left(\frac{\pi}{2} + \gamma\right) \tag{2.25}$$

$$dt = -\sin\{K(\frac{\pi}{2} + \gamma)\}K d\gamma \tag{2.26}$$

Substituting t and dt in equation (2.10), we get dw as a function of γ which can be substituted in turn in equation (2.13) and (2.14) to yield an expression to the projection of the free streamline on the Y axis.

$$Y_{AE} = V_1 (B_y) - (V_1 - V_2)(F_y) - V_2(C_y) \tag{2.27}$$

where

$$B_y = \int_A^E \left[\frac{-K.\sin\{K(\frac{\pi}{2} + \gamma)\}\sin\gamma}{\cos\{K(\frac{\pi}{2} + \gamma)\} - t_B}\right] d\gamma \tag{2.28}$$

$$F_y = \int_A^E \left[\frac{-K.\sin\{K(\frac{\pi}{2} + \gamma)\}\sin\gamma}{\cos\{K(\frac{\pi}{2} + \gamma)\} - t_F}\right] d\gamma$$

$$= \int_A^E f(\gamma)d\gamma \tag{2.29}$$

$$C_y = \int_A^E \left[\frac{-K.\sin\{K(\frac{\pi}{2} + \gamma)\}\sin\gamma}{\cos\{K(\frac{\pi}{2} + \gamma)\} - t_C}\right] d\gamma \tag{2.30}$$

Similarly, the projection on the x-axis is

$$x_{AE} = V_1 B_x - (V_1 - V_2)F_x - V_2 C_x \tag{2.31}$$

The corresponding expressions B_x, F_x and C_x include the term $\cos(\gamma)$ instead of $\sin(\gamma)$ which appears in B_y, F_y and C_y.

The integration limits A and E are the angles that the tangent to the free streamline makes with the X-axis at these two points.

Let

$$A \rightarrow t = 1 \rightarrow \gamma_A = -\left(\frac{\pi}{2}\right)$$

$$E \rightarrow t = -1 \rightarrow \gamma_E = \left(\frac{\pi}{K}\right) - \left(\frac{\pi}{2}\right)$$

$$F \rightarrow t = \cos K\alpha \rightarrow \gamma_F = \alpha - \frac{\pi}{2} \qquad (2.32)$$

The integrands of F_x and F_y include a singular point at the location where the variable γ is equal to $(\alpha - \frac{\pi}{2})$.

To integrate equations (2.29) around the singular point [18], the integration field is divided into two and the infinitesimal increment $|\varepsilon|$ around the singular point F is made to vanish in the limit

$$F_y = \int_A^E \{f(\gamma)\}d\gamma = \int_A^{F+\varepsilon} \{f(\gamma)\}d\gamma +$$

$$= \int_{F-\varepsilon}^{E} \{f(\gamma)\}d\gamma \qquad (2.33)$$

Table 1 provides a summary of the physical models and the corresponding solution types which were obtained.

2.3.2 Physical Models

It is possible to obtain several physical models by varying the magnitude of K. For arbitrary values of K, a closed form solution of equations (2.27) and (2.31) is not possible, in general. However, numerical solutions can be obtained if closed form solutions are not feasible.

2.3.3 Models 1 to 5 (Table 1)

The solutions for these models involve the integration of the expressions shown in equations (2.27) to (2.31).

Since closed form solutions were not feasible, simple numerical techniques were adapted to integrate the expressions B_x, C_x, B_y and C_y.

2.3.4 Models 6 to 9 (Table 1)

For models 6 to 9, closed form solutions can be obtained. The singular point associated with the integrals present no additional difficulties, as the techniques stated earlier can be adopted even here (see equation (2.33)). For the closed form solutions, the increments ε are made to vanish in the limit. The solution for case 6 can be expressed as follows:

$$a/b = \frac{V_1}{2}\{(t_{B_1} - (1-\beta)\, t_{F_1} - \beta t_{C_1} + (\frac{1-\beta}{V_j})\pi \sin\alpha\sqrt{2}\} \quad (2.34)$$

where,

$$t_{B_1} = \sqrt{1 + t_B}\ \ln\{\frac{\sqrt{1 + t_B} + \sqrt{2}}{\sqrt{1 + t_B} - \sqrt{2}}\} \quad (2.35)$$

$$t_{C_1} = \sqrt{1 + t_C}\ \ln\{\frac{\sqrt{1 + t_C} + \sqrt{2}}{\sqrt{1 + t_C} - \sqrt{2}}\} \quad (2.36)$$

$$t_{F_1} = \sqrt{1 + t_F}\ \ln\{-\frac{\sqrt{1 + t_F} + \sqrt{2}}{\sqrt{1 + t_F} - \sqrt{2}}\} \quad (2.37)$$

Also,

$$C/b = \frac{V_1}{\pi\sqrt{2}}\{(t_{B_2} - (1-\beta)\, t_{F_2} - t_{C_2} - (\frac{1-\beta}{V_j})\pi\sqrt{2}\cos\alpha)\} \quad (2.38)$$

where,

$$t_{F_2} = \sqrt{1 - t_F}\ \ln\{\frac{\sqrt{2} - \sqrt{1 - t_F}}{\sqrt{2} + \sqrt{1 - t_F}}\} \quad (2.39)$$

$$t_{B_2} = 2\sqrt{t_B - 1}\ \tan^{-1}\sqrt{\frac{2}{t_B - 1}} \quad (2.40)$$

By replacing t_B by t_C in equation (2.40), one gets the expression for t_{C_2}.

Equation (2.22) along with equations (2.34) and (2.36) constitutes the solution to model 6.

Model 7 is a particular case of model 6. Set the barrier length to infinity ($C \to \infty$). Consequently, α assumes the value of $\pi/2$ in equation (2.34). The latter together with equation (2.22) forms the solution to case 7.

For model 8, a closed form solution is obtained by going through the successive transformations in the same manner as in model 6. From equations (2.23) and (2.24), one gets:

$$\cos\alpha = \{(x_{AE})/\pi\}/(V_1-V_2) \qquad (2.41)$$

$$\frac{a}{b} = -(y_{AE})/\pi + (V_1-V_2)\sin\alpha \qquad (2.42)$$

where,

$$x_{AE} = \frac{\pi}{2}(V_1^2-V_2^2) \qquad (2.43)$$

$$-y_{AE} = V_1 t_B \ln\left[\frac{-1-t_B}{1-t_B}\right] - (V_1 - V_1)t_F \ln\left[\frac{-1-t_F}{-1+t_F}\right] - V_2 t_C \ln\left\{\frac{-1-t_C}{1-t_C}\right\} \qquad (2.44)$$

Using equations (2.43) and (2.44) in equations (2.41) and (2.42), one gets

$$\cos\alpha = \frac{(V_1 + V_2)}{2V_j} \tag{2.45}$$

$$\frac{a}{b} = \frac{V_1}{\pi}\left\{t_B \ln\left[\frac{-1 - t_B}{1 - t_B}\right] - (1-\beta)t_F \ln\left[\frac{-1 - t_F}{-1 + t_F}\right]\right.$$

$$\left. - \beta t_C \ln\left[\frac{-1 - t_C}{1 - t_C}\right] + \frac{(1-\beta)}{V_j}\pi \sin\alpha\right\} \tag{2.46}$$

Equations (2.45) and (2.46) together with equation (2.22) form the complete solution for model 8.

Model 9 is a limiting case for which K becomes infinite. The barrier DE folds over the downstream section DC. Hence this case is identical to model 8.

2.3.5 Model 10($2 < K < \infty$)

Here we consider the particular case for which K assumes values in the closed interval 2 to ∞. Further, let the barrier length C be equal to infinity. One can disregard the barrier in the analysis, if the jet angle α is greater than the angle of the barrier which is denoted by π/K. Under these circumstances, the model is identical to case 8. On the other hand, when the barrier interferes with the jet ($\alpha < \pi/K$), equations (2.22), (2.23), and (2.24) constitute the general solution to case 10.

2.3.6 Remarks

The variable a/b cannot be chosen arbitrarily for fixed values of η and β.

As η approaches unity, the ratio a/b approaches infinity for fixed values of β [17], and C_c takes on vanishingly small values to satisfy the continuity equation.

2.4 LATERAL WEIR OUTLET IN AN OPEN CHANNEL

As stated earlier, the lateral outflow through a free outlet set in a two-dimensional conduit (Fig. 7) has been analysed by a number of investigators in the past [14,17,18]. McNown [17] has hinted at the possibility of extending his theoretical analysis to solve the lateral weir flow problem. The discharge coefficient C_d' for the jet (outflow) issuing out of the conduit can be determined theoretically as a function of the jet velocity ratio η (Fig. 7). For the jet, the inlet velocity V_i (Fig. 1a) provides the axial component while the static head h_o provides the normal component. Under such circumstances, it is common [15,21,27] to add the axial velocity component and the normal velocity component vectorially (Fig. 1a) to obtain the jet velocity V_j. In the following section, the two-dimensional conduit outlet model is adopted to develop an expression for the mean discharge coefficient $\bar{C}_d$

for flow through a lateral weir housed in a rectangular open channel. The bed of the channel is assumed to be horizontal. The flow in the channel upstream of the weir is assumed to be subcritical. For purposes of analysis, the length of the lateral weir is limited to the width of the parent channel ($0<L/B\leq 1$).

The flow through the weir can be assumed to be made up of a large number of infinitessimal horizontal layers. The normal velocity component of the outflow through any layer is a function of its depth below the free surface. The axial jet velocity is assumed to be equal to V_1 in the entire region of outflow. Consequently, the local jet velocity ratio η and the local weir coefficient C_d will be different for the different layers. However, the total outflow can be obtained by summing up the discharge through the infinitessimal layers.

2.4.1 The Polynomial Fit

To simplify the problem, the actual functional relationship between C_d and η in Figure 7, is replaced by a close polynomial fit, given by equation (2.47).

$$C_d = 0.61 + c_1\eta^2 + c_2\eta^4 + c_3\eta^6. \qquad (2.47)$$

for $0<L/B\leq 1$ and $0\leq\eta\leq 1.0$

where

$$c_1 = -0.54 + .25(L/B)$$

$$c_2 = .058 + .234(L/B)$$

$$c_3 = -.13 - .49(L/B) \qquad (2.48)$$

2.4.2 Weir Discharge Computation

For the weir outflow through the infinitesimal layer shown in Figure 1, the jet velocity V_j can be computed. Thus,

$$V_j = \sqrt{V_1^2 + 2gh} \qquad (2.49)$$

The expression for the theoretical discharge can be written as follows:

$$Q_t = \int_0^{h_0} C_d V_j \, L dh \qquad (2.50)$$

where

$$C_d = C_d(\eta, L/B) \qquad (2.51)$$

and

$$h_0 = Y_1 - S \qquad (2.52)$$

Further

$$\eta^2 = \frac{V_1^2}{V_j^2} = \frac{1}{[1 + (2S_y/F_1^2)]} \qquad (2.53)$$

where

$$S_y = \frac{h}{Y_1} \tag{2.54}$$

By replacing the variable h by η in equation (2.50) and simplifying the resulting integral, an expression for the total weir discharge Q_t can be obtained.

Thus

$$Q_t = \frac{V_1^3 L}{g} \eta_0 \int^1 \frac{C_d}{\eta^4} \, d\eta \tag{2.55}$$

with

$$0 < L/B \leq 1.0 \tag{2.56}$$

where

$$\eta_0 = \frac{1}{[1 + (2/F_0^2)]^{\frac{1}{2}}} \tag{2.57}$$

and

$$F_0 = \frac{V}{\sqrt{gh_o}} \tag{2.58}$$

Using equation (2.47) in the above integrand, an expression for Q_t can be obtained in terms of η. The resulting expression can be integrated to yield the following relation for Q_t in terms of η_0. Thus,

$$Q_t = (V_1^3 L/g)\, f(\eta_0, L/B),\quad 0<L/B\leq 1 \qquad (2.59)$$

where

$$f(\eta_0, L/B) = (1-\eta_0^3)\left(\frac{c_3}{3}+\frac{0.203}{\eta_0^3}\right) + (1-\eta_0)\left(c_2+\frac{c_1}{\eta_0}\right) \qquad (2.60)$$

Since η_0 and F_0 are related one can express Q_t in terms of F_0 and L/B.

Further F_0 and F_1 are related as follows.

$$F_0 = \frac{F}{\sqrt{S_{y_1}}} \qquad (2.60a)$$

where

$$S_{y_1} = \frac{h_0}{Y_1} = \left(1-\frac{S}{Y_1}\right) \qquad (2.60b)$$

is the sill height ratio.

2.4.3 Weir Discharge Coefficient

For the weir outflow, an alternate expression can be written in terms of the mean velocity of the jet (outflow) and a mean weir discharge coefficient $\bar{C}_d$.

Thus,

$$Q_t = \bar{C}_d\, L h_0\, \bar{V}_j \qquad (2.61)$$

where

$$\bar{V}_j = \frac{1}{h_0}\left[\int_0^{h_0} (V_1^2 + 2gh)^{\frac{1}{2}}\, dh\right] \qquad (2.62)$$

$$\bar{V}_j = V_1 \frac{F_0^2}{3}\left[\left(1 + \frac{2}{F_0^2}\right)^{\frac{3}{2}} - 1\right] \qquad (2.63)$$

i.e.,

$$Q_t = \bar{C}_d\, L\, h_0 \left\{V_1 \frac{F_0^2}{3}\left[\left(1 + \frac{2}{F_0^2}\right)^{\frac{3}{2}} - 1\right]\right\} \qquad (2.63a)$$

Hence, an expression for $\bar{C}_d$ given by equation (2.64) can be obtained using equations (2.59), (2.61) and (2.63).

$$\bar{C}_d = \frac{3f(\eta_0, L/B)}{\left[\left(1 + \frac{2}{F_0^2}\right)^{\frac{3}{2}} - 1\right]} \qquad (2.64)$$

i.e.,

$$\bar{C}_d = \bar{C}_d\,[\eta_0,\ L/B] \qquad (2.65)$$

or

$$\bar{C}_d = \bar{C}_d\,[F_0,\ L/B] \qquad (2.66)$$

2.5 UNIFORMLY DISCHARGING LATERAL WEIR SYSTEM

The ensuing section deals with the theoretical development related to the geometric contouring of a rectangular channel to obtain a uniformly discharging lateral weir.

For purposes of analysis, it is convenient to examine an equivalent single lateral weir, Fig. 8, in place of multiple weirs housed in the side of the channel. It is reasonable to assume that the outflow through individual weirs of a system of multiple weirs will be equal when the water surface elevation in the channel is uniform along the reach that spans the weirs, when the weir parameter F_0 (see notations) is held constant. Uniformity of water surface elevation for spatially decreasing flow in the channel can be achieved by any one of the following methods:

(1) plane contouring of the channel bed (Fig. 8)

(2) plane contouring of the channel side (Fig. 8)

2.5.1 Channel Bed Contouring

Assume that the channel bed is originally horizontal and that friction losses are negligible in the section considered. For a rectangular channel whose bed is raised locally to a height Z_1 in the vicinity of the weir of length L, (Fig.8) the basic equations of motion are given below.

$$Y_1 + \frac{V_1^2}{2g} = Y + \frac{V^2}{2g} + Z \qquad (2.67)$$

$$Q_1 = Y_1 V_1 B_1 = Q_w + [YVB_1] \text{ exit end} \qquad (2.68)$$

where

Q_w = lateral weir discharge

Q_1 = main channel discharge

B_1 = channel width

Y_1 = depth of flow upstream of the weir

Y = depth of flow in the weir section at the center of the channel

V_1 = mean velocity in the section upstream of the weir

V = mean velocity in the weir section, and

Z = elevation of the bed

Since the water surface elevation has to be set uniformly along the weir span, one can impose the following conditions:

$$Y_1 = Y + Z \qquad (2.69)$$

Consequently, from equations (2.69) and (2.67)

$$V = V_1 \quad \text{and} \quad Q_w = B_1 Z_1 V_1$$

i.e.,

$$\frac{Q_w}{Q_1} = \frac{Z_1}{Y_1} \qquad (2.70)$$

From equation (2.70), one can compute the total rise in the channel bed hump Z_1 required to keep the water surface elevation horizontal for the given Y_1 and the discharge ratio Q_w/Q_1.

2.5.2 Channel Side Contouring

For the case where the channel side is contoured to provide uniform water surface in the vicinity of the weir (Fig. 8), the following equations hold:

$$Y_1 + \frac{V_1^2}{2g} = \left[Y + \frac{V^2}{2g}\right]_{\text{exit end}} \qquad (2.71)$$

$$Q_1 = Y_1 V_1 B_1 = Q_w' + [B_2 Y V]_{\text{exit end}} \qquad (2.72)$$

where

B_2 = the width of the channel at the weir exit section

For the water surface elevation to be uniform

$$Y_1 = Y \quad \text{and} \quad V_1 = V$$

Hence the side contraction b_1 (Fig.8) is related to the discharge ratio as follows:

$$\frac{b_1}{B_1} = \frac{Q_w}{Q_1} \qquad (2.73)$$

where

$$b_1 = B_1 - B_2$$

denotes the channel side contraction (Fig. 8).

2.5.3 Water Profile Indicators, R_H and R_b

Using equations (2.70) and (2.73), two new parameters R_H and R_b given by equations (2.74) and (2.75) are defined as follows:

$$R_H = (Q_w/Q_1)/Z_1/Y_1) \qquad (2.74)$$

$$R_b = (Q_w/Q_1)/(b_1/B_1) \qquad (2.75)$$

When the variable R_H has the value of unity, the water surface will be horizontal in the channel reach spanning the weir, for the case where bed contouring is adopted. Similarly, when the variable R_b has the value of unity, the water surface profile will be horizontal in the channel reach spanning the weir, for the case where side contouring is adopted. These two variables are useful in the analysis of the experimental data.

Experimental data was obtained to verify the various theoretical results obtained in this section.

A brief outline of the test set-up for each test series is given in the next chapter.

CHAPTER III

EXPERIMENTAL STUDY

CHAPTER III

EXPERIMENTAL STUDY

3.1 GENERAL REMARKS

Two different flumes were used to conduct the tests related to the lateral weir characteristics and their uniformly discharging irrigation outlets. These are described in the following sections.

3.2 LATERAL WEIR SET-UP

Some tests were conducted to obtain a verification of the proposed theoretical expressions for the discharge coefficient of the lateral weir. The rectangular test flume used in the tests was horizontal and had a smooth painted surface (Fig. 9). The flume was 25.4 centimeters (10") wide and 43.2 centimeters (17") deep. Plexiglass sheets were used to form six sharp edged lateral weirs which were housed in the side of the flume.

The discharge from the flume and the weir were measured with the help of standard V notches. The point gages used to measure the water levels in the flume and the V notch tanks could be read to the nearest 0.1 milimeters (0.04").

Section A, 25.4 centimeters (10") upstream of the weir (Fig. 9) was chosen to measure the upstream depth Y_1. This section was preceded by a system of baffles and screens

to reduce large scale turbulence at the inlet section, where the depth Y_1 was measured. The measurement of Y_1 was done at the centre of the flume. In all the series, the experimental data presented are related to fully ventilated nappes.

The tests for series 1 to 6 (Table 4) were conducted in the flume whose width was 25.4 cm (10"). However, the data for series 7 was obtained from an earlier exploratory study which was conducted in a flume (Fig. 10) that was 45.7 cm (18") wide.

3.3 UNIFORMLY DISCHARGING LATERAL WEIR SET-UP

To verify the theoretical results related to uniformly discharging lateral weirs, tests were conducted in a rectangular steel plate flume which housed a lateral weir. The flume (Fig. 10) was 18 inches (457 mm) wide and the channel sides were given a smooth painted finish. The sharp edged lateral weirs were 18 inches (45.7 cm) long. The sill height of the weirs above the channel floor was variable (Tables 5a and 5b). Sufficient entry and exit end lengths were provided to reduce external interference effects in the vicinity of the weir. The depth measurements were made with a point gage and the inflow into the test flume was metered by an orifice meter. The weir flow was measured with the help of a Standard (ASME) V notch.

The tests were conducted to determine the effectiveness of changing the channel geometry to ensure a uniform water surface profile, which in turn, was assumed to provide uniform spanwise weir outflow distribution. To this end, either the channel bed profile was changed (Fig. 8) or the side wall of the channel was contoured (Fig. 8) to the requirements imposed by equations (2.70) and (2.73) respectively.

The depth measurements were made along the centerline of the channel using a point gage which could register the depth to the nearest .001 ft (0.3 mm). Tables 5a and 5b show the modified channel geometries. Plexiglass sheets were used to provide the changes to the channel geometry.

In all the tests, it was desirable to maintain a high value for the inlet Froude number to get an appreciable change in the velocity head as the flow negotiated the weir. On the other hand, it was also felt that the inlet Froude number should not be excessively high in order to reduce the turbulence in the channel upstream of the weir.

Based on these considerations, the inlet Froude number was set in a range close to 0.4 (Tables 5a and 5b).

CHAPTER IV

ANALYSIS OF RESULTS

CHAPTER IV

ANALYSIS OF RESULTS

4.1 GENERAL REMARKS

In the following section an analysis of the theoretical and the experimental results is presented.

4.2 LATERAL OUTLET STUDY

4.2.1 Results of Numerical Solutions

Figures 11 to 16 indicate the graphical solution for the models 1 to 5. The coefficient of contraction C_c, which is the principal parameter of the lateral outlet flow has been plotted as a function of the jet velocity ratio η. The exit velocity factor β is used as the group parameter.

In these five models, the length of the barrier is assumed to be infinite. This assumption provides considerable mathematical simplifications in the development of the solution. It must be noted that this assumption does not reduce the generality of the results to practical cases in which the barrier length is finite. In a practical case, the contraction occurs well within a distance corresponding to four or five times the outlet width a(Fig. 2a). Therefore, in a physical model, the length of the barrier in excess of 5a is redundant in determining the contraction coefficient. Hence,

the present model is valid for the physical models, which are fitted with a barrier which is at least four to five times the width of the outlet.

For fixed barrier angles [π/K], the contraction coefficient decreases with the jet velocity ratio η for all values of the exit velocity ratio β. The top-most curve in figures 11 to 16 corresponds to vanishing values of β. This denotes the dead end conditions for the conduit ($V_2 = 0$). The case for which the value of η vanishes ($V_1 = 0$) denotes the so-called reservoir conditions. The corresponding contraction coefficient C_{co} for reservoir conditions are plotted in Figure 17 for a range of K values. This parameter attains the value of 0.61 in the limit, when the barrier is set at right angles to the inlet pipe (K 2). This value agrees favourably with the known solution for C_{co} corresponding to the flow through a very narrow slit [7]. For the symmetric outflow from the slit, the central streamline can be viewed as a barrier.

Consider the lower most curves of Figures 11 to 16 for which the velocity factor β is close to unity. Based on these curves, Figure 18 is developed to show the functional relationship between K and C_c with η as the group parameter. When the value of β approaches unity, the normalized value of the contraction coefficient C_c denoted by C_c/C_{co} can be very closely represented by the following equation:

$$(C_c/C_{co}) = 1 - 0.93\ \eta^{1.4} \qquad (4.1a)$$

For $1.2 < K \leq 2$ and $0 \leq \eta < .9$, the above function is plotted in Figure 19. Flow past a small aperture can yield β values approaching unity. In this context, small irrigation outlets taking off from a bigger parent channel can be considered to provide a practical application of this model. In general, the angle of take-off for such a branch channel is a variable. Figures 17 and 19 provide a consolidated version of the results to the most important range of parameters K, η and (C/C_{co}) for lateral flow past an outlet fitted with a barrier.

To overcome the difficulties associated with the singularities pertaining to the free streamline model a ten-point Gaussian quadrature technique was used for the numerical solution. The results were checked against the closed form solution for the particular case in which an infinite barrier was at a right-angle to the conduit (K = 2, Model 7).

4.2.2 Results of Closed Form Solutions

As shown in Table 1, closed form solutions for Models 6 and 7 were obtained by the present method. The results were found to be in agreement with the existing solutions to these models [14,17,18].

Model 6 refers to a finite barrier whose length is adjusted to render the jet angle to be the same as that for the free outlet (C = 0). Figure 20 displays the results for model 6.

For the free outlet model (C = 0) represented by case 8, the contraction coefficient C_c is represented in terms of the square of the jet velocity ratio η^2 for all possible β values. This linear range increases as β increases. Hence, it is not surprising to note that empirical linear relationship between C_c and η^2 for small sharp edge outlets were proposed by earlier investigators [21]. A typical result quoted by Vigander [27] related to the discharge coefficient of small sharp edged holes in a circular pipe is given below. It was based on the experiments of Rawn et al, [21] (see also Fig. 21).

$$C_c = 0.63 - 0.58\eta^2 \qquad (4.1b)$$

The agreement between the present two-dimensional solution ($\beta \to 1.0$) and the empirical relation (Equation (4.1b)) appears to be reasonable, considering the fact that the outlet had a finite thickness in the experiments of Rawn et al [21].

The relationship between the jet angle α and the jet velocity factor η is shown in Figure 22. The relationship is almost linear for low β values. This linear range shrinks as

the β value increases.

The set of curves in Figure 21 for the values of β above 0.5 can be approximated by the equation

$$C_c = .611 - \frac{\eta^2}{[3.85 - 2.13\beta]}, \qquad (4.2)$$

$$0 < \eta \leq .836$$

For the above relation, the approximation improves as the value of β reaches unity (Fig. 23). For the particular case of the small orifice ($\beta \to 1$), one can reduce Equation (4.2) to the following form:

$$C_c = 0.611 - 0.58\eta^2 \qquad (4.3)$$

The relationship based on the theoretical results in Equation (4.3) compares very well with Equation (4.1b) which is empirical.

In the present analysis, the jet velocity ratio η is considered as the main variable. This is in conformity with the usual method of plotting experimental data related to the design of diffusers [21] used for diluting effluents. However, the geometric parameter a/b may also be used to represent the results [17]. The solid lines in Figure 24 show the locus of the points corresponding to fixed values of a/b. The locus for

very small values of a/b approaches the curve for which β is close to unity. Hence, the curve in which β tends to unity can represent the case of multiport diffusers [27] in which the outlets are very small compared with the main conduit.

Since pressures can be measured more easily than velocities in an existing conduit system, it is desirable to denote the velocity parameters η and β in terms of the upstream pressure p_1, the downstream pressure p_2 and the atmospheric pressure p_{atm}. Accordingly, one can obtain the following relationship using the energy equation:

$$(p_1 - p_{atm})/\rho V_1^2/2) = (1/\eta^2) - 1 \qquad (4.4)$$

$$(p_1 - p_2)/(\rho V_1^2/2) = \beta^2 - 1 \qquad (4.5)$$

4.3 LATERAL WEIR STUDY

4.3.1 The Main Parameters

In the foregoing discussions, the local weir coefficient C_d is expressed in terms of the inlet Froude number F_1, the sill ratio S_y and the width ratio L/B, while the average weir coefficient $\bar{C}_d$ is expressed in terms of the jet velocity ratio η_o and the width ratio L/B. The results are valid for subcritical flows in the channel upstream of the weir, whose length can be as large as the width of the parent channel.

4.3.2 Theoretical Results

Figures 25 and 26 were obtained with the help of equations (2.47) and (2.53). They indicate the variation of C_d with the layer depth ratio S_y for fixed values of L/B and F_1. The uppermost graphs in Figures 25 and 26 denote the "reservoir conditions". For a given inlet Froude number F_1, the theoretical value of the local weir coefficient is a maximum for the infinitesimal layer which is just above the weir sill and decreases as one moves towards the upper layers. For instance, the curve 1-2-3 of Figure 25 denotes the progressive reduction of C_d as one moves from the lowest layer to the topmost layer, when the inlet Froude number is 0.5 and L/B is unity. For the cases where S_y is low ($0 < S_y < 0.1$), the variation of C_d among the infinitesimal factor (Fig. 1a) is large, particularly at low values of F_1. Further, for fixed values of S_y and F_1, Figures 25 and 26 also indicate that C_d decreases when the width ratio L/B is reduced. The dependence of C_d on L/B is significant only when the sill height is relatively high ($S_y \to 0$) and the Froude number is at least moderate ($F_1 > 0.4$).

The variation of the average discharge coefficient $\bar{C}_d$ with the jet velocity ratio η_Q and the weir parameter F_o are shown in Figures 27 and 28. The sill height is an important parameter in the design of lateral weirs used in irrigation and urban sewer systems since S determines the ratio of surface flow to the bedflow that is deflected through the weir.

One may set the sill height to be sufficiently high so that the sand in an irrigation channel or the foul flow in a sewer system will not form a large part of the weir outflow. In so doing, a compromise has to be made while choosing S since, $\bar{C}_d$ is drastically reduced at higher weir sill ratios due to the increase of η_o (Fig.27). It should be noted that the value of $\bar{C}_d$ is significantly influenced by L/B at larger values of η_o (Fig.27). Figure 28 indicates the variation of $\bar{C}_d$ in terms of the weir parameter F_o. It is an alternative representation to the variation of $\bar{C}_d$ and η_o since F_o and η_o are related to each other by Equation (2.57). The value of $\bar{C}_d$ reaches zero asymptotically for large values of F_o. For a weir whose sill height ratio is zero, the upper bound of F_o is unity in Figure 28 since the present analysis is limited to subcritical flows ($F_1 < 1$). Similar upper bounds for F_o can be established in Figure 28 for other sill height ratios (Table 6).

4.3.3 Experimental Results

The results of the series of experiments conducted to verify the theoretical predictions are shown in Figures 29 to 34. For all these graphs, Table 4 provides the details of the test weir geometry. In Figures 27 and 28, the theoretical curves based on equations (2.65) and (2.66) are plotted to indicate the dependence of $\bar{C}_d$ on η_o and F_o. Curves AB and CD in Figures 29 to 32 denote the locus of the points for which the theoretical value of $\bar{C}_d$ is reduced by 5% and 10% respect-

ively. The experimental values of η_o covered a very wide range of subcritical flows ($0 < \eta_o < 0.9$). The theoretical curves overestimate the average discharge coefficient $\overline{C}_d$ in all cases. In the derivation of the theoretical formula, the velocity distribution was assumed to be uniform in the main channel. However, in the experiments, the velocity in the upper layers will be more than the mean velocity V_1. This, in turn, tends to increase the local value of η. Hence, under such circumstances, the value of the experimental discharge coefficient $\overline{C}_d$ will be lower than the theoretically predicted $\overline{C}_d$. In other words, the net result will be a slight reduction in the total weir outflow. Nevertheless, the effect of the velocity distribution on $\overline{C}_d$ is not excessive. For instance, the energy coefficient was 1.04 for flow in one of the test flumes used in an earlier investigation [23], which had a geometric configuration similar to the present flume.

For the curves AB shown in Figures 29 and 30, the value of the total weir discharge Q_t is 5% lower than the theoretical value (Eq. 2.63a) and the experimental data appears to cluster around the curves denoted by AB. Eq.(4.6) provides the modified relationship between Q_t', η_o and L/B.

$$Q_t' = .95\ \overline{C}_d\ Lh_o\{V_1\frac{F_0^2}{3}\ [(1 + \frac{2}{F_0^2})^{\frac{3}{2}} - 1]\} \quad (4.6)$$

The results of the series of experiments made to check the validity of the proposed equations for series 2,4 and 6 are shown in Figures 31 and 32 for the upper range of η_o and F_o. At low η_o and F_o values, the nappe had a tendency to cling to the weir when the value of L/B was 0.5. However, the data presented validates the theoretical predictions as in the other series for which L/B was unity.

Figures 33 and 34 indicate the correlation of the actual discharge and the predicted discharge for all the 7 series (Table 4) of tests. The correlation appears to be reasonable when one adopts the theoretical equation modified to accomodate the correction for velocity distribution.

4.4 UNIFORMLY DISCHARGING LATERAL WEIRS

A brief discussion of the results of the experimental data is presented in the following section. Tables 5(a) and 5(b) indicate the range of the main variables covered in the tests.

4.4.1 Bed Contouring

Figure 35 shows the water surface profiles for the case in which bed contouring was adopted to ensure a horizontal water surface in the channel reach that spanned the weir. For values of R_H (water level indicator) close to unity which denotes the design conditions, the water surface was nearly horizontal in the reach spanning the weir.

Figure 36 indicates the water surface profiles for off design and design conditions for a typical test. For the values of R_H which are much less than unity, the water surface had a falling profile and for values of R_H much more than unity, the water surface had a raising profile.

Clearly, the water surface profiles shown in Figures 35 and 36 validate the theoretical predictions indicated by equations (2.70) and (2.74).

4.4.2 Side Contouring

Figure 37 shows the water surface profile for the case in which the side contouring was adopted to ensure a horizontal water surface in the channel reach that spanned the weir. For values of R_b (water level indicator) close to unity, the water surface was nearly horizontal in the reach spanning the weir. Figure 38 indicates the water surface profiles for off design and design conditions for a typical test. Thus for values of R_b which are much less than unity the water surface had a falling profile and for values of R_b much more than unity, the water surface had a raising profile, and again the experimental results shown in Figures 37 and 38 validate the theoretical predictions indicated by equations (2.73) and (2.75).

4.4.3 Other Remarks

The hydrodynamic weir model was used to obtain the theoretical discharge through the lateral weir. For the cases in which the bed contouring and the side contouring were effective (design conditions), the correlation between theoretical discharge Q_t and the measured discharge Q_w are shown in Figures 39 and 40, respectively.

The agreement between the theoretical discharge and the experimental discharge can be considered to be reasonable for both the bed contouring and side contouring. It should be noted that the comparison of the experimental data with theory should be viewed qualitatively, since the weir model is related to a channel which is free from bed contouring or side contouring. It may be added that under design conditions, the velocity V_1 is constant in the channel reach spanning the weir. From equations (2.70) and (2.73) one can infer that a small bed contouring can be very effective in a wide channel and a small side contouring can be very effective in a deep channel to limit the size of the structural changes required to provide a given weir outflow under design conditions.

Besides bed contouring and side contouring designs for the weir assembly one may also vary the sill heights to compensate for the changes in the mean velocities at the weir inlets and the water surface profile. However, in this design, the water surface profile is not horizontal and further, each weir

should be designed separately using individual values of F_o and C_d.

4.4.4 Field Applications

The main objective of the study was to determine the necessary geometric changes that are required to be made in the channel to ensure a horizontal water surface in the reach of the channel that spans the lateral weir. In practice, one may get a horizontal water surface across a battery of weirs by providing the necessary contouring to the side or bed of the channel. Figure 41 shows a typical weir assembly arrangement which yields equal outflow through the individual weirs.

Two weirs, six inches (15.24 cm) long and spaced twelve inches (30.48 cm) apart were set in the test flume to conduct a few tests to verify the effectiveness of the bed contouring. The test results indicated that the water level was nearly horizontal and that the discharge through the two weirs agreed within five per cent of the theoretical discharge when design conditions (R_H close to unity) were satisfied. It should be noted that the value of F_o is constant for all weirs of the weir battery, when design conditions are ensured.

Although the proposed designs can be adopted in the field, a few remarks are included to indicate the comparative merits of the proposed designs. For instance, when the channel carries a good deal of sediment, the side contouring

design is preferred to bed contouring. If there is a need to have pairs of weirs housed on either side of the channel, the bed contouring design is to be preferred. However, identical weirs whose center lines coincide will not provide identical outflows in practice. More flow will tend to go through one of them than through the other, because of self-instability.

As such, the designer should stagger such weirs along the center line and provide adequate spacing between them. In a field application, the design can be easily extended to the case where the rates of outflow through subassembles of weirs follow prescribed design requirements.

The additional cost of construction due to changes in the channel geometry will not be excessive for any of the designs discussed, as the main costs are related to the construction of the parent channel. As a matter of fact, for the side contouring design, the design can be modified to act as a transition structure (if any) which links the upstream and downstream channels.

CHAPTER V

SUMMARY AND CONCLUSIONS

CHAPTER V

SUMMARY AND CONCLUSIONS

5.1 LATERAL OUTLET IN A TWO-DIMENSIONAL CONDUIT

The problem of flow past a lateral outlet housed in a two-dimensional conduit has been solved using the well-known Schwarz-Cristoffel transformation and the free streamline theory. The solution presented can be applied to the general case of a lateral outlet which is fitted with a barrier that is set at arbitrary angles. The jet contraction coefficient and the jet inclination constitute the primary parameters of the problem. These are expressed as functions of the velocity ratio parameters η and β. For particular cases such as the free outlet or the outlet fitted with a normal barrier, closed form solutions are obtained. The results for the free outlet agrees very well with the empirical formula suggested by earlier investigators.

For the general case of flow past a barrier fitted at arbitrary angles, numerical techniques were used to solve the problem. To this end, a ten point Gaussian quadrature technique was adopted and was found to be satisfactory. Although the theoretical analysis assumes the barrier to be infinitely long, the results are not restrictive, since the jet contraction in a physical model occurs within a short distance from the outlet.

The conclusions that can be drawn from the present analysis are briefly outlined below.

(1) For all values of β and K, the contraction coefficient C_c decreases for increasing values of the jet velocity ratio η.

(2) The contraction coefficient C_{co} for the reservoir condition ($\eta \to o$) increases from 0 to 0.61, as the barrier inclination varies from π to $\pi/2$.

(3) For a large number of outlet barrier inclinations, functional relationships between C_c and η can be obtained from the graphical solutions which are presented.

The general case of flow through an outlet fitted with a barrier finds an application in the design of branch conduits set at arbitrary angles to the main conduit. The case of flow through a free outlet also finds extensive applications. These include the design of multiport diffusers which are used to dilute the effluent of thermal plants in a stream. Based on curve fitting techniques, several approximate relationships are provided to aid the design of physical models.

5.2 LATERAL WEIR OUTLET

Based on the theoretical and experimental study, the following conclusions can be drawn about the characteristics of lateral weirs.

(1) The variation of the local weir discharge coefficient C_d among the different infinitesimal layers (Fig. 1a) which constitute the weir outflow is very large when the values of F_1 and S_y are low. C_d appears to decrease when the width ratio L/B is decreased. The average discharge coefficient of the weir $\bar{C}_d$ is highly dependent on the jet velocity ratio η_0. The width ratio L/B emerges as a significant parameter and $\bar{C}_d$ appears to depend on L/B.

(2) The present experimental data provides a good verification of the theoretical predictions when the minor correction to the theoretical model is made to account for the velocity distribution of the flow in the channel. Based on the experimental results, one can conclude that the proposed model is applicable to lateral weirs which can be as wide as the parent channel.

5.3 UNIFORMLY DISCHARGING LATERAL WEIRS

Based on a simple theory, it is shown that for spatially varied subcritical flow, the water surface profile in a rectangular channel weir system can be maintained horizontally

if the geometry of the channel is properly altered by bed contouring or side contouring. Experimental data has been obtained to verify the nature of water surface profiles predicted by the theory. Tests on the battery of two weirs set in the test flume indicate that proper contouring of the channel geometry does provide a horizontal water surface in the channel reach spanning the weir. This in turn, ensures equal discharge through the individual weirs.

Side contouring designs are more applicable to field conditions where the water carries a high sediment load. Bed contouring is more desirable when the weirs are to be housed on either side of the channel. In such a case, one adopts a staggered arrangement for housing the weirs.

The proposed system can be easily adopted to design weirs which are required to provide a predetermined outflow distribution.

5.4 SCOPE FOR FURTHER STUDIES

It may be interesting to extend the present lateral weir study to the case where the parent channel is trapezoidal since the present study is limited to rectangular channels.

The general principles of the present theory can be applied to other types of outlet assemblies (Ex: uniformly discharging siphon outlets) and the resulting theoretical

models can be verified through experimental studies.

REFERENCES

REFERENCES

[1] Ackers, P., "A Theoretical Consideration of Side Weirs as Storm Water Overflows", Proceedings of the Institute of Civil Engineers, Vol.6, 1957, pp.250-269.

[2] Allen, J.W., "The Discharge of Water Over Side Weirs in Circular Pipes", Proceedings of the Institute of Civil Engineers, Vol. 6, 1957, pp.270-287.

[3] Arbhabhirama, A. "Free Streamline Analysis of Two Dimensional Jet", Journal of the Hydraulics Division, ASCE, (95,4), 1969, pp.1139.

[4] Babbit, M.E., Sewage and Sewage Treatment. Wiley, New York. 7th edition. 1953.

[5] Coleman, G.S. and Smith, D. "The Discharging Capacity of Side Weirs", Selected Engineering Paper No.6, Institution of Civil Engineers, London, 1923.

[6] Collinge, V.K., "The Discharge Capacity of Side Weirs", Proceedings of the Institute of Civil Engineers, London, England, Vol.6, 1957, pp.288-304.

[7] De Marchi, G., "Essay on the Performance of Lateral Weirs", L'Energia Elettrica, Milano, Italy, Vol.11, No.11, Nov.1934, pp.849.

[8] El-Khashab, A., Smith, K.V.H., "Experimental Investigation of Flow Over Side Weirs", Journal of the Hydraulics Division,ASCE,Vol.102,No.HY9, Proc. Paper 12402, Sept. 1976, pp.1255-1268.

[9] Engels, H., "Mitlerlungen ausdem Dresdonet Flusbaulaboratorium", Forsch Arb. Ing. Wes., 1917.

[10] Favre, H., "Contribution à l'etude des courants liquides". Rascher et cie, Zurich, 1933.

[11] Frazer, W., "The Behaviour of Side Weirs in Prismatic Rectangular Channels", Proceedings of the Institution of Civil Engineers, London, England, Vol.6, Feb. 1957, pp.305-328.

[12] Garton,J.E., "Designing an Automatic Cutback Furrow Irrigation System", Oklahoma State University, Exptl. Station, Bulletin B-651, Oct.1966.

[13] Gentilini, B., "Richerche Specimentali Sagli Spioratori Longitudinali"(prima serie di prove). L'Energia E Lettrica, Vol.15, Sept.1938.

[14] Gurevitch, M.I., The Theory of Jets in an Ideal Fluid. 1st Ed., Vol.1, Pergamon Press, N.Y. 1966.

[15] Harlock, J.H., "An Investigation of the Flow in Manifolds With Open and Closed Ends", Journal of the Royal Aeronautical Society, England, Vol.60, Nov.1956, pp.749-753.

[16] Humphreys, A.S., "Mechanical Structures for Farm Irrigation", Journal of the Irrigation and Drainage Division, ASCE, Vol.98, IR4, 1969, pp.463-479.

[17] McNown, J.S., and Hsu, E., "Application of Conformal Mapping to Divided Flow", Proceedings of the Mid-Western Conference on Fluid Dynamics, State University of Iowa, Reprints in Engineering, Reprint No. 96, 1951, pp.143-154.

[18] Mitchell, J.M., "On the Theory of Free Stream Lines", Philosophical Transactions of the Royal Society, London, Vol.A181, 1890,pp.389-431.

[19] Nimo, W.H.R., "Side Spillways for Regulating Diversion Canals", Transactions of the Society of Civil Engineers, Vol.92, 1928, pp.1561.

[20] Ramamurthy, A.S., Subramanya, K., and Carballada,L., "Uniformly Discharging Outlets for Irrigation Systems", Proceedings of the Second World Congress on Water Resources, New Delhi, 1975.

[21] Rawn, A.M., Bouerman, F.R., and Brooks, N.H., "Diffusers for Disposal of Sewage in Seawater, Journal of the Sanitary Engineering Division, ASCE, Vol.86, No. SA2, Proc. Paper 2424, Mar.1960, pp.65-105.

[22] Smith, K.V.H., "Computer Programming for Flow Over Side Weirs", Journal of the Hydraulics Division, ASCE, Vol.99, No. HY3, Proc. Paper 9626, March 1973, pp.495-506.

[23] Subramanya, K., and Awasthy, S.C., "Spatially Varied Flow Over Side Weirs", Journal of the Hydraulics Division, ASCE, Vol.98, No.HY1, Proc.Paper 8627, Jan. 1972, pp.1-9.

[24] Sweeten, J.M., and Garton,J.E., "The Hydraulics of an Automated Furrow Irrigation System With Rectangular Side Weir Outlets", Transactions of the American Society of Agricultural Engineers, Vol.13, No.6, 1970, pp.746-751.

[25] Sweeten, J.M., Garton,J.E., and Mink,A.L., "Hydraulic Roughness of an Irrigation Channel With Decreasing Spatially Varied Flow", Transactions of the American Society of Agricultural Engineers, Vol.12, No.4, 1969, pp.466-470.

[26] Vallentine, H.R., Applied Hydrodynamics, Butterworths Publications, 1969.

[27] Vigander, S., Elder, R.A., and Brooks, N.H., "Internal Hydraulics of Thermal Discharge Diffusers", Journal of the Hydraulics Division, ASCE, Vol.96, No.HY2, Proc. Paper 7085, Feb. 1970, pp.509-527.

APPENDIX I

DETAILS OF THE PROCEDURAL OUTLINES ASSOCIATED WITH THE TRANSFORMATIONS FOR THE LATERAL OUTLET IN A TWO-DIMENSIONAL CONDUIT

APPENDIX I

DETAILS OF THE PROCEDURAL OUTLINES ASSOCIATED WITH THE TRANSFORMATIONS FOR THE LATERAL OUTLET IN A TWO-DIMENSIONAL CONDUIT

(1) Figure 2a denotes the outlet model in the physical plane. The barrier is set at an arbitrary angle π/K.

(2) The complex potential w is obtained by successive transformations from the physical plane to the ξ, ξ' and t-planes. The final transformation adopts the Schwarz-Christoffel technique.

(3) The technique of integration along the free streamline for simple flows is described in standard texts [26] and further it may be added that the factors Y_{AE} and X_{AE} are the Cauchy principal values of the integrals [3]. One can obtain the value of ds on the free streamline as it is equal to dw. In figures 6a and 6b, AFE defines the boundary of the free streamline and it includes a discontinuity at F (Figs. 6a and 6b). The origin is located at A and as such, integration of equations (2.11) and (2.12) provides the coordinates of any point on the free streamline boundary.

(4) Equations (2.13) and (2.14) yield the projections of the free streamline on the axis of y and x respectively. Since the origin is at A (Figures 6a and 6b) and the outlet width "a" is defined as a positive

quantity, Y_{AE} carries a negative sign.

(5) The pair of equations (2.20) and (2.21) are derived from the equations (2.15) and (2.16). The former, together with equation (2.22) provide the solution to the problem.

(6) For all specific values of the barrier length (C) and the parameter K, closed form solutions could not be obtained. Under these circumstances, numerical solutions were sought. For the specific case of the free outlet (K = 1, C = 0), the existing experimental results [21] were compared with the closed form solution.

APPENDIX II

LATERAL WEIR DESIGN EXAMPLE

APPENDIX II

LATERAL WEIR DESIGN EXAMPLE

A2.1 LATERAL WEIR DESIGN EXAMPLE

Let the following data be related to the design of a lateral weir set in a rectangular channel. The Manning's roughness coefficient and the slope are 0.0149 and 0.0016 respectively. The rest of the data are shown below.

Data: B = 10 ft (3.05 m), L = 10 ft (3.05 m), S = 2 ft (0.61 m), and Q_1 = 368 cfs (10.42 c.m./sec).

We obtain Y_1 = 5 ft (1.52 m), V_1 = 7.37 ft/sec (2.25 m/sec), $h_o = (Y_1 - S)$ = 3 ft (0.91 m) and L/B = 1.

From Equations (2.58) and (2.57), F_o = 0.75 and η_o = 0.47. From Equations (2.65) and (2.66) from Figures 27, or from Figure 28, C_d = 0.48 for L/B = 1.0. The corresponding weir outflow Q_t is 173.58 cfs (4.92 c.m./sec) form Equation (2.63a). Hence the expected weir outflow is $Q_t' = 0.95$. Q_t = 165 cfs (4.67 m^3/sec).

APPENDIX III

EFFECT OF VARIATIONS IN Q_1 ON THE UNIFORMITY OF WEIR DISCHARGES IN CHANNELS HAVING CONTOURED SIDES

APPENDIX III

EFFECT OF VARIATIONS IN Q_1 ON THE UNIFORMITY OF WEIR DISCHARGES IN CHANNELS HAVING CONTOURED SIDES

The effect of the variations in the discharge Q_1 through the main channel on the weir outflow Q_w can be analysed approximately using "an order of magnitude analysis". The following assumptions which are not too restrictive are made.

(1) (a) Main channel discharge range →

$$0.90\ Q_1]_{design} < Q_1 < 1.10\ Q_1]_{design} \qquad \text{(A3.1)}$$

(Total Variation = 20%)

(b) Weir Assembly Design → Modular [identical weirs, fixed value of weir height (S).]

(c) Weir type → Deep Weirs, $(Y_1 - S) \rightarrow Y_1$ (A3.2)

(2) (a) Design procedure → Side contouring

Design criteria →

$$\frac{Q_w}{Q_1} = \frac{b_1}{B} = \text{constant} \qquad \text{(A3.3)}$$

(b) Water surface → Horizontal; for fixed Q_1 values, Y_1 is constant

(at the channel center)

Mean velocity in the channel → V_1 = constant (when Q_1 is fixed.)

Parameters F_o and F_1 → F_o and F_1 are constant (when Q_1 is fixed and $Y_1 - S \simeq Y_1$).

As a first approximation, one can use the following relationships to complete the order of magnitude analysis.

$$Q_1 \propto V_1 Y_1, \quad V_1 \propto Y_1^{2/3} \tag{A3.4}$$

i.e.,

$$\left.\begin{aligned} &Q_1 \propto Y_1^{5/3} \quad \text{and} \quad Y_1 \propto Q_1^{3/5} \\ &F_o \quad V_1/\sqrt{g(Y_1-S)}, \ [Y_1 - S] \simeq Y_1 \end{aligned}\right] \tag{A3.5}$$

i.e.,

$$F_o \propto Y_1^{1/6}, \quad F_o \propto Q_1^{1/10} \tag{A3.6}$$

Hence, it is reasonable to assume that F_o is essentially constant

$$(0.99F_o]_{design} < F_o < 1.01F_o]_{design}),$$

when the variations in Q_1 are limited to ±10% of the design discharge. Further, using the assumed conditions of deep

weirs, $h_o \approx Y_1$ and the relationship for $Q_w (=Q_t)$ as given by equations (2.28) and (2.30), one gets,

$$Q_t = Q_w = \bar{C}_d L h_o \bar{V}_j \tag{A3.7}$$

and

$$\bar{V}_j = V_1 . f_1[F_o] \tag{A3.8}$$

where, f_1 denotes a function.

i.e.,

$$\bar{V}_j \propto V_1$$

Further,

$$Y_1 + h_o (=Y_1 - S) \tag{A3.9}$$

$$Q_w = \bar{C}_d L Y_1 \bar{V}_j = \bar{C}_d L Y_1 V_1 f_1[F_o] \tag{A3.10}$$

$$Q_w \propto Q_1 \bar{C}_d \tag{A3.11}$$

i.e.

$$\frac{Q_w}{Q_1} \propto \bar{C}_d \tag{A3.12}$$

$\bar{C}_d$ is a weak function of L/B and as such, approximately $\bar{C}_d$, F_o and F_o variations for off design conditions are too small for normal operating conditions. Consequently, Q_w/Q_1 will remain essentially constant and will be close to the ratio b_1/B, which is a constant design parameter.

APPENDIX IV

COMPUTER PROGRAMS AND SAMPLE COMPUTATION

Program to verify the closed form solution with regard to McNown solution and corresponding output.

```
...

 *TERMINATED*

READY.

LIST

00100 PROGRAM LUI(INPUT,OUTPUT)
00110 DIMENSION XK(45),YK(56)
00120 DATA (XK(I),I=1,10)/.0001,.1,.2,.3,.4,.5,.6,.7,.8,.9/
00130 DATA (YK(I),I=1,9)/.1,.2,.3,.4,.5,.6,.7,.8,.9999/
00140 VJ=1.
00150 DO 14 J=1,10
00160 VV=XK(J)
00170 PRINT 17,VV
00180 DO 15 I=1,9
00190 V1=YK(I)
00200 TF=(1.+VV)/(2.*V1)
00210 XN=1./(1.-VV)
00220 XN1=1.-(1./XN)
00230 XN2=1.-(1./(2.*XN))
00240 PT=(3.1416*SQRT(1.-(TF**2.)))/XN
00250 PT1=-((TF/XN)*ALOG((1.+TF)/(1.-TF)))
00260 PT2=((XN2*XN2+TF*TF)/(XN2*TF))*ALOG((XN2+TF)/(XN2-TF))
00270 PT3=-((((XN2*XN2+XN1*XN1*TF*TF)/(XN2*TF)))*ALOG((XN2+XN1*TF)/
00280+(XN2-(XN1*TF))))
00290 P=1./3.1416
00300 A=PT+PT1+PT2+PT3
00310 FT=TF/XN2
00320 BL=P*(P*FT)
00330 EK=(2.*TF)/(BL*(2.*XN-1.))
00340 G1=(((1.+V1)**2.)/((1.-V1)**2.))*((2.-V1-VV*V1)/(2.+V1+VV*V1))
00350 G2=((1.-VV*V1)/(1.+VV*V1))*((1.+V1)/(1.-V1))
00360 G3=A.-(V1+VV*V1)**2.
00370 GA=(1.+(VV*V1)**2)/((1.-(VV*V1))*V1)
00380 CCI=.5*(1.+VV)*V1*ALOG(G1)+(GA)*ALOG(G2)+.5
00390+*3.1416*SQRT(G3)
00400 CCV=3.1416/CCI
00410 TB=.5*(V1+(1./V1))
00420 TC=.5*(V1*VV+(1./(VV*V1)))
00430 TB1=TB*ALOG((-1.-TB)/(1.-TB))
00440 TF1=-(1.-VV)*TF*ALOG((-1.-TF)/(-1.+TF))
00450 TC1=-VV*TC*ALOG((-1.-TC)/(1.-TC))
00460 TR=(1.-VV)*3.1416*SQRT(1.-TF*TF)
00470 AC=(V1/3.1416)*(T=1+TF1+TC1+TR)
00480 CC=(1.-VV)/(AB/V1)
00490 AA1=ACOS(TF)
00500 AA=ACOS(TF)*(360./6.2832)
00510 GA=(2./3.1416)*TF*ALOG(1./(TAN(AA1/2.)))-SQRT(1.-TF*TF)
00520 FV1=(2./3.1416)*(1.+(V1*V1))*(.5*ALOG((1.+V1)/(1.-V1)))
00530 FV2=(2./3.1416)*(1.+((V1*VV)**2))*(.5*ALOG((1.+(V1*VV))/(1.
00531+-(V1*VV))))
00540 AEM=FV1-FV2-(((V1-(V1*VV))*GA))
00550 CCM=(1.-VV)/(AEM/V1)
00560 PRINT 13,AEM,CCM,AB,CC
00570 15 CONTINUE
00580 14 CONTINUE
00590 17 FORMAT(2X,F16.8,//,2X)
00600 13 FORMAT(4(2X,E15.7))
00610 STOP
00620 END
READY.
```

PNh

V_2/V_1=.20010000

McNown's (a/b)	McNown's C_c	Author's (a/b)	Author's C_c
.1642133E+00	.6089031E+00	.1642133E+00	.6089031E+00
.3319128E+00	.6025076E+00	.3319128E+00	.6025076E+00
.5070060E+00	.5916498E+00	.5070060E+00	.5916498E+00
.6943810E+00	.5759950E+00	.6943810E+00	.5759950E+00
.9008352E+00	.5549850E+00	.9008352E+00	.5549850E+00
.1136918E+01	.5276899E+00	.1136918E+01	.5276899E+00
.1421288E+01	.4924617E+00	.1421288E+01	.4924617E+00
.1793770E+01	.4459435E+00	.1793770E+01	.4459435E+00
.6995053E+01	.1429296E+00	.6995054E+01	.1429296E+00
.10000000			
.1478373E+00	.6087773E+00	.1478373E+00	.6087773E+00
.2990021E+00	.6020024E+00	.2990021E+00	.6020024E+00
.4572350E+00	.5905060E+00	.4572350E+00	.5905060E+00
.6272392E+00	.5739438E+00	.6272392E+00	.5739438E+00
.8155984E+00	.5517421E+00	.8155984E+00	.5517421E+00
.1032604E+01	.5229497E+00	.1032604E+01	.5229497E+00
.1296592E+01	.4858892E+00	.1296592E+01	.4858892E+00
.1646964E+01	.4371680E+00	.1646964E+01	.4371680E+00
.6796373E+01	.1324103E+00	.6796373E+01	.1324103E+00
.20000000			
.1314472E+00	.6086093E+00	.1314472E+00	.6086093E+00
.2660766E+00	.6013305E+00	.2660766E+00	.6013305E+00
.4074744E+00	.5889941E+00	.4074744E+00	.5889941E+00
.5601697E+00	.5712555E+00	.5601697E+00	.5712555E+00
.7305390E+00	.5475409E+00	.7305390E+00	.5475409E+00
.9286147E+00	.5168990E+00	.9286147E+00	.5168990E+00
.1172393E+01	.4776556E+00	.1172393E+01	.4776556E+00
.1500811E+01	.4264361E+00	.1500811E+01	.4264361E+00
.6598101E+01	.1212349E+00	.6598102E+01	.1212349E+00
.30000000			
.1150562E+00	.6083993E+00	.1150562E+00	.6083993E+00
.2331422E+00	.6004918E+00	.2331422E+00	.6004918E+00
.3576827E+00	.5871126E+00	.3576827E+00	.5871126E+00
.4930230E+00	.5679248E+00	.4930230E+00	.5679248E+00
.6453187E+00	.5423677E+00	.6453187E+00	.5423677E+00
.8243208E+00	.5095104E+00	.8243208E+00	.5095104E+00
.1047647E+01	.4677148E+00	.1047647E+01	.4677148E+00
.1353697E+01	.4136821E+00	.1353697E+01	.4136821E+00
.6396769E+01	.1094193E+00	.6396769E+01	.1094193E+00
.40000000			
.9866033E-01	.6081472E+00	.9866033E-01	.6081472E+00
.2001716E+00	.5994852E+00	.2001716E+00	.5994852E+00
.3077669E+00	.5848582E+00	.3077669E+00	.5848582E+00
.4255759E+00	.5639417E+00	.4255759E+00	.5639417E+00
.5594940E+00	.5361988E+00	.5594940E+00	.5361988E+00
.7189394E+00	.5007[illegible]		

INTERRUPTED
STOP

Program to obtain the numerical solution for the lateral outlet case.

```
      PROGRAM TK5(INPUT,OUTPUT,TAPE4,TAPE2)
       DIMENSION XK(14),X1(14),A2(55)
      DIMENSION Z(2,10,300),AX(2),NPTB(2),NPT(300),LTYP(300)
      EXTERNAL FCT
      COMMON XXK,VA,VV,TC,TB,TF
       DATA (X2(I),I=1,56)/0.01,0.011,.012,.013,.014,.015,.016,.017
     +,.018,.019,.02,.021,
     +.03,.04,.05,.06,.07,.08,.09,.1,.16,.2,.25,.3,.35,.4,.45,.5,.55,
     +.56,.57,.58,.59,.60,.62,.65,.67,.69,.71,.75,.77,.79,.82,.83
     +,.86,.88,.89,.90,.92,.94,.96,.98,.99,.995,.9999,.99999/
      DATA (XK(I),I=1,5)/2.,1.75,1.33333,1.25,1.1/
       DATA (X1(I),I=1,10)/.1,.2,.3,.4,.5,.6,.7,.8,.9,1./
      DATA (NPTB(I),I=1,2)/.5,.5/
      DATA (AX(I),I=1,2)/10.,7./
      MM=1
         PRW=0.0
      NSET=10
       NNN=56
      NS=NNN
      NB=1
      DO 1 II=1,NSET
      NPT(II)=NS
    1 LTYP(II)=NB
      Y<=1.
      VJ=1.
      FCV=.00001
      CF=.99999999
      DO 77 IK=1,10,2
      KI=IK+1
   77 CONTINUE
      DO 14 J=1,10
        DC=FLOAT(J)
        F7=DC/10.
         VV=X1(J)
          SY=X1(J)
           A1=-.538+.254*VV
             A2=.058+.234*VV
             A3=-.129-.469*VV
      DO 15 I=1,NNN
        CF=1./(1.+((2.*X2(I))/(X1(J)**2)))
            DSQ=1./SQRT(1.+((2.*SY)/(F7**2)))
              ETS=X2(I)
              CONTINUE
        FW=SQRT((2.*(ETS**2))/(1.+(ETS**2)))
           AW=(1.-(ETS**3))*(A3+(A1/(ETS**3)))+(3.*
     +(1.-ETS))*(A2+(A1/ETS))
          CZ=((1.+(2./(FW**2)))**1.5)-1.
         CDB=AW*(1./3.)*X1(J)*(FW**2)
         DCB=AW*(1./3.)*VV*(1.**2)
             IF(CDB.GT.1.)     CDB=1.
           FD=(2.*(ETS*ETS))/(1.-(ETS*ETS))
              RQ=VV*SY*FD*AW
        IF(RQ.GT.1.)     RQ=1.
        IF(RQ.LT.0.)  RQ=0.
         CD3=.A1+A2*V1+(A2*(V1**2))+(A3*(V1**3))
           IF(CDB.LT..0)     CDB=0.
           IF(FW.GT.3.)     FW=3.
        GO TO 4567
      AA=.5*(V1+VV*V1)
      AAA=COS(AA)
      XAA=(3.1416/YK)
      IF(AA.LT.XAA.AND.YK.GT.2.) AA=XAA
      TF=COSTY**AA)
      TC=.5*(((VV*V1)**YK)+(1./((VV*V1)**YK)))
      TB=.5*((V1**YK)+(1./(V1**YK)))
      IF(AA.LT.XAA.AND.YK.GT.2.) GO TO 98
      TB1=TB*ALOG((1.-TB)/(1.-TB))
      TF1=-(1.-VV)*TF*ALOG((1.-TF)/(1.+TF))
```

```
      TC1=-VV*TC*ALOG((-1.-TC)/(1.-TC))
      TB=(1.-VV)**3.1416*SQRT(1.-TF*TF)
      AB=(V1/3.14(6)*(TB)+TF)+TC1+T3)
      GO TO 74
   98 CONTINUE
      PX=.1E-20
      XXK=YK
      XA=-(3.1416/2.)
      XE=(-(3.1416/2.)-PX)+AA
      X_=-(3.1416/2.)
      D1=(XE-XA)/MM
       XOC=.0
       YOC=.0
      DO 456 NN=1,MM
       XU=XL+D1
      CALL QG16 (XL,XU,FCT,Y)
      X_=XU
      YOC=YOC+Y
  456 CONTINUE
       YO=YOC
      R=YO
      C9=0.
      AY=(3.1416/XXK)-(3.1416/2.)
      AB=(((-R)/3.1416)+(V1-(VV*V1)))/COS(AY)
   78 CONTINUE
      CC=(V1-(VV*V1))/AB
        VV2=V1*V1
        AO=AA*(180./3.1416)
          ERT=1./(1.+((2.*V1)/(VV*VV)))
            AS=.472-(.456*VV)
          ASO=.1794+(.44594*VV)
          DF=SQRT(1.+(2.*V1))
           DV=SQRT(1.+1.33*V1)
             CDM=(1./(V1*DM))*((.203*((DF**3)-1.))-(AS*(DF-1.))+ASO*((1.
     +/DF)-1.))
             CD1=.61+(.01*ERT)-(.62*ERT*ERT)
                IF(FS.GT.100.)       FS=100.
 4567  CONTINUE
        IF(ETS.GT..8)    ETS=.8
       IF(FH.GT.1.)    FH=1.
          CDSF=0.61+A1*ETS+A2*(ETS**2)+A3*(ETS**3)
          RW=1./DCBW
           IF(RW.GT.2.)     RW=2.
      Z(2,J,T)=FH
      Z(1,J,T)=BX
   15 CONTINUE
   14 CONTINUE
   13 CONTINUE
   97 CONTINUE
      CALL MPGRAPH(6,4,10,NPT,LTYP,Z,ORIG,AX)
   17 FORMAT(//,2X,'V2/V1=',FA.4,2X,'K=',F8.4,//)
   99 FORMAT(2X,6(4X,E15.8,2X))
   31 FORMAT(2X,E15.7,3X,E15.7)
      REWIND 4
      STOP
      END
      FUNCTION  FCT(BTA)
      COMMON XXK,V1,VV,TC,TB,TF
      A_F=XXK*((3.1416/2.)+BTA)
      BTE=BTA+(3.1415/XXK)+(3.1416/2.)
      FCF=(-SIN(ALF)*XXK*SIN(BTE))/(COS(ALF)-TF)
      FCR=(-SIN(ALF)*XXK*SIN(BTE))/(COS(ALF)-TB)
      FCC=(-SIN(ALF)*XXK*SIN(BTE))/(COS(ALF)-TC)
      FCT=V1*FCR-((V1)-((VV*V1)))*FCF-(VV*V1)*FCC
      RETURN
      END
```

Program for lateral weir data (L/B =.0.5) reduction and output.

```
      PROGRAM LW(INPUT,OUTPUT,TAPE4,TAPE7)
      DIMENSION Y1(154),Y2(154),QW(154),Q2(154)
      DIMENSION Z(2,10,300),AX(2),ORIG(2),NPT(300),LTYP(300)
      DATA (AX(I),I=1,2)/10.,7./
      DATA (ORIG(I),I=1,2)/0.,0./
      READ 12,(Y1(I),I=1,46)
      READ 12,(Y2(I),I=1,46)
      READ 13,(QW(I),I=1,46)
      READ 13,(Q2(I),I=1,46)
      NSET=1
      NS=46
      NR=0
      DO 1 II=1,NSET
      NPT(II)=NS
    1 LTYP(II)=NR
      XL=5./12.
      H=10./12.
      S=4.0/12.
      G=32.2
      DO 75 I=1,46
      Y22=Y2(I)/12.
      Y11=Y1(I)/12.
      V1=(QW(I)+Q2(I))/(B*Y11)
        QA=QW(I)+Q2(I)
      V2=Q2(I)/(B*Y22)
      VS=V1**2.
      V12S=((V1+V2)/2.)**2.
        IF(I.GT.18.AND.I.LT.35)  S=(2./12.)
           IF(I.GT.34)           S=6./12.
           C1=-.538+.254*(.5)
             C2=.058-.234*(.5)
          RS=2.*G*(Y11-S)
             C3=-.129-.489*(.5)
        ETS=V1/SQRT((V1**2)+RS)
        FR=V1/SQRT(G*Y11)
          FO=V1/SQRT(.5*RS)
       FR=V1/SQRT(G*Y11)
        AH=(1.-(ETS**3))*((C3)+(.611/(ETS**3)))+(1.-ETS)*(C2+(C1
     +/FTS))*3.
          CXW=(QA*(FR**2))/QW(I)
            QT=(XL*(V1**3)*AH)/(3*G)
             DC=(QW(I)-QT)/QT
               PO=((1.+(2./(FO*FO)))**1.5-1.)
             CDT=(1.*AH)/PO
               VMJ=V1*FO*FO*(PO/3.)
             CDW=QW(I)/(XL*VMJ*(Y11-S))
             DCD=(CDW-CDT)/CDT
           S1=S*12.
  798      CONTINUE
           WRITE(4,79)
     +Y11,QA,QW(I),FO,S1,CDW,CDT,DC,I
   51      CONTINUE
   43    FORMAT(2X,I3,3(2X,E10.3),2X))
        Z(1,1,I)=CDW
        Z(2,1,I)=FO
           Z(1,1,1)=0.
           Z(2,1,1)=1.
           Z(2,1,9)=1.
           Z(2,1,9)=0.
   75 CONTINUE
   79    FORMAT(4X,F5.3,6X,F5.3,6X,F5.3,6X,F5.3,6X,F4.2,6X,F4.2,3(6X,F5.3),
     +6X,I4)
           CALL HPGRAPH(6,7,
      STOP
   12         FORMAT(20F4.2,/,20F4.2,/,20F4.2)
   13         FORMAT(16F5.3,/,16F5.3,/,16F5.3,/,12F5.3)
      END
```

y_1 in feet	Q_1 in cfs	Q_w in cfs	F_o	s in inches	C_{dw}	C_d	$\frac{C_{dw} - C_d}{C_d}$	Run
.743	.930	.317	.42	4.00	.489	.537	-.089	1
.594	.832	.1163	.58	4.00	.448	.491	-.088	2
.658	.857	.335	.37	4.00	.501	.552	-.092	3
.691	.834	.214	.49	4.00	.469	.518	-.095	4
.513	.461	.108	.41	4.00	.491	.341	-.093	5
.681	.937	.245	.50	4.00	.466	.515	-.094	6
.627	.426	.195	.27	4.00	.526	.577	-.088	7
.707	.428	.287	.21	4.00	.548	.589	-.069	8
.423	.430	.033	.72	4.00	.429	.454	-.055	9
.510	.432	.043	.43	4.00	.505	.536	-.058	10
.495	.436	.075	.48	4.00	.500	.521	-.040	11
.392	.352	.017	.79	4.00	.408	.434	-.059	12
.448	.352	.097	.49	4.00	.477	.518	-.079	13
.507	.332	.091	.35	4.00	.524	.556	-.057	14
.428	.333	.037	.57	4.00	.478	.497	-.038	15
.578	.160	.160	.12	4.00	.586	.603	-.028	16
.575	.151	.151	.11	4.00	.565	.604	-.064	17
.553	.147	.130	.12	4.00	.559	.603	-.072	18
.573	.438	.338	.25	2.00	.550	.581	-.053	19
.618	.437	.368	.22	2.00	.555	.586	-.053	20
.458	.444	.444	.20	2.00	.563	.590	-.045	21
.716	.522	.522	.21	2.00	.561	.589	-.046	22
.274	.044	.044	.10	2.00	.556	.605	-.081	23
.339	.092	.092	.14	2.00	.568	.601	-.054	24
.213	.074	.013	.34	2.00	.539	.559	-.037	25
.249	.146	.036	.39	2.00	.525	.547	-.041	26
.297	.146	.081	.28	2.00	.554	.573	-.032	27
.340	.291	.044	.36	2.00	.540	.554	-.025	28
.716	1.250	.496	.50	2.00	.478	.516	-.073	29
.469	.716	.204	.59	2.00	.459	.491	-.066	30
.642	.716	.427	.33	2.00	.529	.561	-.056	31
.243	.236	.039	.61	2.00	.486	.483	.006	32
.345	.228	.046	.33	2.00	.534	.561	-.048	33
.348	.228	.132	.26	2.00	.545	.577	-.055	34
.771	1.204	.184	.64	6.00	.436	.477	-.086	35
.681	.936	.093	.64	6.00	.431	.463	-.069	36
.770	.929	.135	.56	6.00	.464	.498	-.068	37
.681	.554	.089	.40	6.00	.524	.542	-.033	38
.759	.531	.171	.30	6.00	.569	.569	-.035	39
.779	.548	.190	.28	6.00	.549	.573	-.042	40
.671	.269	.082	.19	6.00	.571	.593	-.037	41
.613	.758	.049	.79	6.00	.434	.434	.001	42
.653	.790	.076	.63	6.00	.464	.479	-.030	43
.605	.655	.382	.72	6.00	.433	.453	-.045	44
.443	.672	.102	.49	6.00	.511	.520	-.018	45
.524	.307	.036	.37	6.00	.551	.552	-.002	46

CONTINUED

Program for lateral weir (L/B = 1) data reduction and output.

```
      PROGRAM LW(INPUT,OUTPUT,TAPE4,TAPE5)
      DIMENSION Y1(92),Y2(92),QW(92),Q2(92)
      DIMENSION Z(2,10,300),AX(2),ORIG(2),NPT(300),LTYP(300)
        DATA (AX(I),I=1,2)/10.,7./
      DATA (ORIG(I),I=1,2)/0.,0./
      READ 12,(Y1(I),I=1,92)
      READ 12,(Y2(I),I=1,92)
      READ 13,(QW(I),I=1,92)
      READ 13,(Q2(I),I=1,92)
      NSET=1
      NS=92
      NB=0
      DO 1 II=1,NSET
      NPT(II)=NS
    1 LTYP(II)=NB
      XL=10./12.
      B=10./12.
      S=2.0/12.
      G=32.2
      DO 75 I=1,92
      Y22=Y2(I)/12.
      Y11=Y1(I)/12.
      V1=(QW(I)+Q2(I))/(B*Y11)
        QA=QW(I)+Q2(I)
      V2=Q2(I)/(B*Y22)
      VS=V1**2.
      V12S=((V1+V2)/2.)**2.
          IF(1.GT.33.AND.I.LT.53)    S=(A.07/12.)
            IF(I.GT.52)      S=4./12.
            IF(I.GT.91)      S=A.07/12.
          C1=-.53A*.254
            C2=.0*S+.234
          RS=2.*G*(Y11-S)
            C3=-.129-.489
        ETS=V1/SQRT((V1**2)+RS)
        FR=V1/SQRT(G*Y11)
        FO=V1/SQRT(.5*RS)
       FR=V1/SQRT(G*Y11)
      AH=(1.-(ETS**3))*((C3)+(.611/(ETS**3)))+(1.-ETS)*(C2+(C1
     +/FTS))*3.
        XDC=(QA*(FR**2))/QW(I)
          QT=(XL*(V1**3)*AH)/(3*G)
          DC=(QW(I)-QT)/QT
            PD=((1.+(2./(FO*FO)))**1.5-1.)
          CDT=(1.*AH)/PD
            VMJ=V1*FO*FO*(PD/3.)
           CDW=QW(I)/(XL*VMJ*(Y11-S))
          DCD=(CDW-CDT)/CDT
          S1=S*12.
798         CONTINUE
        WRITE(4,79)
     +Y11,QA,G,(I),FO,S1,CDW,CDT,DQ,I
 51       CONTINUE
 43     FORMAT(2X,13,3(2X,E2.3,2X))
          IF(XDC.GT.2.)    XDC=2.
           IF(FO.GT.1.)     FO=1.
      Z(1,1,I)=CDW
      Z(2,1,I)=FO
           Z(1,1,A3)=0.
            Z(2,1,A3)=0.
            Z(1,1,A4)=2.
            Z(2,1,A4)=1.
   75 CONTINUE
   79   FORMAT(6X,F5.3,6X,F5.3,6X,F5.3,6X,F5.3,6X,F4.2,6X,F4.2,3(6X,F5.3),
     +6X,I4)
   12   FORMAT(5(20F4.2,/),4F4.2,/,1JF4.2,/,20F4.2,/,5F4.2,/,12F4.2)
   13         FORMAT(6(16F5.3,/),8F5.3,/,1JF5.3,/,14F5.3,/,9F5.3,/,12F5.3)
        CALL HPGRPH(A,5,1,NPT,LTYP,Z,ORIG,AX)
      STOP
      END
```

r_1 in feet	Q_1 in cfs	Q_o in cfs	r_o	s in inches	C_{dv}	C_d	$\frac{C_{dv} - C_d}{C_d}$	Run number
.448	.769	.696	.81	2.88	.638	.676	-.079	71
.583	.756	1.019	.66	2.88	.812	.864	-.072	2
.594	.936	.729	.81	2.88	.861	.943	-.096	3
.661	1.296	.871	.87	2.88	.874	.981	-.107	4
.573	1.442	.946	.83	2.88	.883	.917	-.060	5
.547	.629	.747	.66	2.88	.843	.878	-.031	6
.606	1.418	.664	.68	2.88	.889	.968	-.073	7
.632	.648	.899	.89	2.88	.898	.929	-.004	8
.648	.767	.621	.68	2.88	.875	.934	-.062	9
.674	1.321	.916	.56	2.88	.876	.926	-.054	10
.582	.879	.699	.80	2.88	.811	.844	-.043	11
.685	.688	.644	.93	2.88	.888	.938	-.071	12
.649	.887	.816	.88	2.88	.880	.912	-.044	13
.630	.917	.868	.88	2.88	.839	.868	-.046	14
.588	.588	.699	.75	2.88	.843	.895	-.108	15
.891	.894	.894	.93	2.88	.883	.913	-.090	16
.868	.868	.868	.98	2.88	.883	.873	-.011	17
.595	.878	.843	.87	2.88	.888	.875	-.086	18
.599	.898	.898	.83	2.88	.888	.893	-.008	19
.583	.874	.874	.89	2.88	.846	.898	-.087	20
.838	.847	.847	.86	2.88	.886	.888	-.087	21
.821	.860	.860	.87	2.88	.866	.887	-.017	22
.676	.893	.893	.86	2.88	.886	.871	-.036	23
.836	.812	.812	.79	2.88	.836	.866	-.052	24
.767	1.148	1.148	.83	2.88	.826	.866	-.063	25
.842	.886	.886	.89	2.88	.841	.867	-.044	26
.697	.898	.898	.84	2.88	.881	.896	-.065	27
.818	.888	.847	.68	2.88	.832	.861	-.031	28
.861	.879	.828	.86	2.88	.836	.872	-.068	29
.822	.884	.844	.83	2.88	.861	.877	-.042	30
.837	.884	.838	.84	2.88	.823	.868	-.049	31
.889	.895	.898	.86	2.88	.826	.868	-.047	32
.898	.898	.898	.86	2.88	.821	.866	-.043	33
.718	.894	.894	.86	6.87	.871	.881	-.099	34
.683	.897	.196	.86	6.87	.886	.896	-.031	35
.665	.886	.171	.81	6.87	.887	.896	-.013	36
.830	.844	.188	.82	6.87	.871	.844	-.036	37
.796	.876	.876	.89	6.87	.899	.896	-.078	38
.787	.836	.836	.86	6.87	.876	.868	-.059	39
.868	.884	.884	.88	6.87	.812	.868	-.066	40
.667	.879	.196	.77	6.87	.833	.884	-.187	41
.727	.883	.868	.81	6.87	.878	.892	-.033	42
.848	.886	.182	.77	6.87	.881	.886	-.078	43
.863	.884	.888	.84	6.87	.896	.918	-.036	44
.849	.884	.844	.87	6.87	.862	.861	-.025	45
.862	.843	.823	.89	6.87	.878	.896	-.060	46
.884	.838	.899	.84	6.87	.818	.832	-.041	47
.884	.837	.838	.74	6.87	.844	.887	-.058	48
.826	.827	.118	.83	6.87	.863	.868	-.029	49
.871	.884	.844	.96	6.87	.863	.933	-.078	50
.828	.897	.113	.84	6.87	.838	.878	-.067	51
.881	1.896	.193	.79	6.87	.846	.888	-.074	52
.583	1.852	.328	.76	6.88	.866	.887	-.083	53
.766	1.831	.868	.87	6.88	.883	.881	-.008	54
.727	.867	.837	.68	6.88	.818	.888	-.071	55
.828	.889	.875	.78	6.88	.834	.888	-.100	56
.878	.888	.144	.87	6.88	.893	.831	-.071	57
.891	.886	.283	.98	6.88	.829	.868	-.084	58
.898	.886	.288	.84	6.88	.866	.878	-.056	59
.811	.849	.288	.87	6.88	.883	.878	-.068	60
.889	.893	.132	.88	6.88	.866	.888	-.043	61
.812	.895	.194	.89	6.88	.868	.898	-.058	62
.672	.893	.868	.87	6.88	.867	.882	-.066	63
.883	.892	.868	.87	6.88	.866	.867	-.068	64
.817	.868	.862	.81	6.88	.831	.876	-.068	65
.866	.837	.837	.74	6.88	.868	.884	-.058	66
.812	.853	.858	.15	6.88	.856	.867	-.086	67
.382	.826	.826	.87	6.88	.867	.869	-.182	68
.636	.884	.884	.13	6.88	.868	.868	-.068	69
.781	.738	.738	.31	6.88	.881	.881	-.001	70
.681	.878	.878	.87	6.88	.868	.887	-.043	71
.826	.826	.826	.78	6.88	.868	.887	-.047	72
.567	.344	.333	.28	6.88	.856	.885	-.049	73
.663	.397	.388	.27	6.88	.862	.867	-.044	74
.758	.794	.724	.32	6.88	.881	.879	-.048	75
.733	.756	.668	.34	6.88	.851	.875	-.046	76
.727	.754	.649	.35	6.88	.847	.874	-.046	77
.633	1.183	.878	1.78	6.88	.761	.785	-.071	78
.498	.888	.188	1.16	6.88	.847	.868	-.131	79
.395	.877	.837	1.88	6.88	.839	.894	-.058	80
.668	.898	.891	1.13	6.88	.891	.881	-.128	81
.625	.872	.878	.98	6.88	.882	.838	-.016	82
.668	1.638	.838	2.72	6.88	.826	.857	-.288	83
.833	1.817	.868	1.88	6.88	.888	.884	-.188	84
.387	.811	.838	1.72	6.88	.841	.888	-.167	85
.888	.813	.868	1.86	6.88	.886	.898	-.081	86
.887	.813	.856	1.86	6.88	.811	.811	-.008	87
.811	.995	.867	1.77	6.88	.888	.874	-.178	88
.883	.899	.869	1.86	6.88	.842	.859	-.054	89
.881	.871	.828	1.81	6.88	.862	.861	-.008	90
.383	.736	.829	1.86	6.88	.852	.862	-.008	91
.868	1.648	.836	2.14	6.87	.199	.219	-.090	92

Let us consider run number 1 of this serie (L/B = 1.) A sample computation is as follows

From the print-out we have

$y_1 = 0.4$ feet

$Q_1 = 0.742$ cfs

$Q_w = 0.296$ cfs

$S = 2$ inches

We know that B = 10 inches and L = 10 inches. So,

$$V_1 = \frac{Q}{y\ B} = \frac{0.742}{0.4(\frac{10}{12})} = 2.22 \text{ fps}$$

$$h_o = y_1 - S = 0.4 - \frac{2}{12} = 0.233 \text{ ft}$$

and

$$F_o = \frac{V_1}{\sqrt{gh_o}} = \frac{2.22}{\sqrt{32.2(0.233)}} = 0.81$$

Since we have F_o and L/B from Figure 28, the weir mean coefficient $\bar{C}_d$ is 0.438.

To obtain $\bar{C}_{dw}$, i.e., the actual weir coefficient equation (2.63a) is used and the measured weir discharge Q_w(=0.296 cfs), the upstream weir velocity V_1(=2.22 fps), the weir length L(=10 inches), h_o(=0.233 ft) and the weir parameter

F_o (=0.81) are substituted and C_{dw} = 0.476 is obtained.

Column $(C_{dw}-C_d)/C_d$ shows the percentage error.

FIGURES

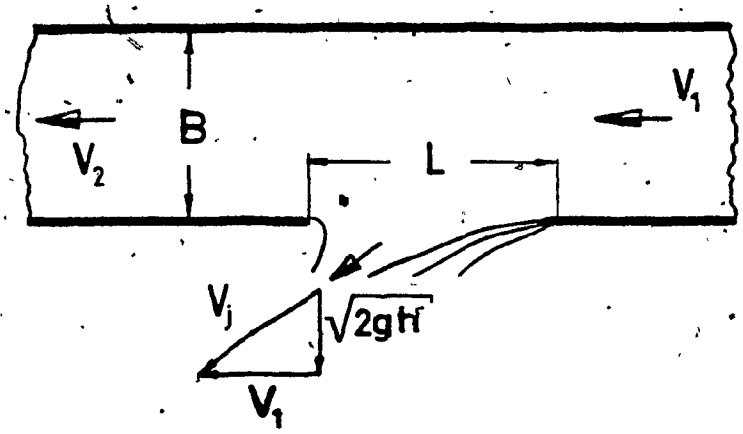

(a) PLAN VIEW

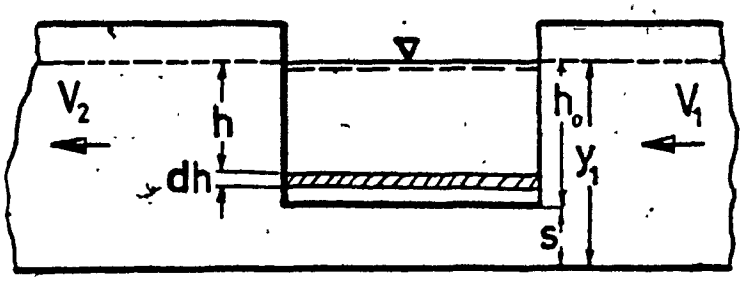

(b) FRONT VIEW

FIG. 1 LATERAL WEIR MODEL

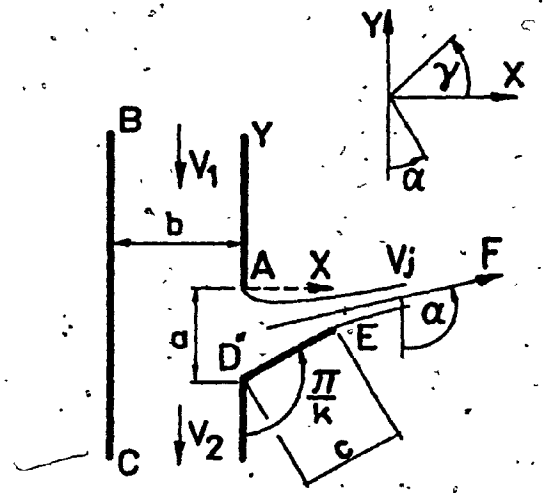

FIG. 2(a) THE PHYSICAL (Z) PLANE

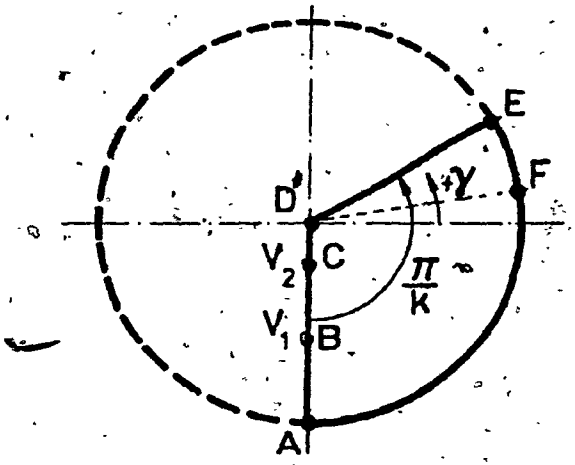

FIG. 2(b) THE INVERSE HODOGRAPH (ξ) PLANE

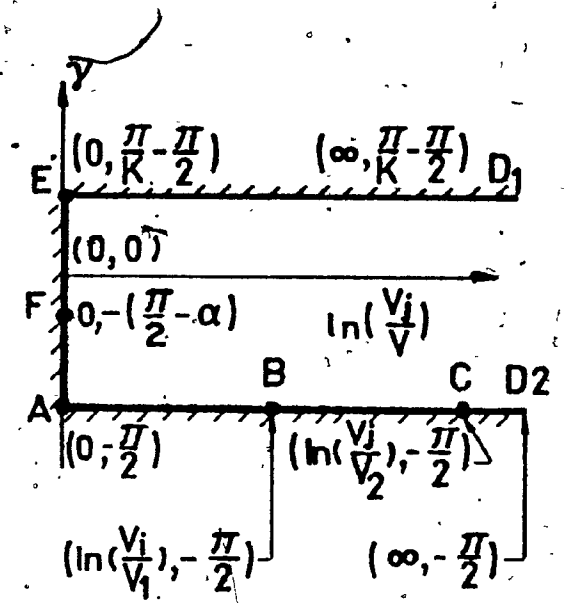

FIG. 3 THE ξ PLANE

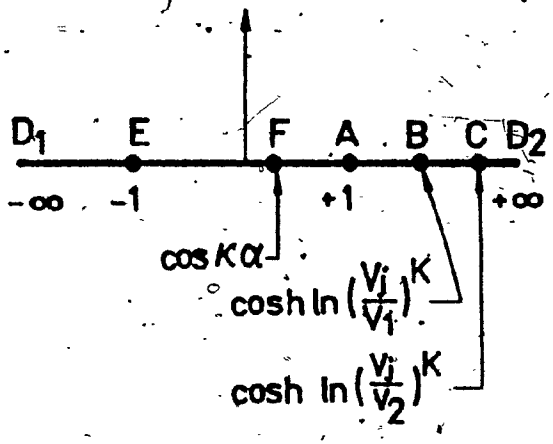

FIG. 4 THE t PLANE

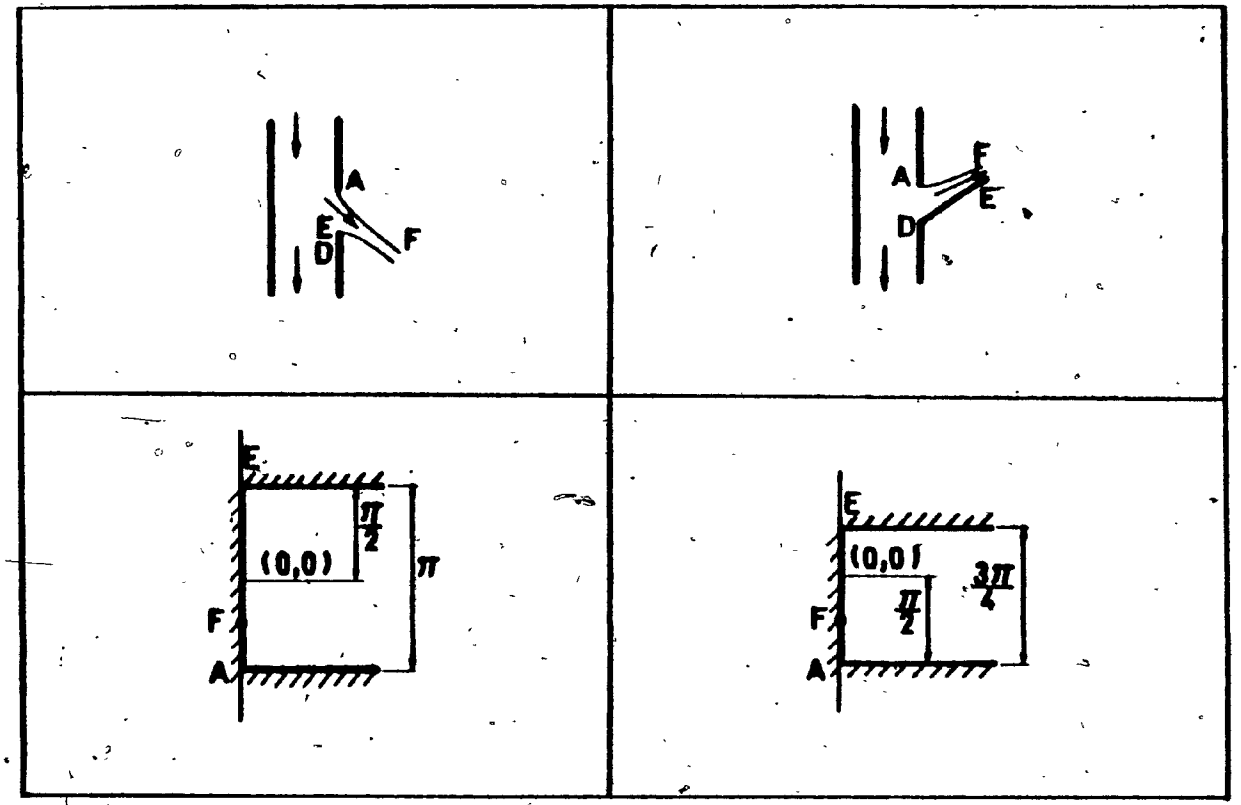

FIG.5(a) THE FREE OUTLET MODEL (K = 1)

FIG. 5(b) THE BARRIER MODEL (K = 3/4)

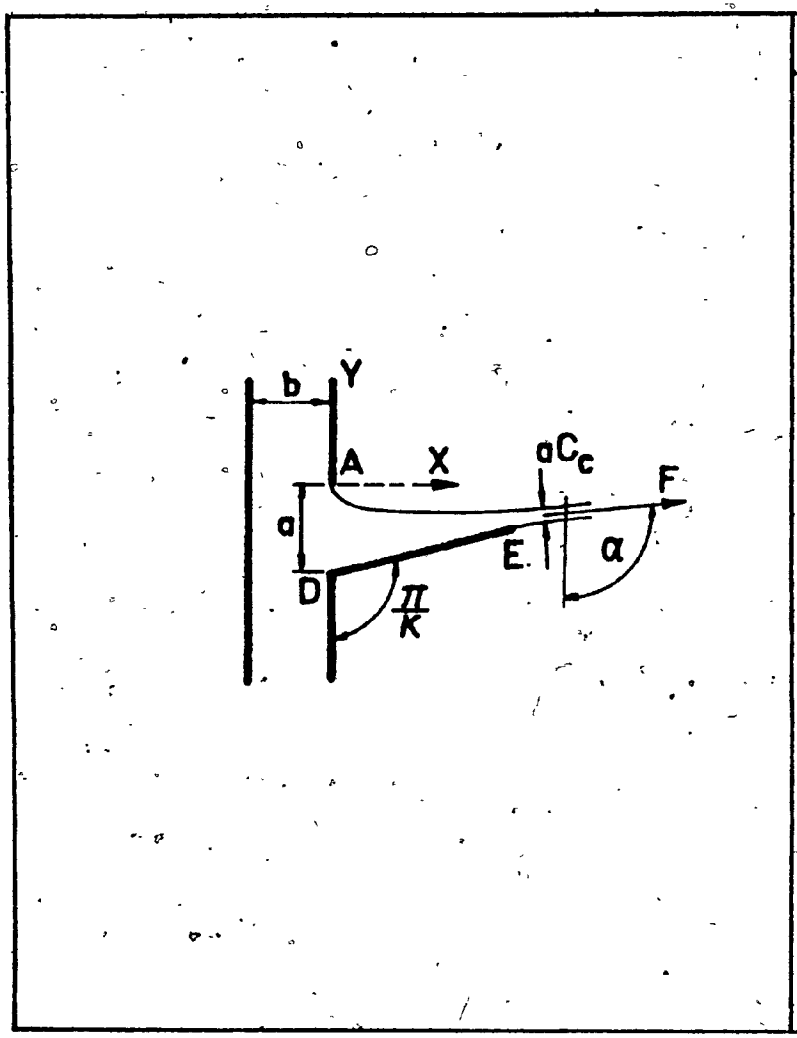

FIG. 6(a) FREE STREAMLINE PATTERN FOR K < 2

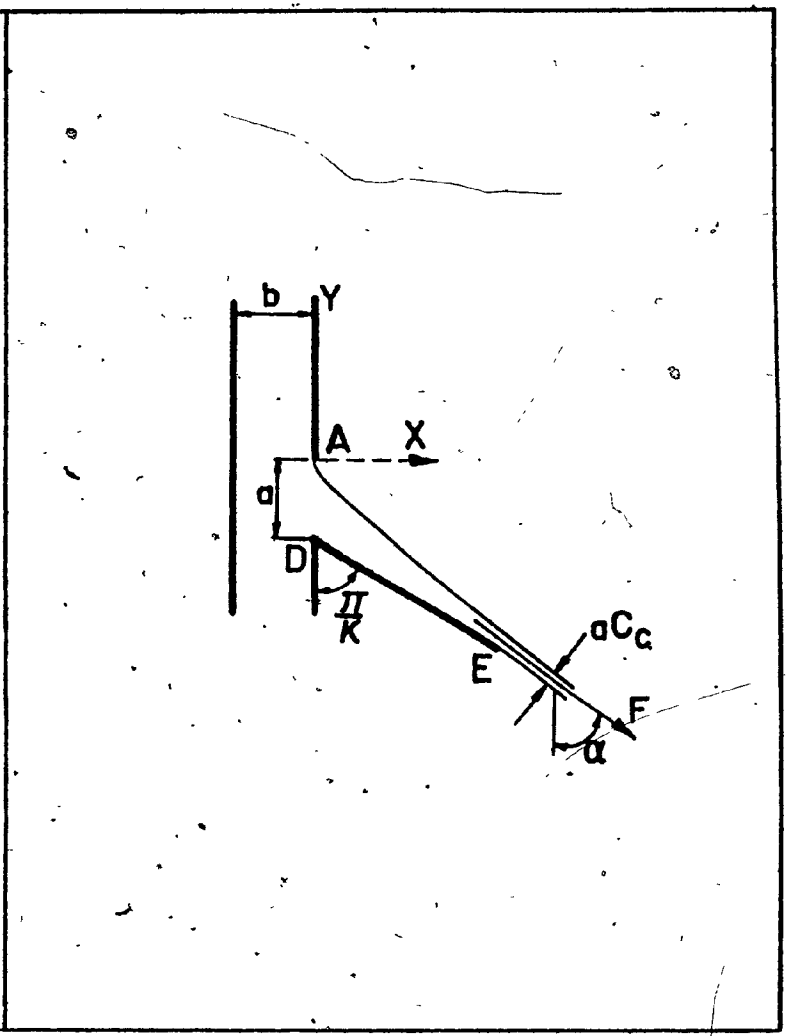

FIG. 6(b) FREE STREAMLINE PATTERN FOR K > 2

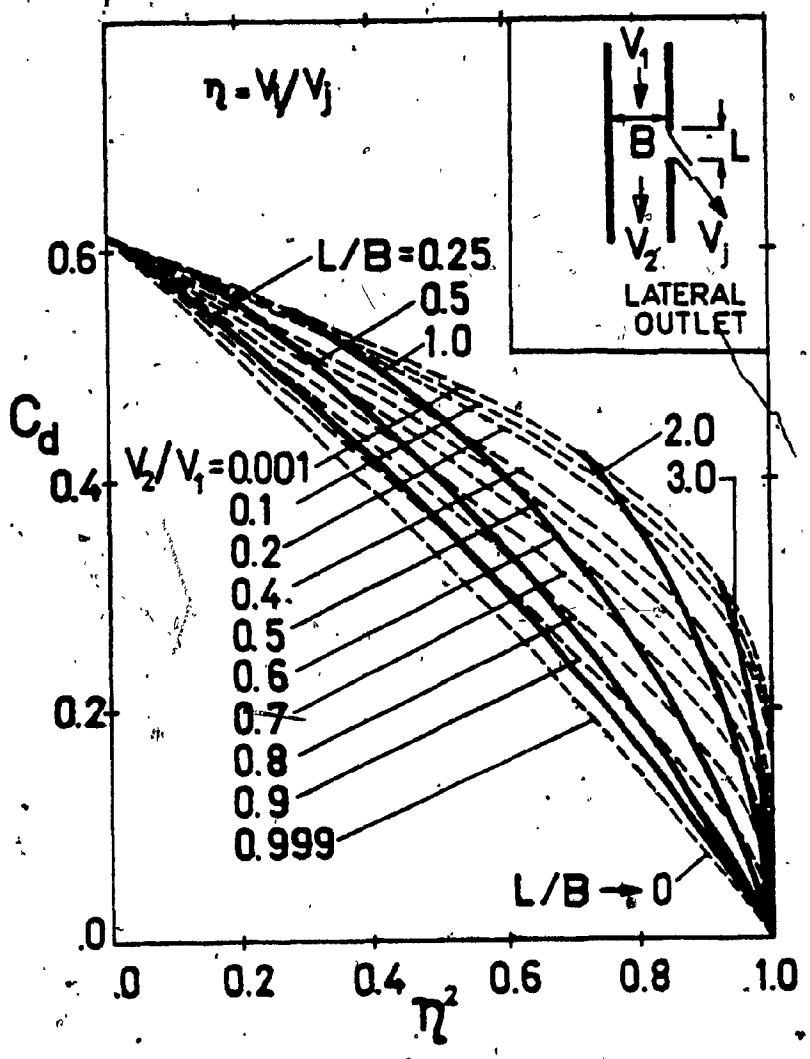

FIG. 7 VARIATION OF THE COEFFICIENT C_d WITH THE SQUARE OF THE JET VELOCITY RATIO η^2, $0 \leq \eta < 1$

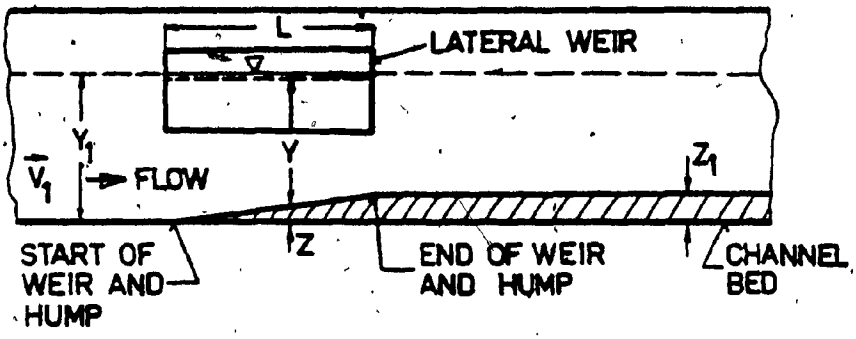

(a) CONTOURING OF CHANNEL BED (ELEVATION)

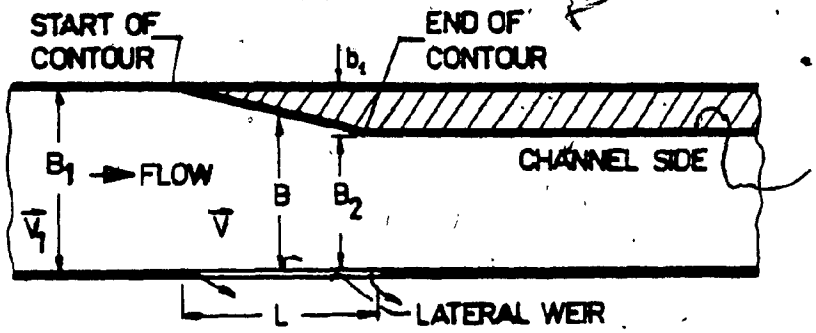

(b) CONTOURING OF CHANNEL SIDE (PLAN)

FIG. 8 GEOMETRIC CONFIGURATION OF THE CHANNEL

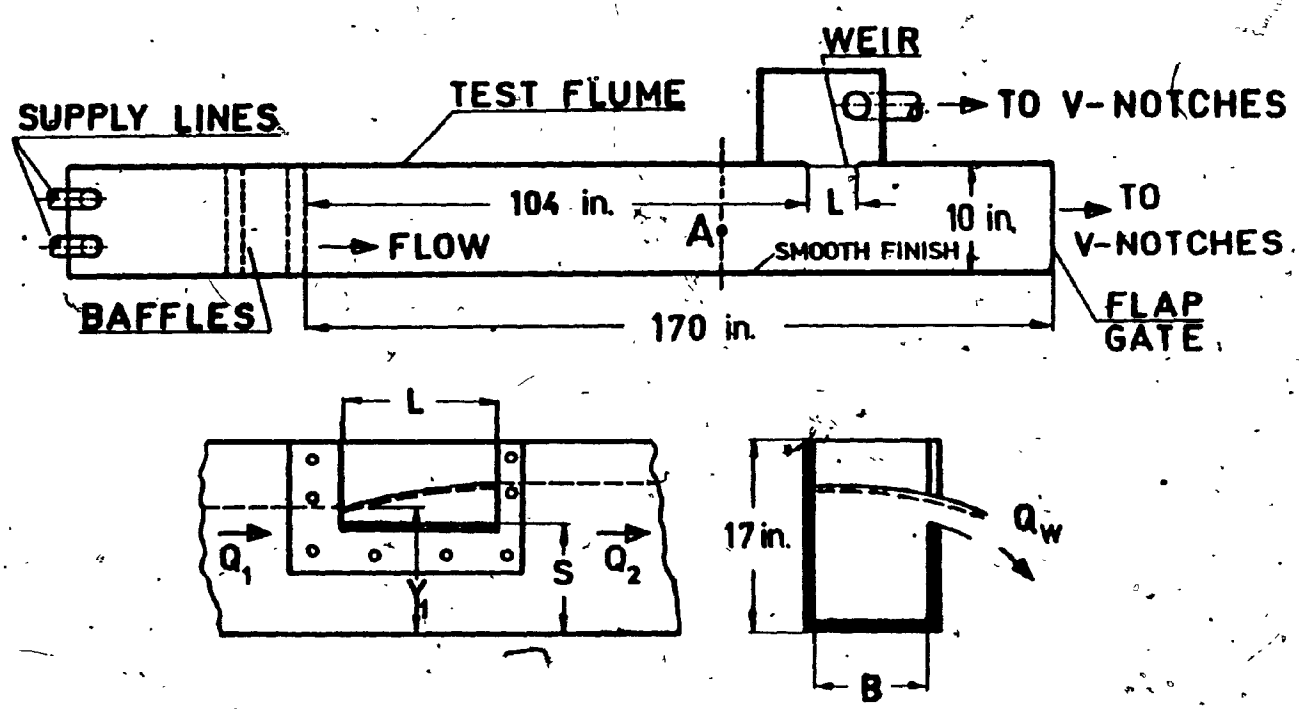

FIG. 9 EXPERIMENTAL SET-UP FOR LATERAL WEIR STUDY
(1" = 25.4 mm)

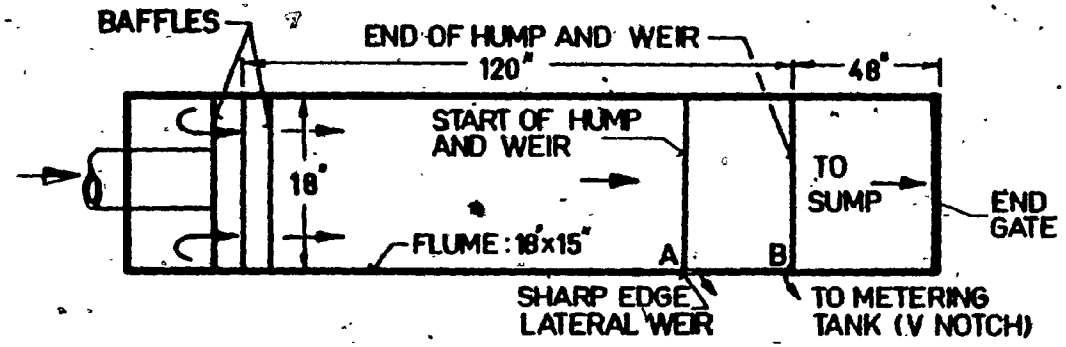

(a) PLAN VIEW, LATERAL WEIR FLUME

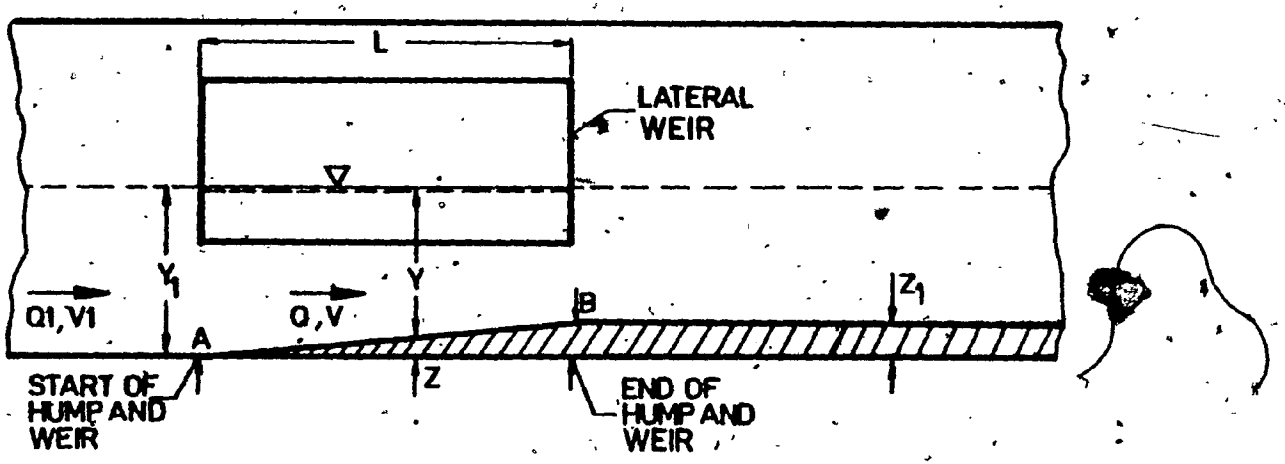

(b) DETAILS - HUMP LOCATION (SECTION)

FIG. 10 EXPERIMENTAL SET-UP WITH HUMP IN PLACE (1 inch = 25.4 mm)

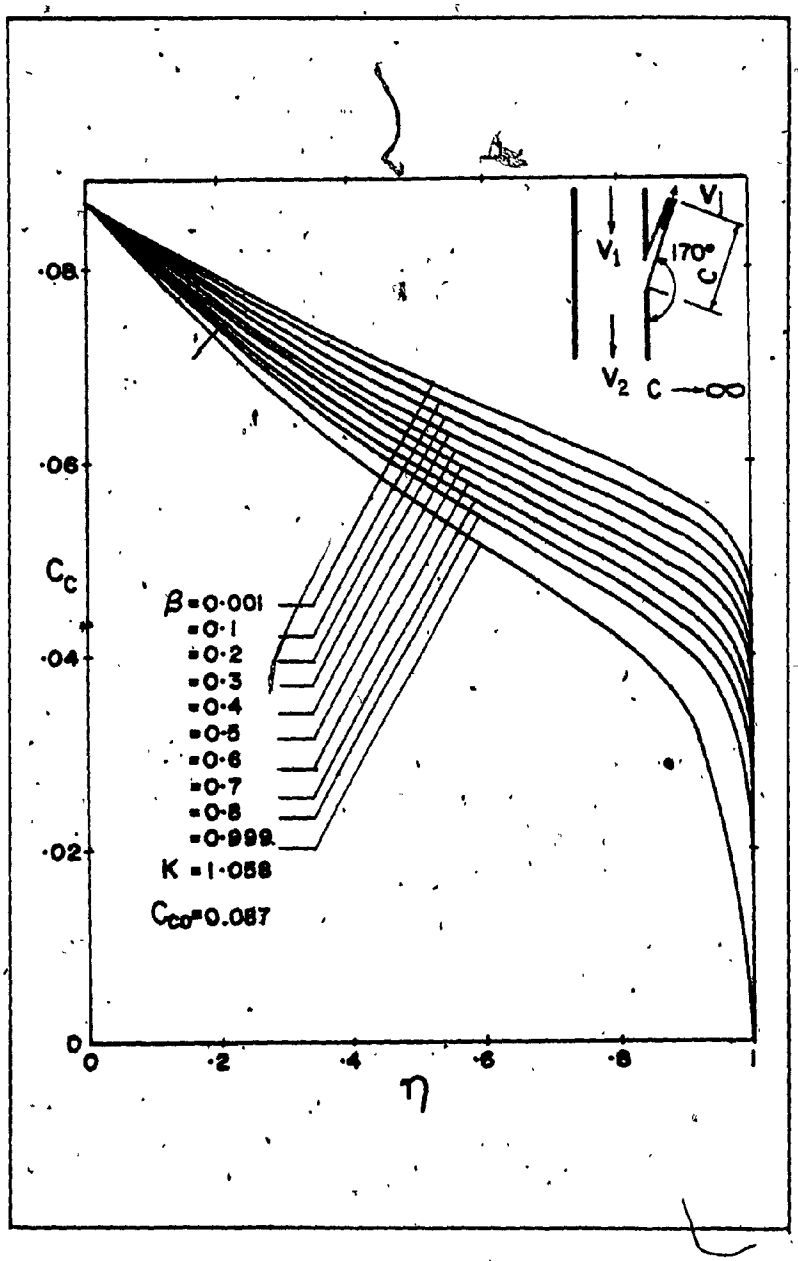

FIG. 11 THE CONTRACTION COEFFICIENT C_c AS A FUNCTION OF η AND β, $[(\pi/K) = 170^{\circ}, C \to \infty]$

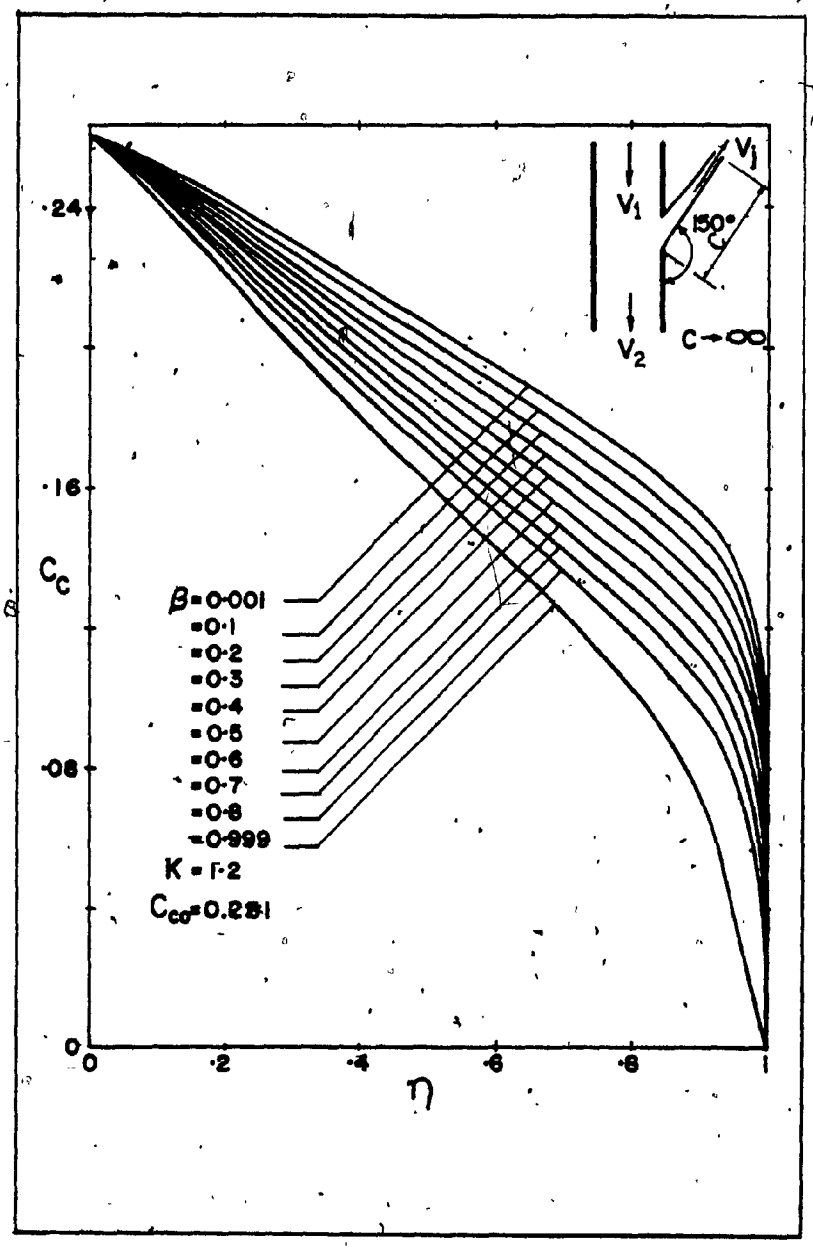

FIG. 12 THE CONTRACTION COEFFICIENT C_C AS A FUNCTION OF η AND β[$(\pi/K)_1 = 150^o$, $C \to \infty$]

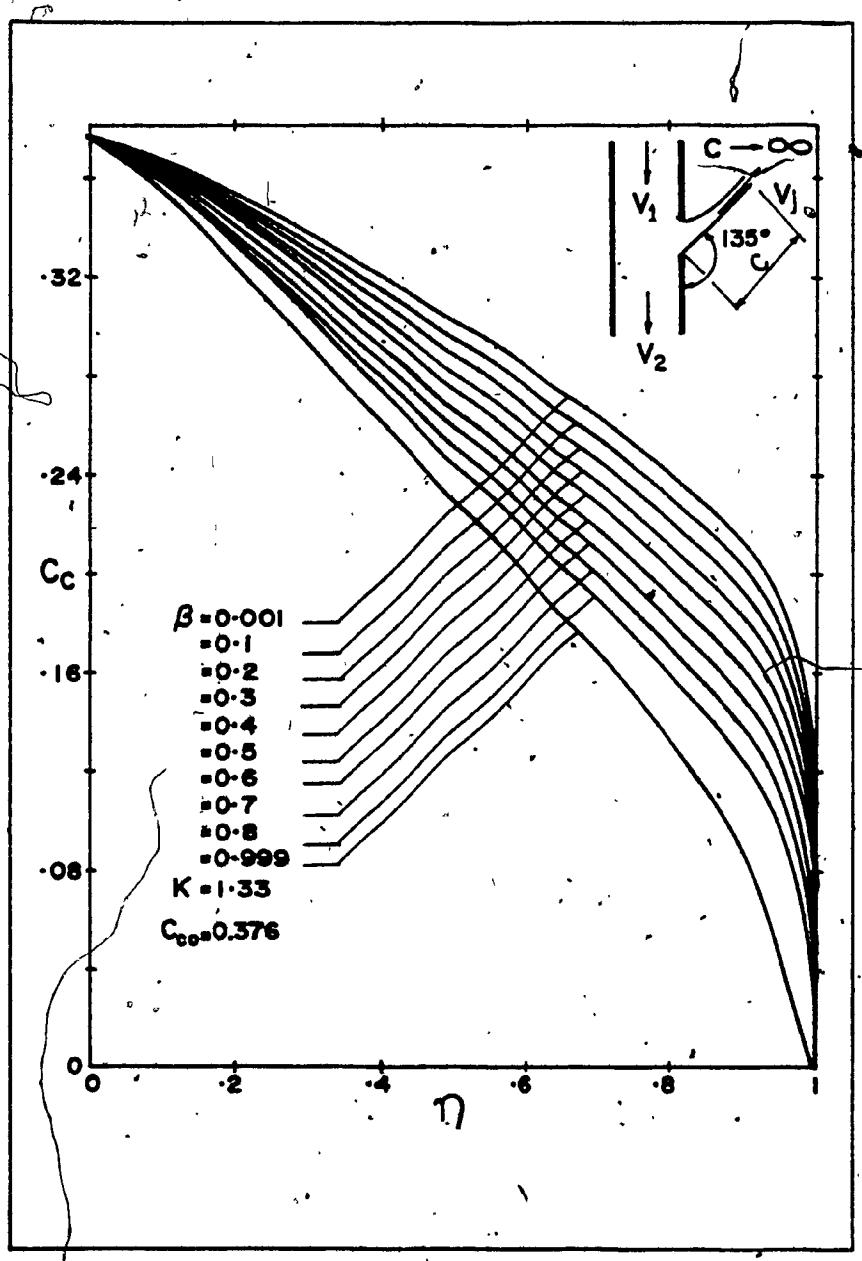

FIG. 13 THE CONTRACTION COEFFICIENT, C_c AS A FUNCTION OF η AND β, $[(\pi/K) = 135^{\circ}, C \to \infty]$

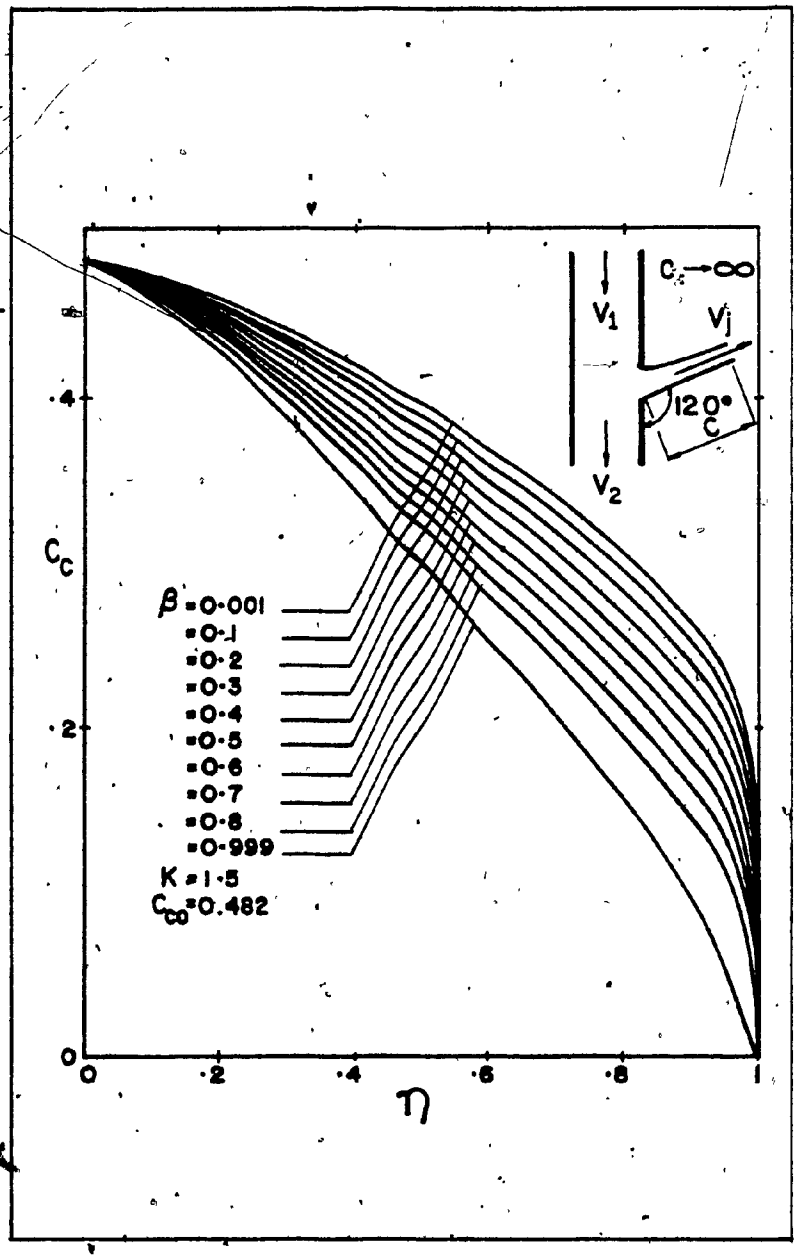

FIG. 14. THE CONTRACTION COEFFICIENT C_c AS A FUNCTION OF η AND β, [(π/K) = 120°, C → ∞]

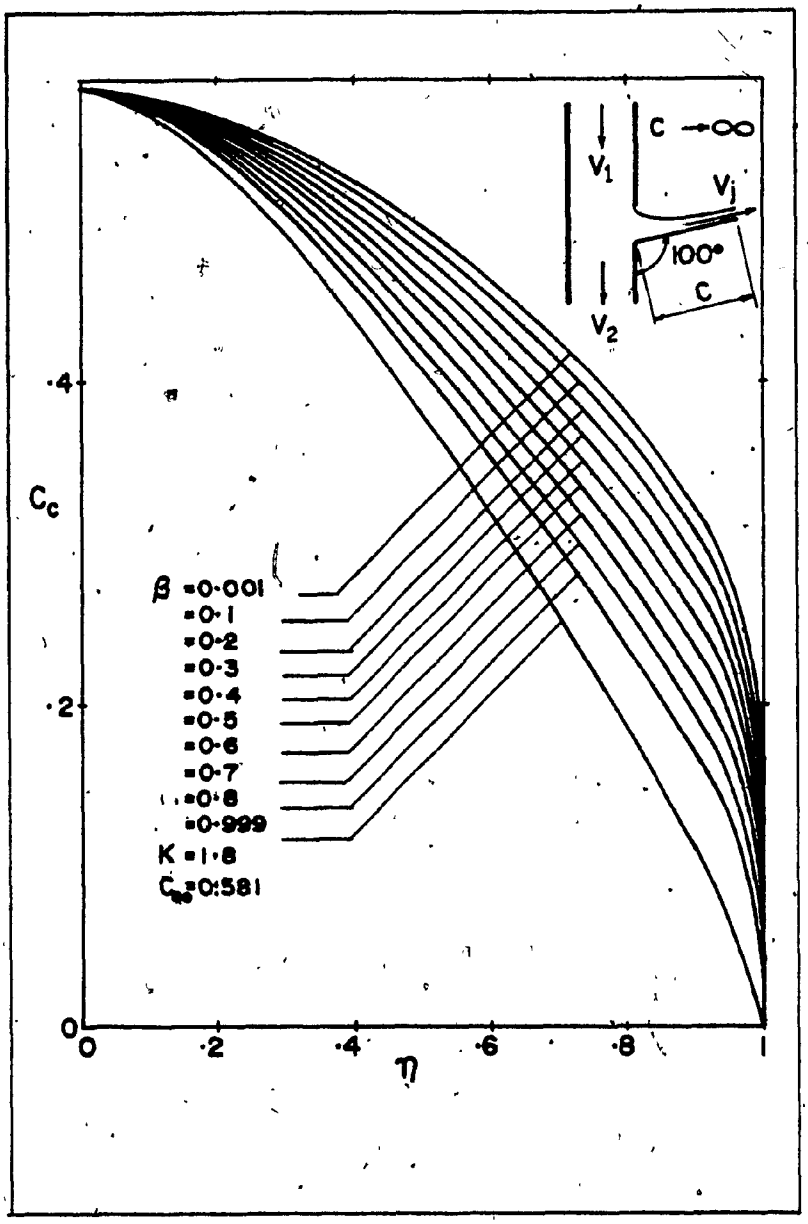

FIG. 15 THE CONTRACTION COEFFICIENT C_c AS A FUNCTION OF η AND β, $[(\pi/K) = 100^{\circ}, C \to \infty]$

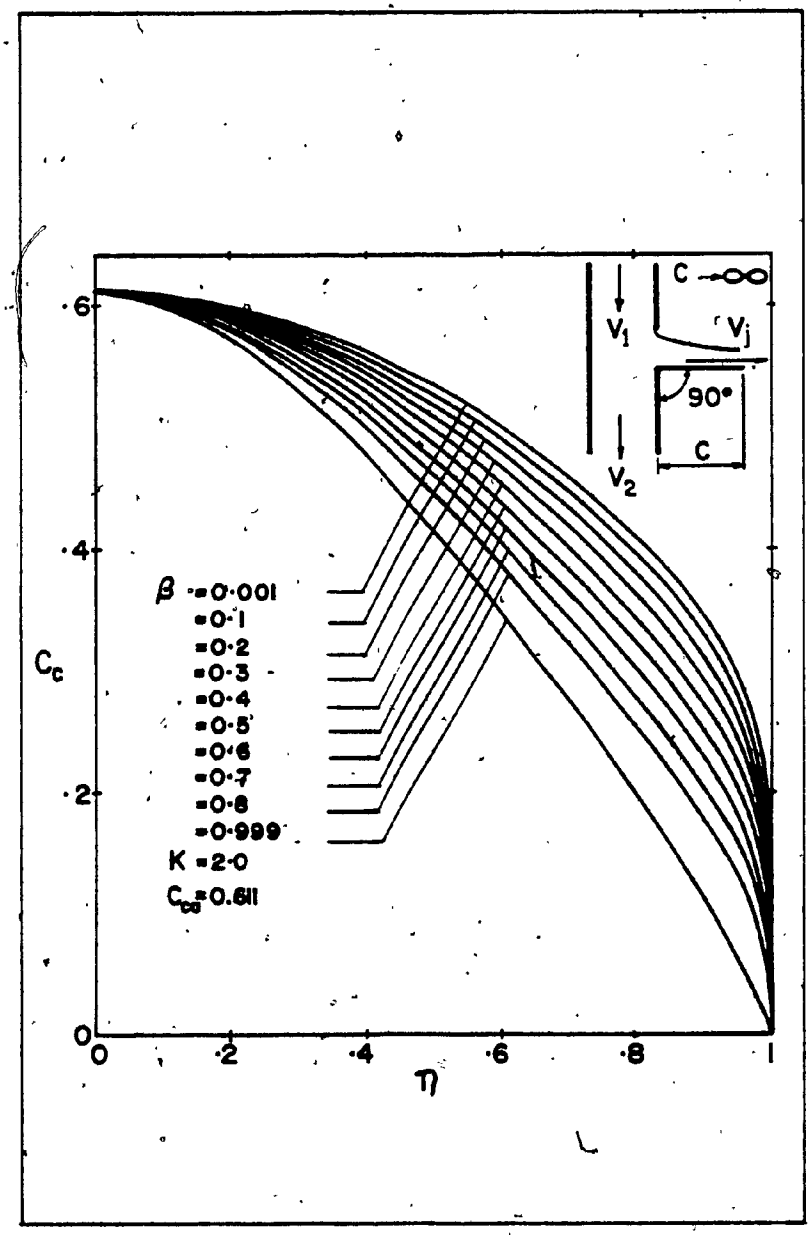

FIG. 16 THE CONTRACTION COEFFICIENT C_c AS A FUNCTION OF η AND β, $[(\pi/K) = 90^{\circ}, C \to \infty]$

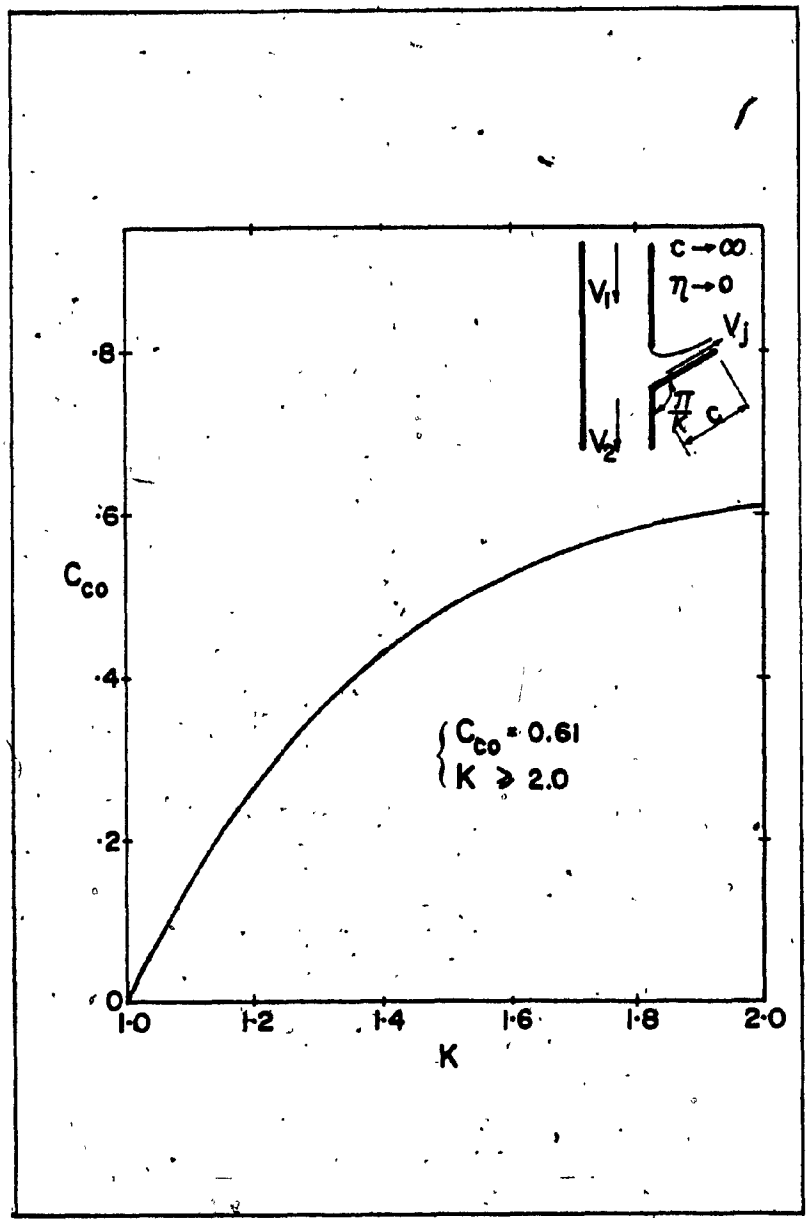

FIG. 17 THE CONTRACTION COEFFICIENT C_{co} AS A FUNCTION OF K, [$\eta \to 0$, $C \to \infty$]

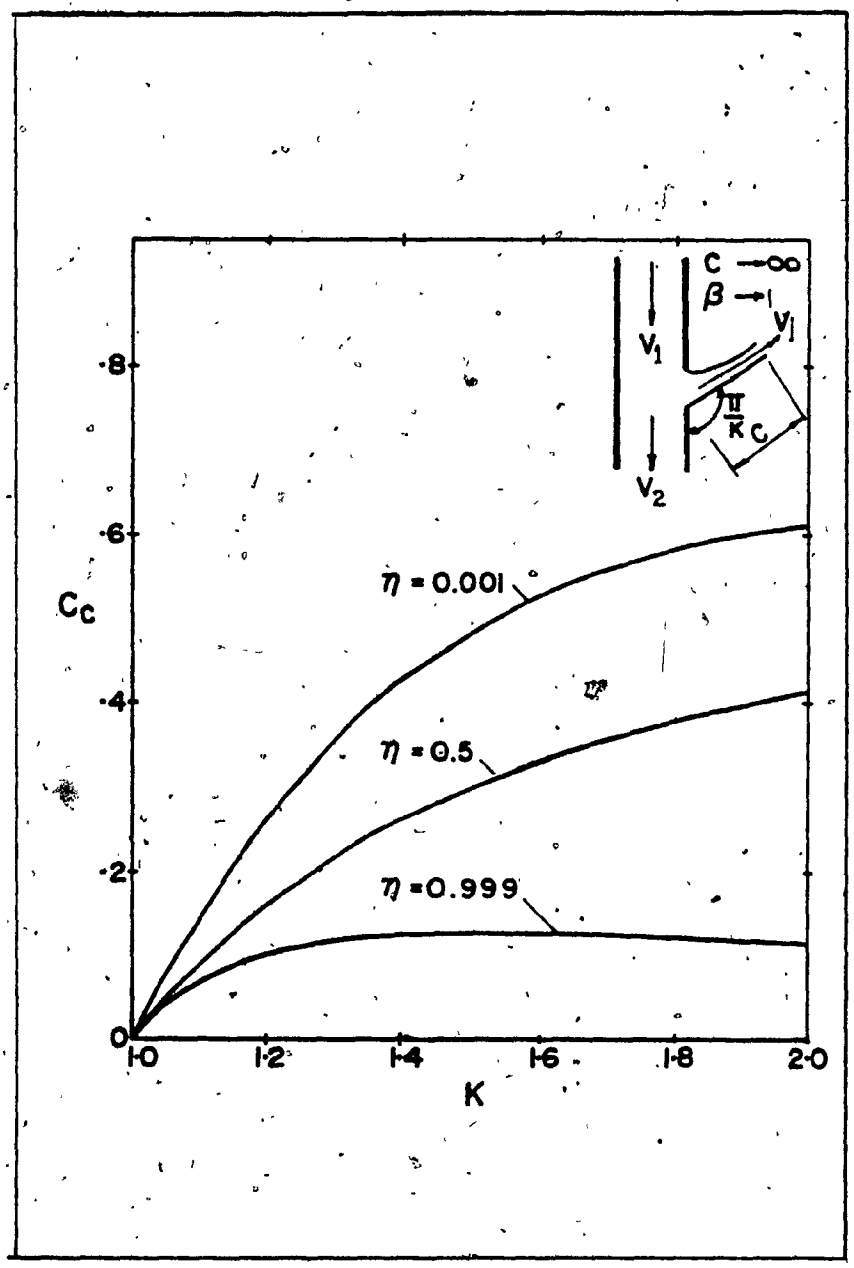

FIG. 18 THE CONTRACTION COEFFICIENT C_c AS A FUNCTION OF K, $[o \leq \eta < 1.0, C \to \infty]$

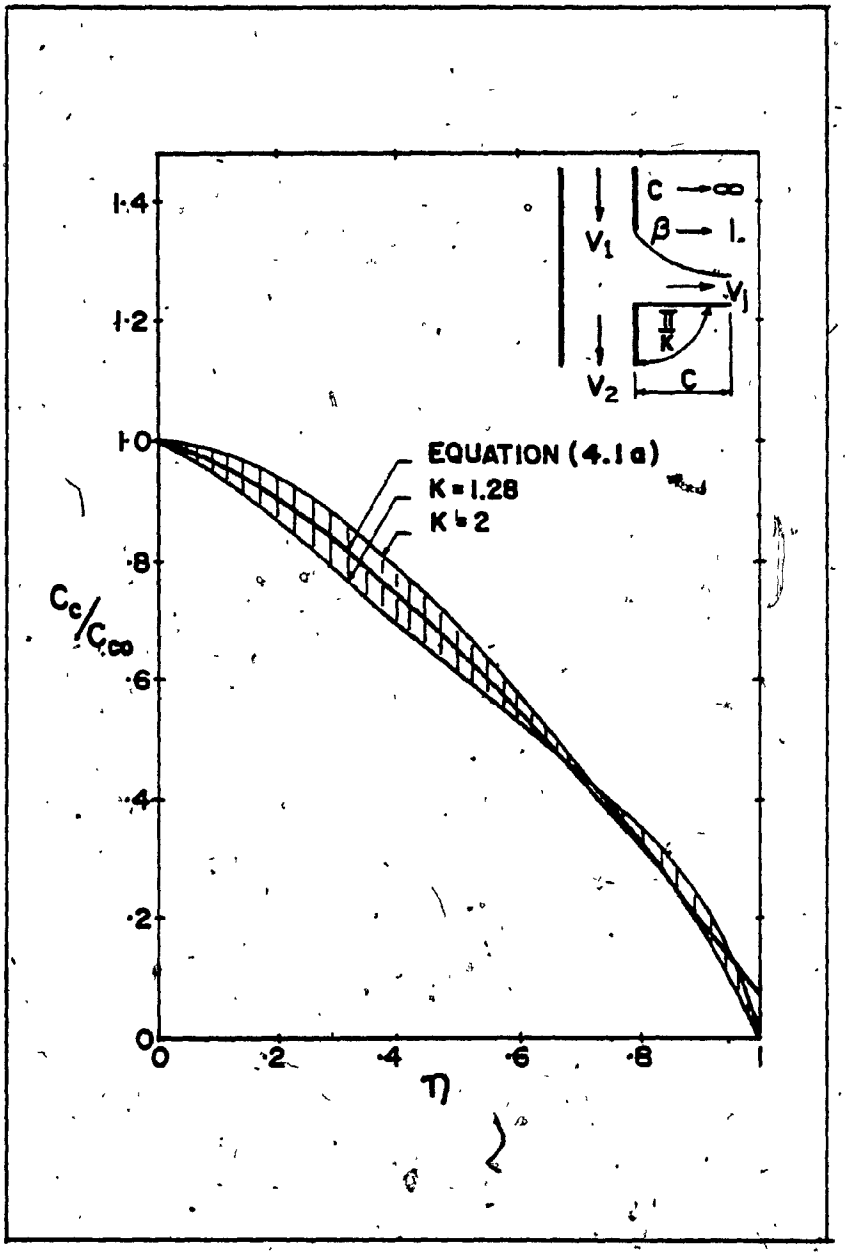

FIG. 19 THE VARIATION OF C_c/C_{c_∞} AS A FUNCTION OF η, $[1.28 \leq K < 2.0]$

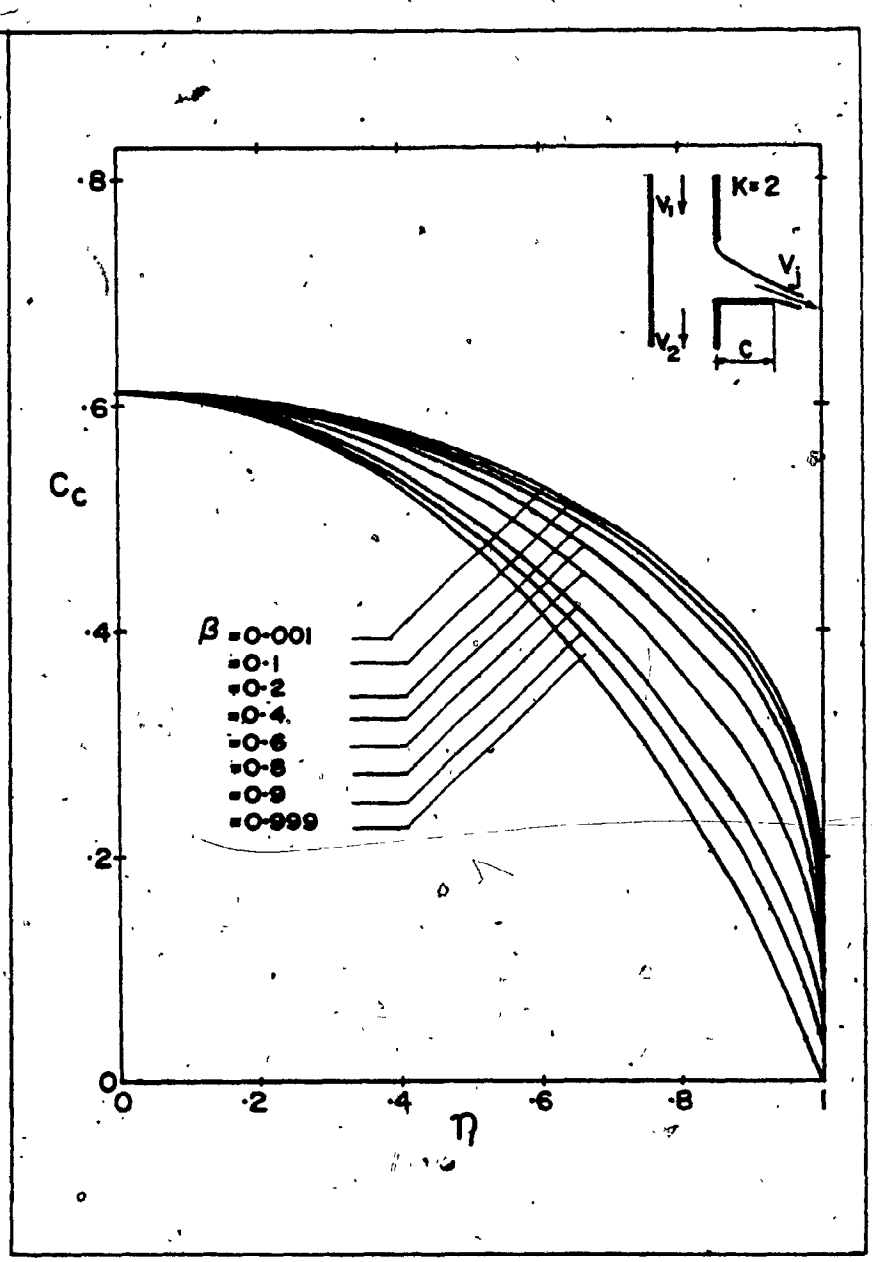

FIG. 20 THE CONTRACTION COEFFICIENT C_c AS A FUNCTION OF η [$K = 2, 0 \leq \beta < 1.0$]

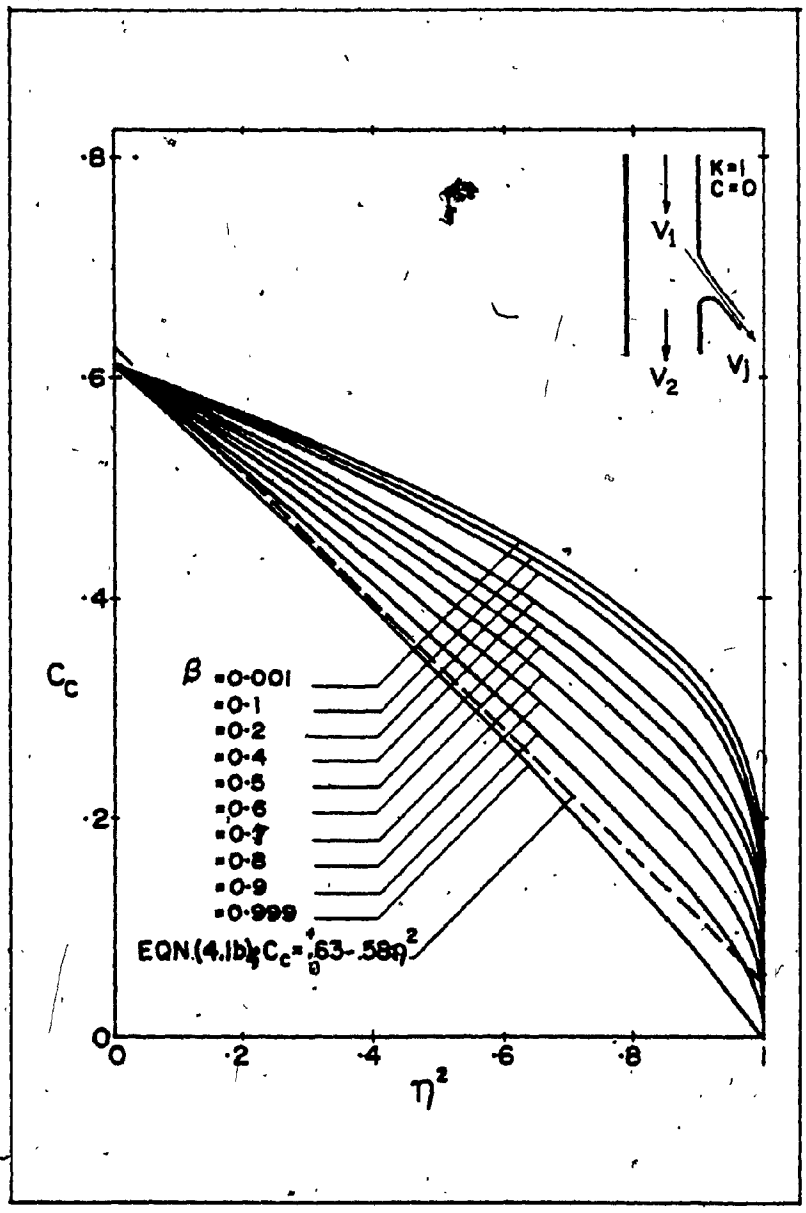

FIG. 21 THE CONTRACTION COEFFICIENT C_c AS A FUNCTION OF η^2 AND β, [K = 1, C = o]

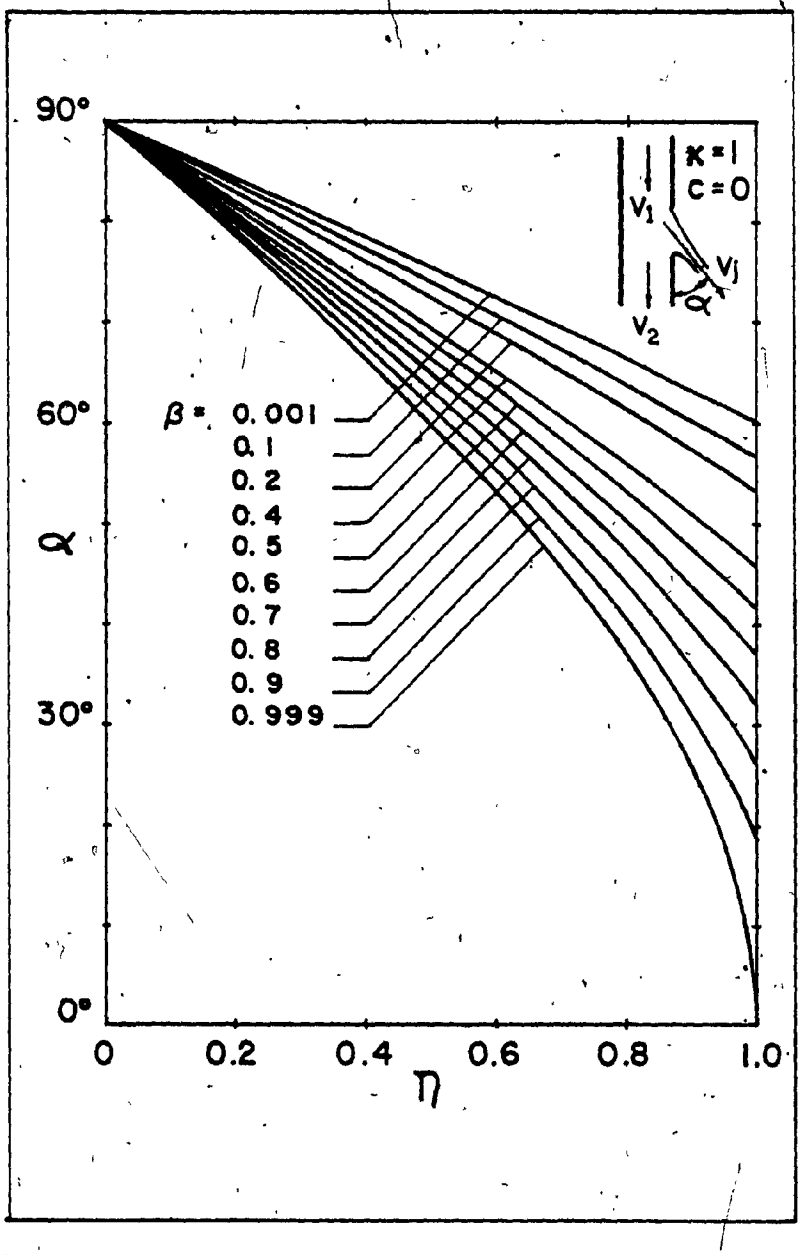

FIG. 22 THE ANGLE OF THE JET α AS A FUNCTION OF η AND β, [K = 1, C = o]

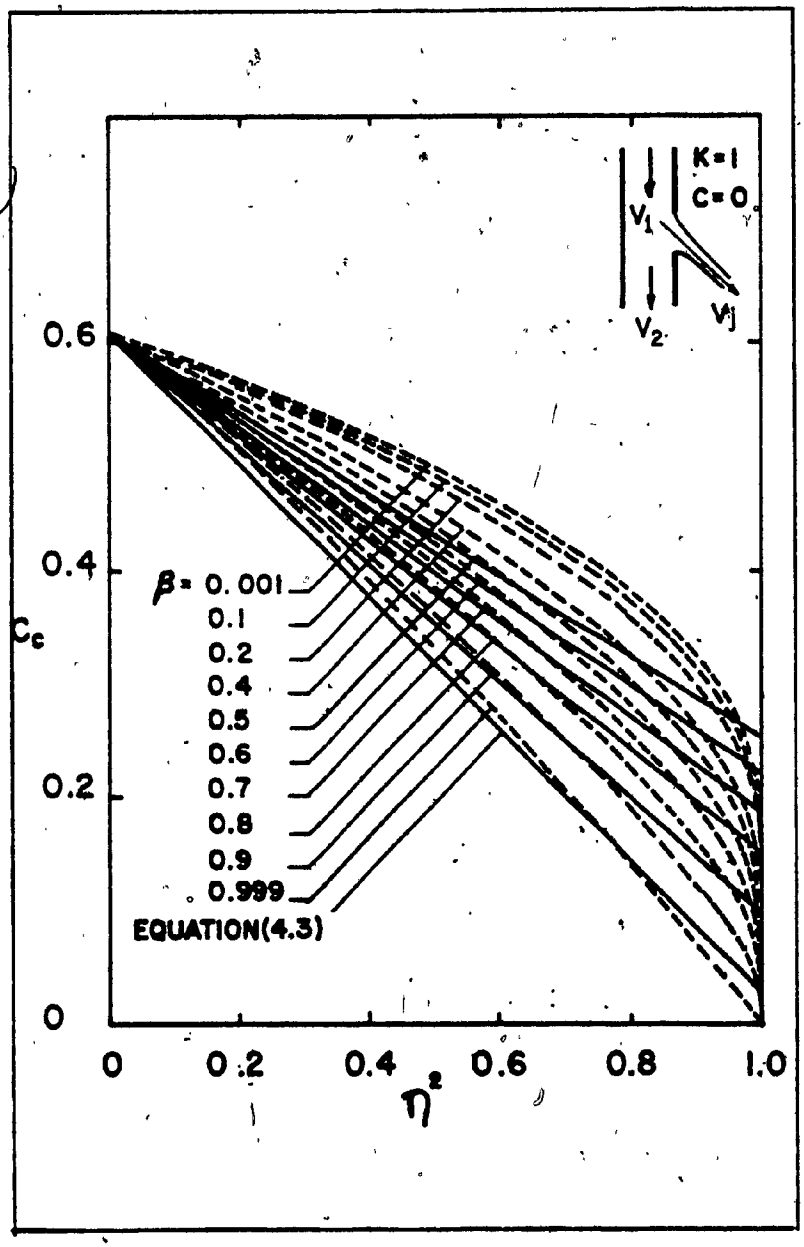

FIG. 23 THE CONTRACTION COEFFICIENT C_c AS A FUNCTION OF η^2, [K = 1, C = o, o $\leq \eta \leq$ .836, β > 0.5]

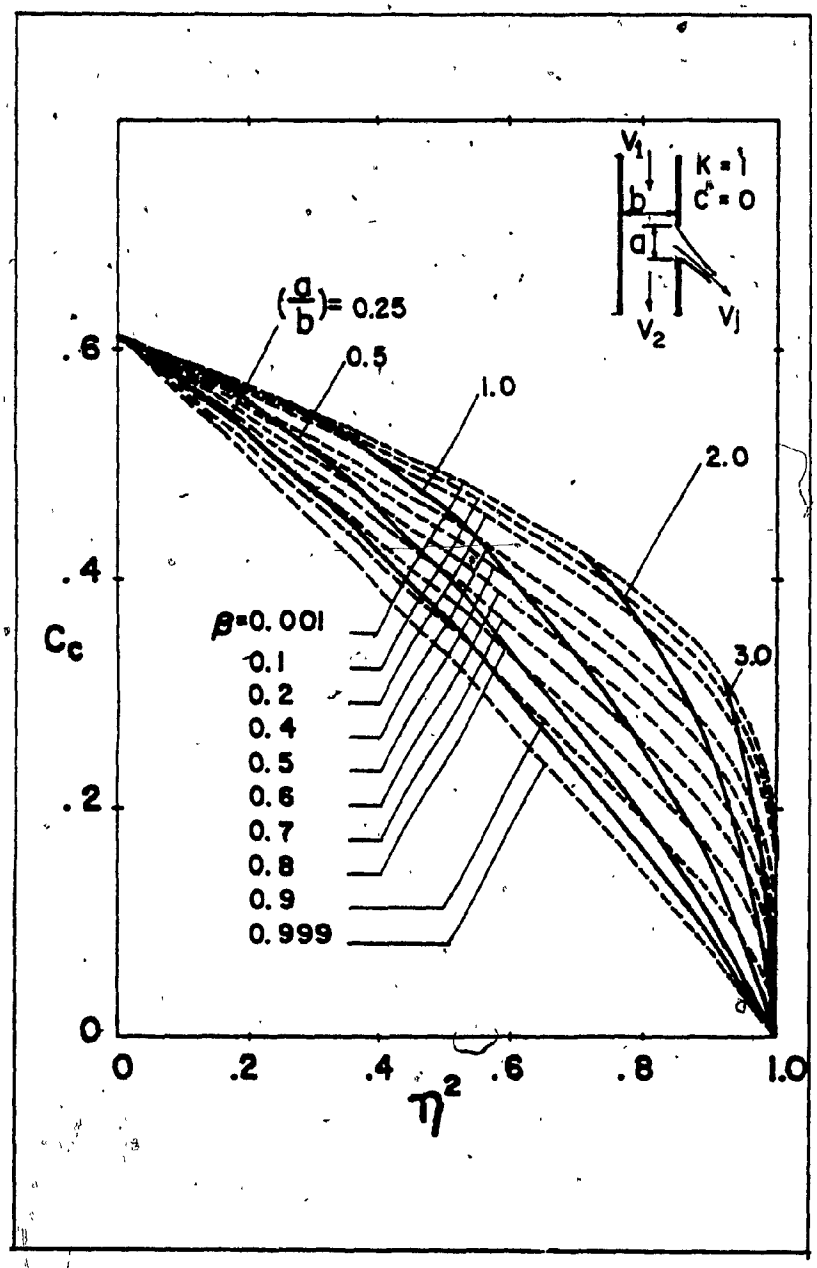

FIG. 24 THE CONTRACTION COEFFICIENT C_c AS A FUNCTION OF η^2 [K = 1, $C^* = o$, (a/b) = constant]

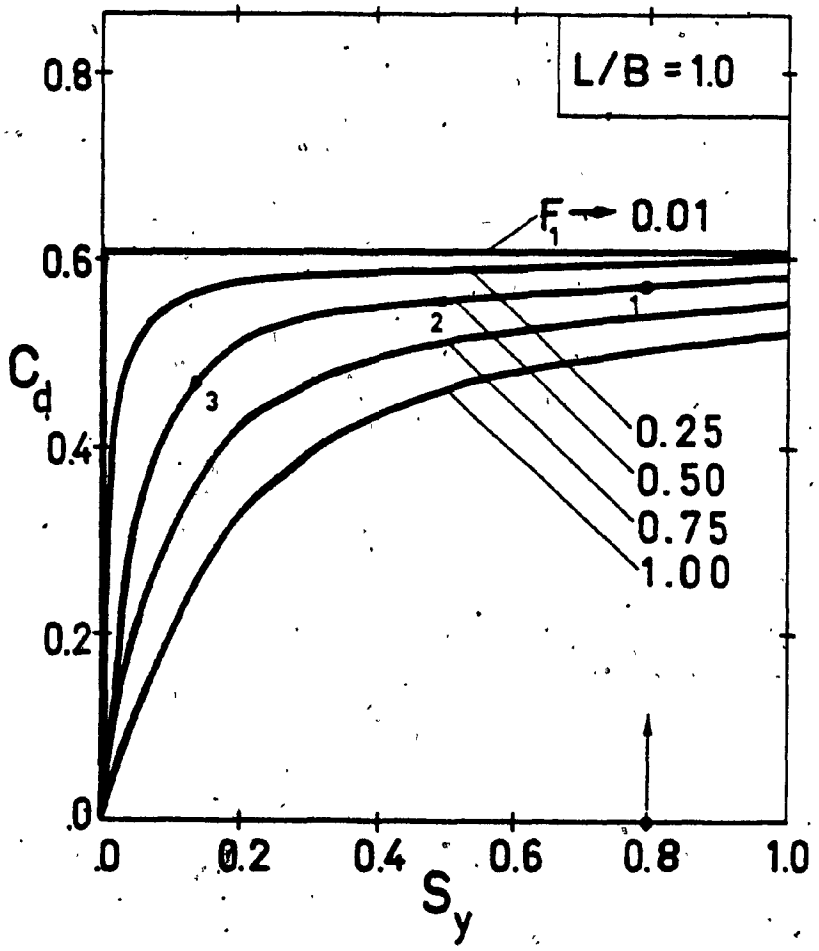

FIG. 25 VARIATION OF THE LOCAL DISCHARGE COEFFICIENT C_d WITH THE LAYER DEPTH RATIO S_y FOR L/B = 0.5

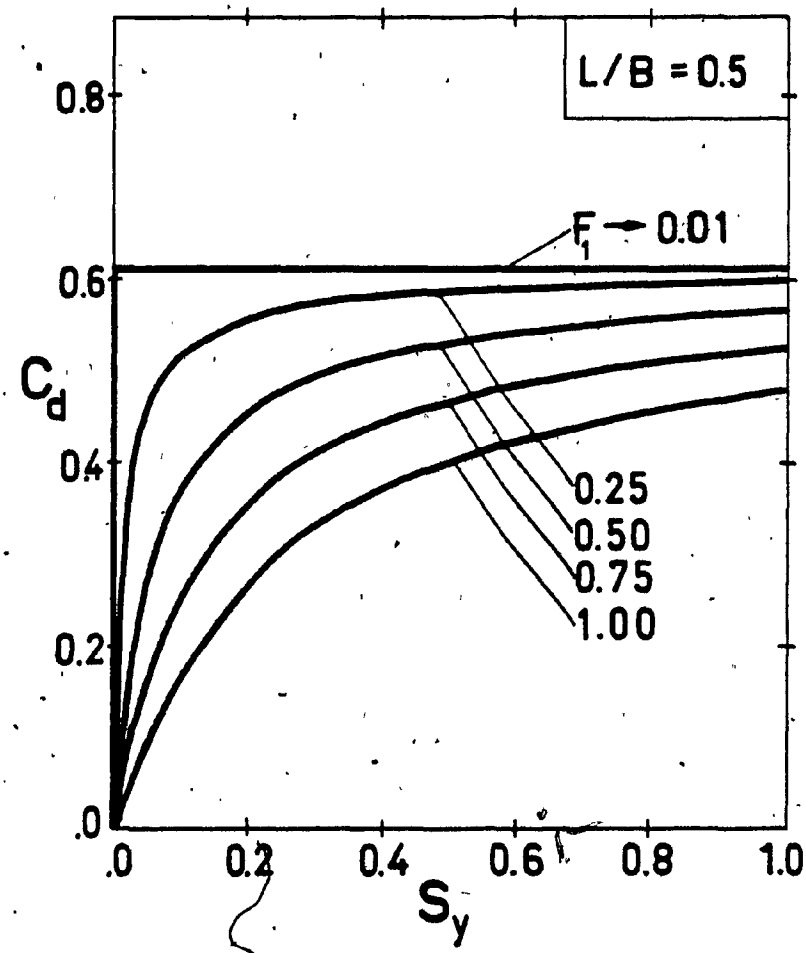

FIG. 26 VARIATION OF THE LOCAL DISCHARGE COEFFICIENT C_d WITH THE LAYER DEPTH RATIO S_y FOR L/B = 0.5

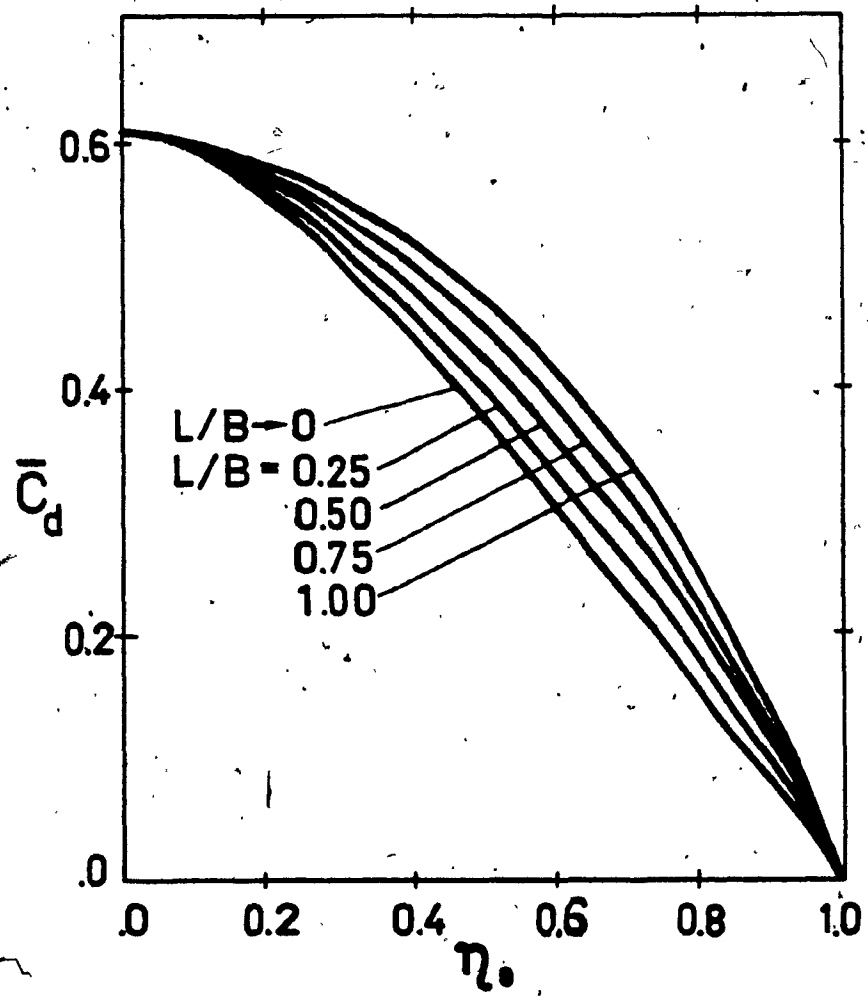

FIG. 27 VARIATION OF THE MEAN DISCHARGE COEFFICIENT $\bar{C}_d$ WITH THE WEIR VELOCITY RATIO η_o FOR THE L/B RANGE $0.001 \leq (L/B) \leq 1.0$

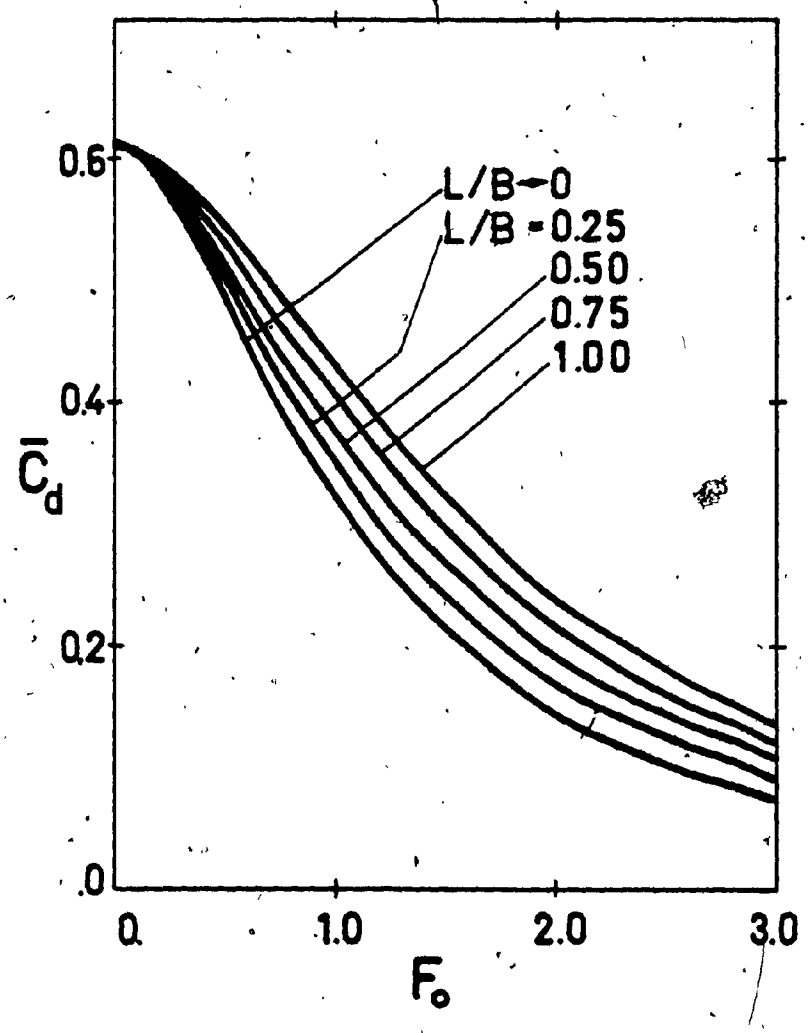

FIG. 28 VARIATION OF THE MEAN DISCHARGE COEFFICIENT $\bar{C}_d$ WITH THE WEIR PARAMETER F_o FOR $.001 \leq L/B \leq 1$

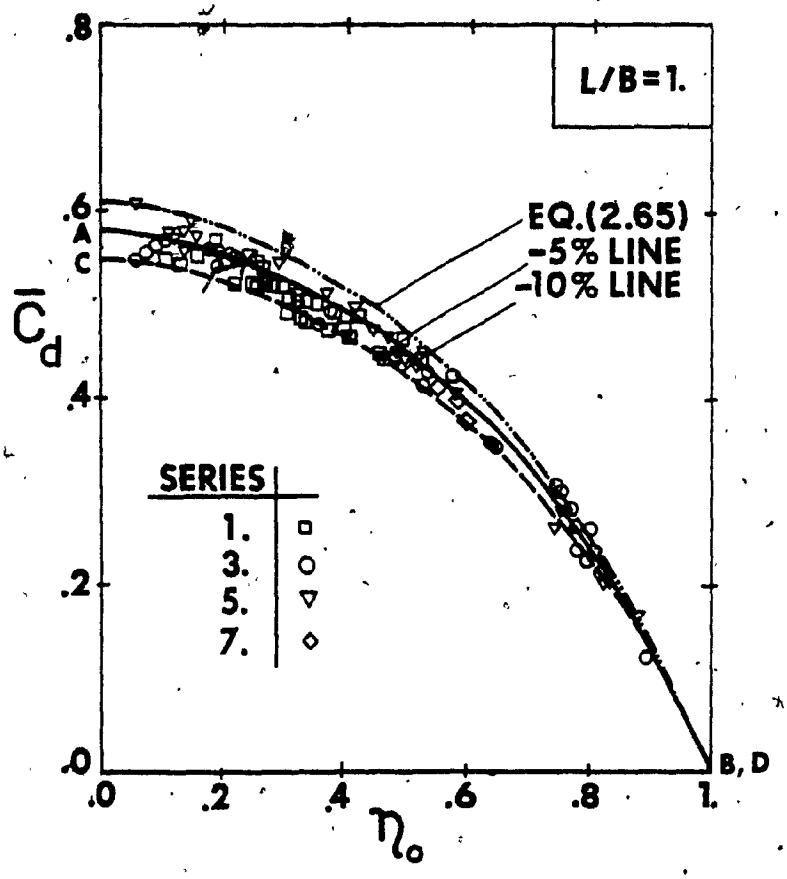

FIG. 29 VARIATION OF THE MEAN DISCHARGE COEFFICIENT $\bar{C}_d$ WITH THE WEIR VELOCITY RATIO η_o FOR L/B = 1.0

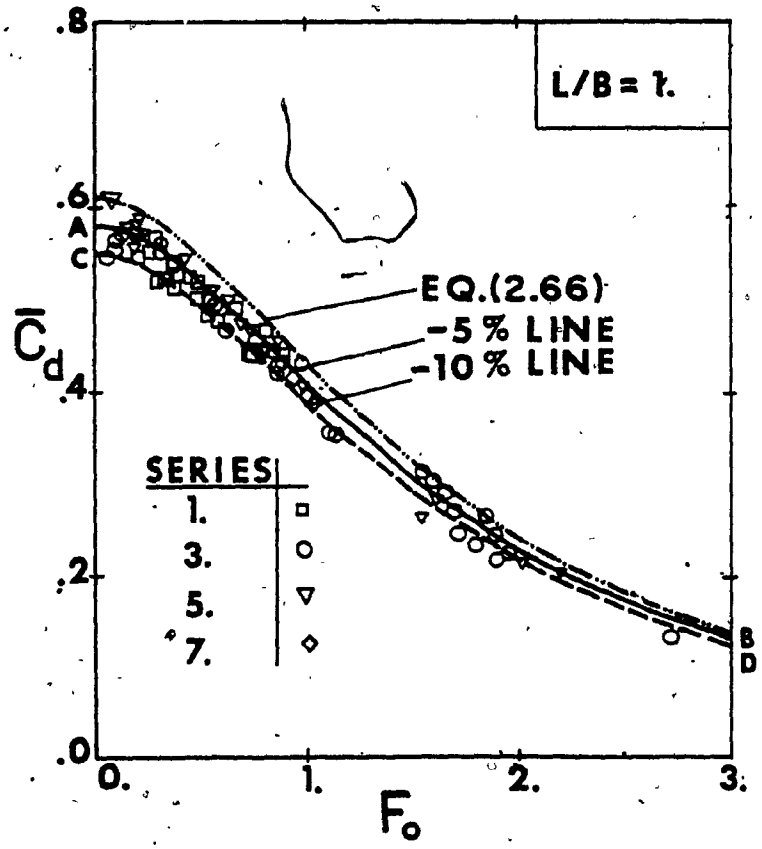

FIG. 30 VARIATION OF THE MEAN DISCHARGE COEFFICIENT $\bar{C}_d$ WITH THE WEIR PARAMETER F_o FOR L/B = 1.0

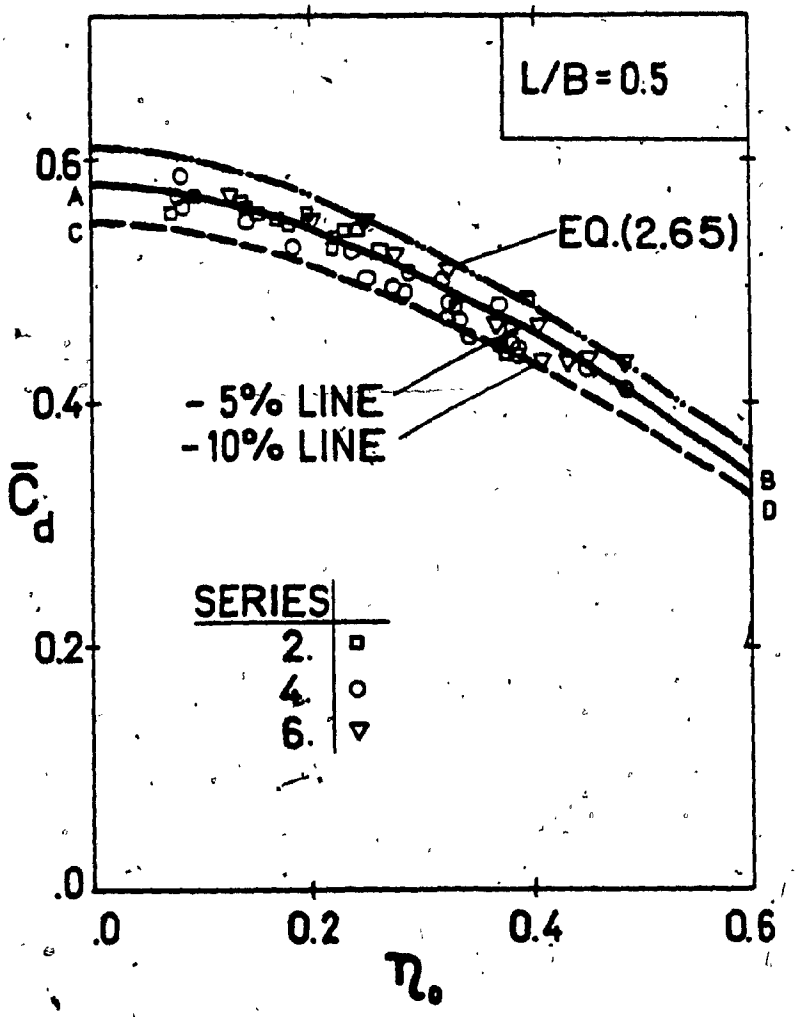

FIG. 31 VARIATION OF THE MEAN DISCHARGE COEFFICIENT $\bar{C}_d$ WITH THE WEIR VELOCITY RATIO η_o FOR L/B = 0.5

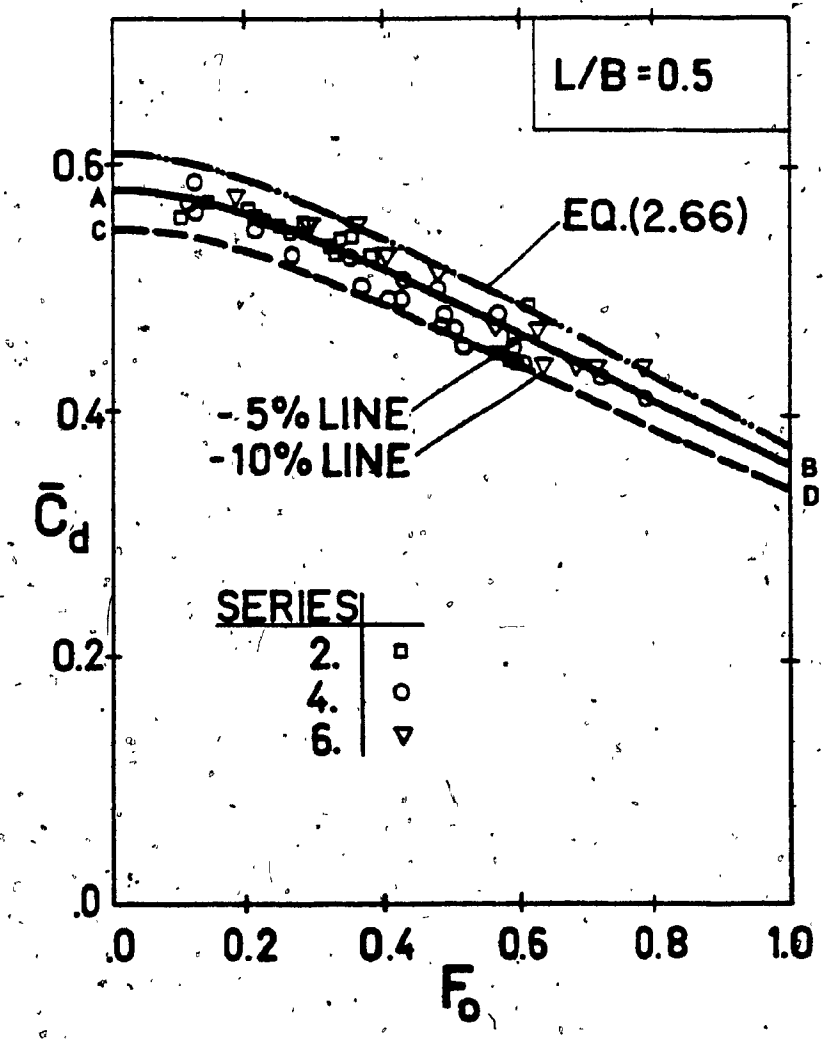

FIG. 32 VARIATION OF THE MEAN DISCHARGE COEFFICIENT $\bar{C}_d$ WITH THE WEIR-PARAMETER F_o FOR L/B = 0.5

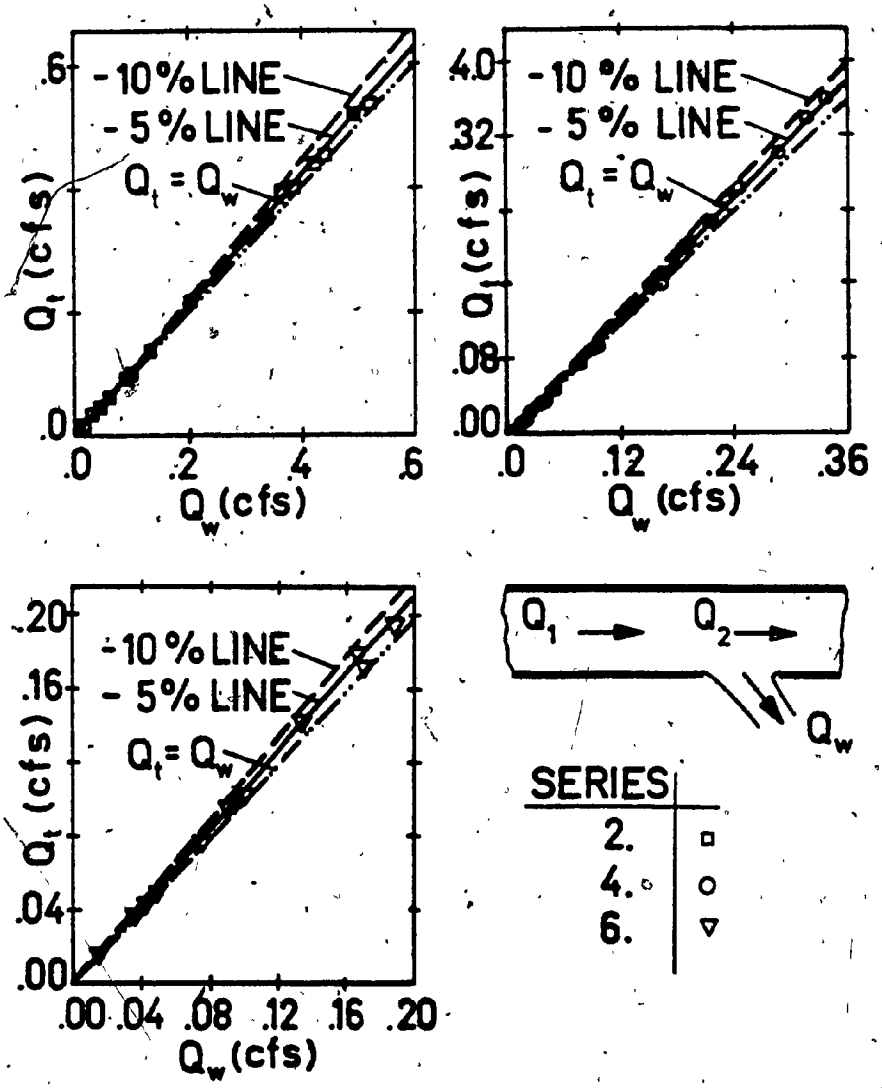

FIG. 33 CORRELATION OF THEORETICAL WEIR DISCHARGE Q_t AND ACTUAL WEIR DISCHARGE Q_w FOR SERIES 2,4 AND 6 (1 cfs = 0.028m^3/sec)

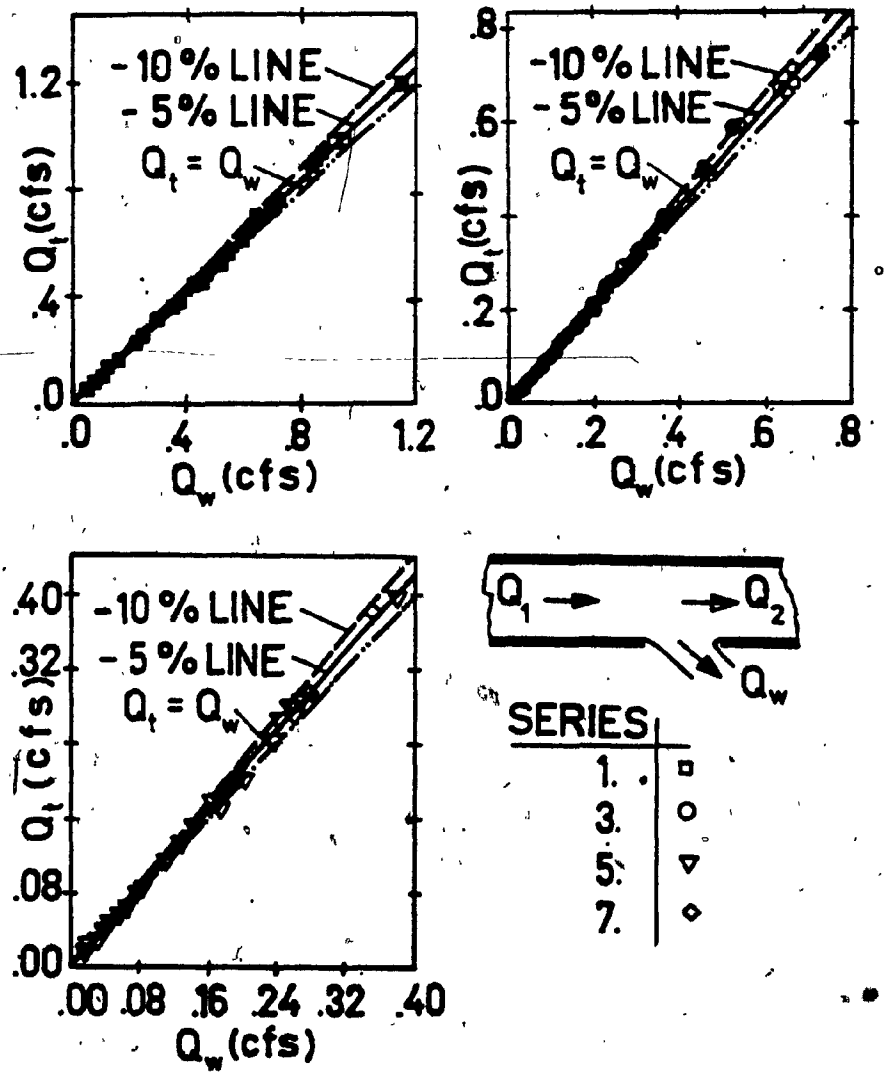

FIG. 34 CORRELATION OF THEORETICAL WEIR DISCHARGE Q_t AND ACTUAL WEIR DISCHARGE Q_w FOR SERIES 1,3,5 AND 7 (1 c/s ≙ 0.028 m^3/sec)

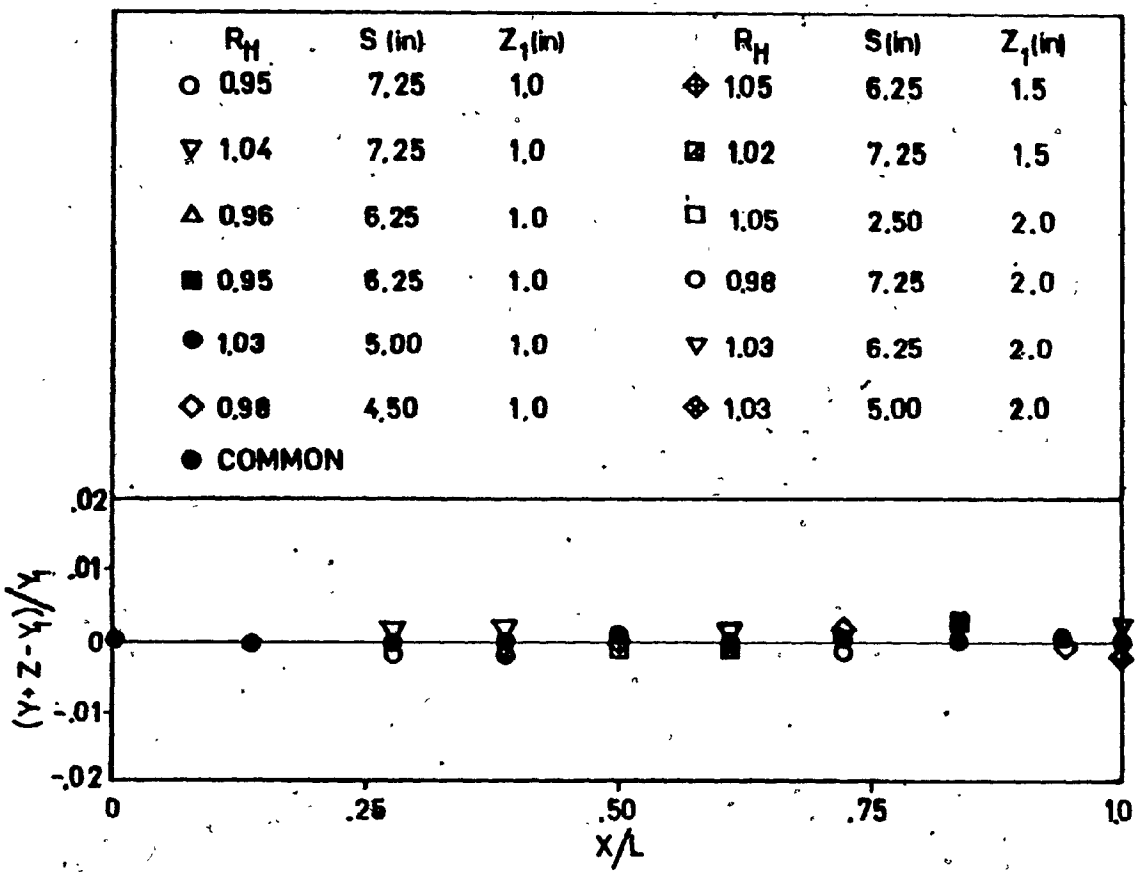

FIG. 35 VARIATION OF THE RATIO $(y + z - y_1)/y_1$ ALONG WEIR SPAN FOR BED CONTOURING

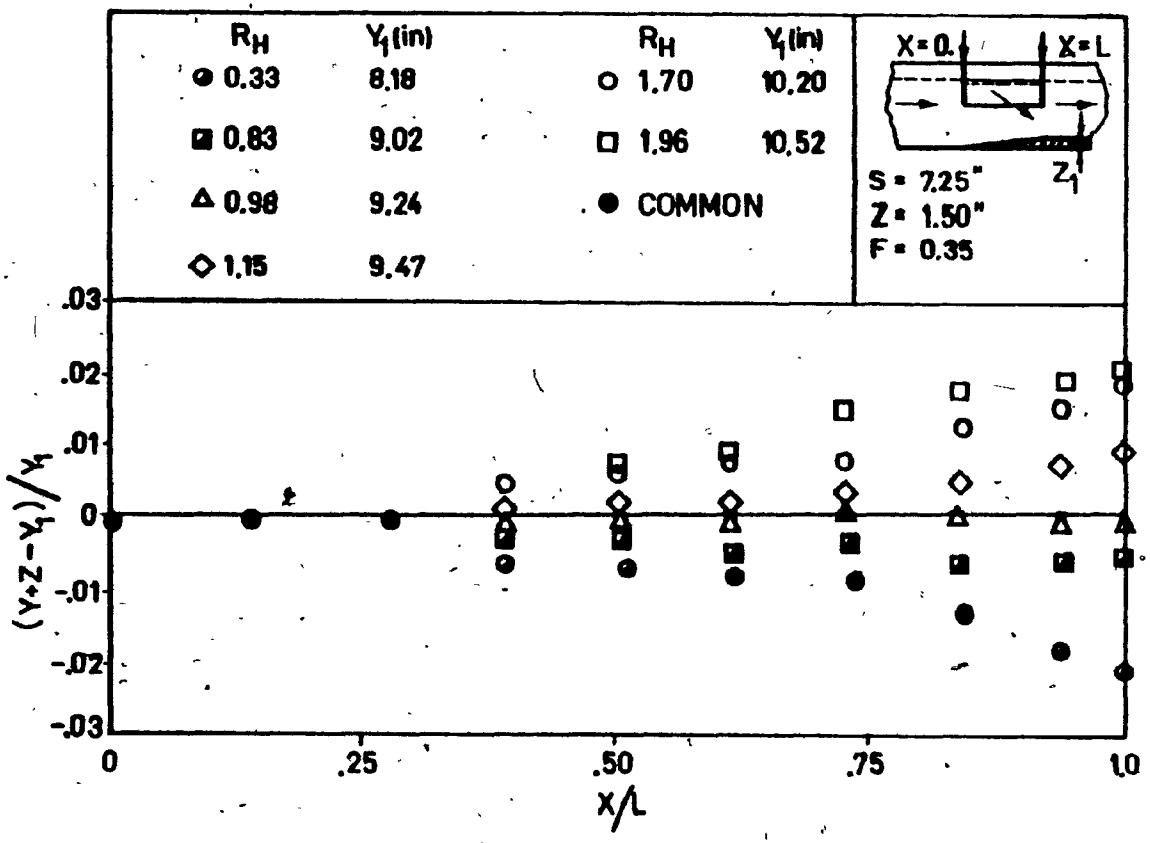

FIG. 36 VARIATION OF THE RATIO $(y + z - y_1)/y_1$ ALONG WEIR SPAN FOR BED CONTOURING IN A TYPICAL CASE (1 inch = 25.4 mm)

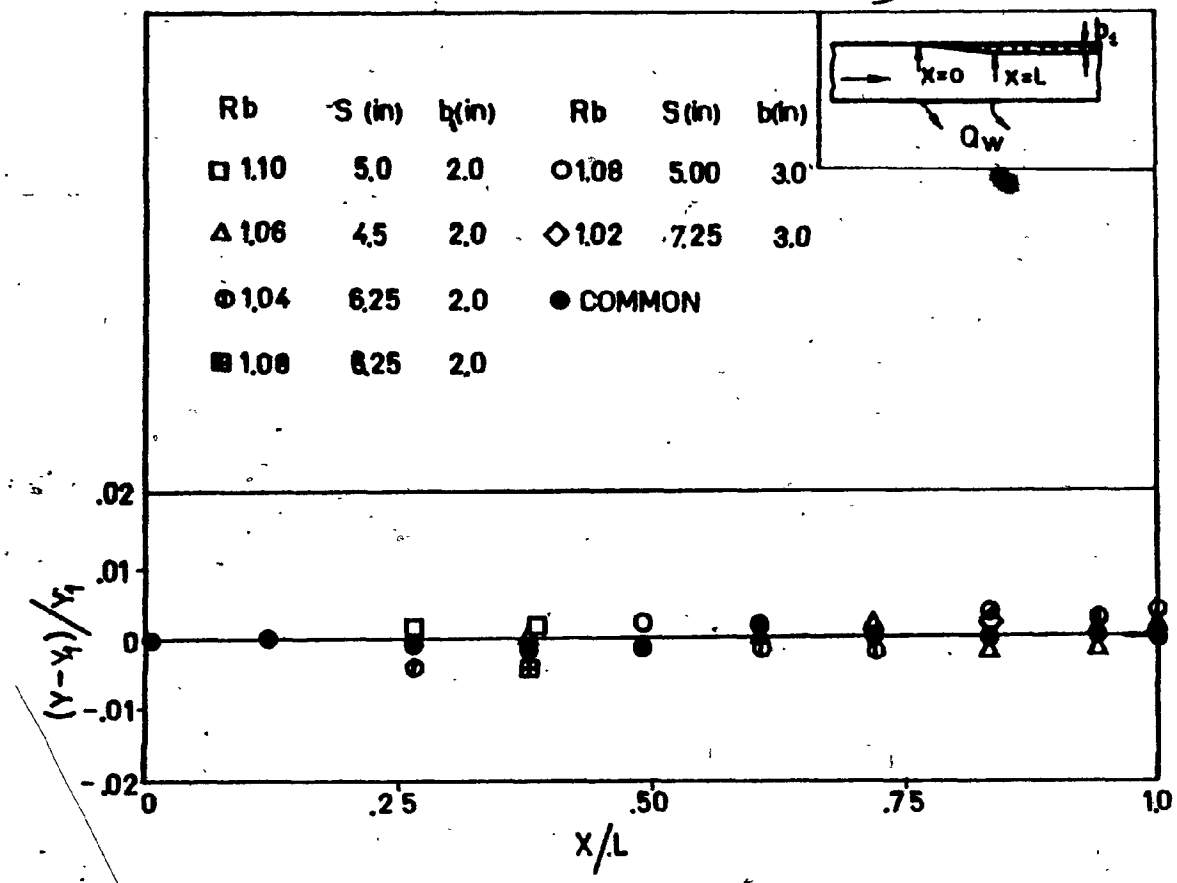

FIG. 37 VARIATION OF THE RATIO $(y - y_1)/y_1$ ALONG WEIR SPAN FOR SIDE CONTOURING (1 inch = 25.4 mm)

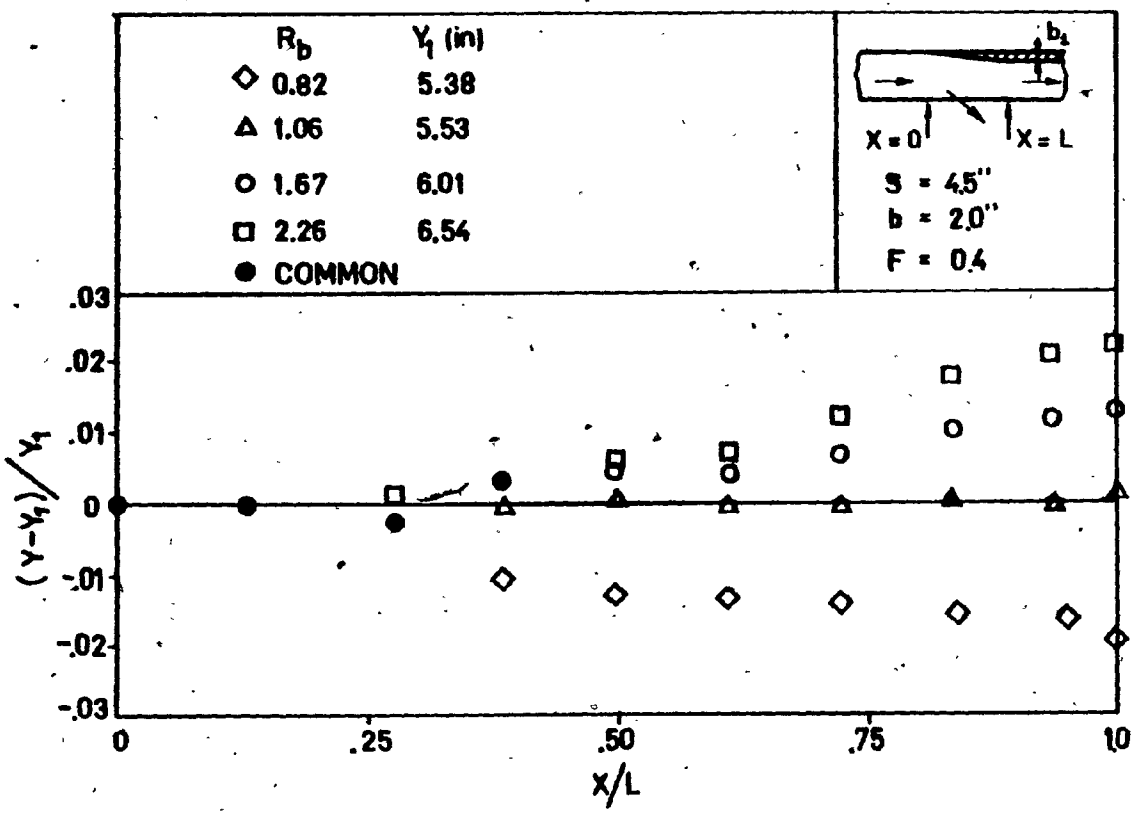

FIG. 38 VARIATION OF THE RATIO $(y - y_1)/y_1$ ALONG WEIR SPAN FOR SIDE CONTOURING IN A TYPICAL CASE (1 inch = 25.4 mm)

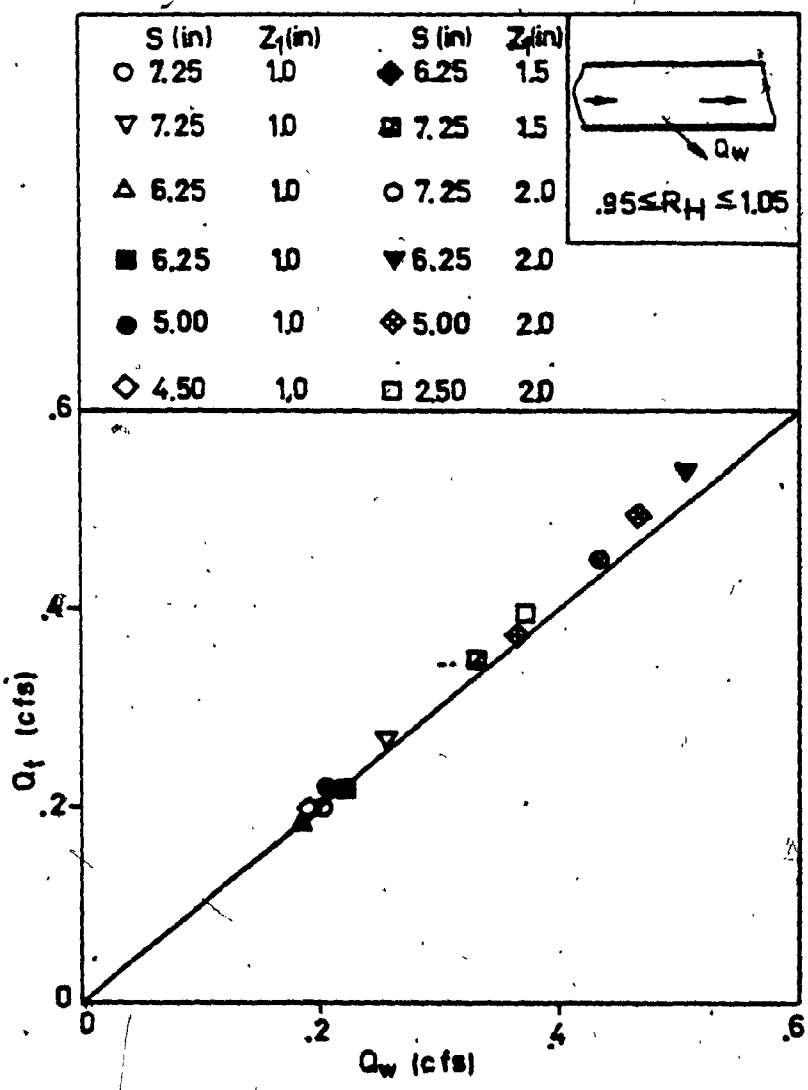

FIG. 39 CORRELATION OF THEORETICAL WEIR DISCHARGE Q_t AND ACTUAL WEIR DISCHARGE Q_w FOR BED CONTOURING (1 cfs = 0.028 m^3/sec, 1 inch = 25.4 mm)

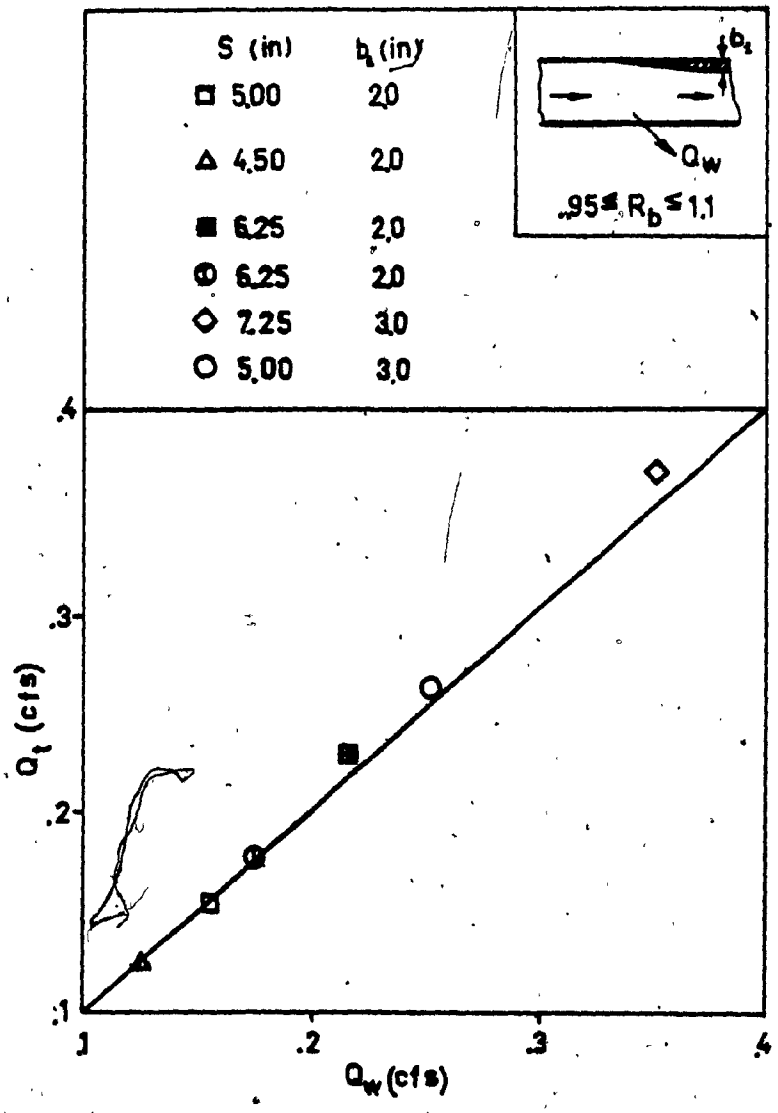

FIG. 40 CORRELATION OF THEORETICAL WEIR DISCHARGE Q_t AND ACTUAL WEIR DISCHARGE Q_w FOR SIDE CONTOURING (1 cfs = 0.028 m /sec, 1 inch = 25.4 mm)

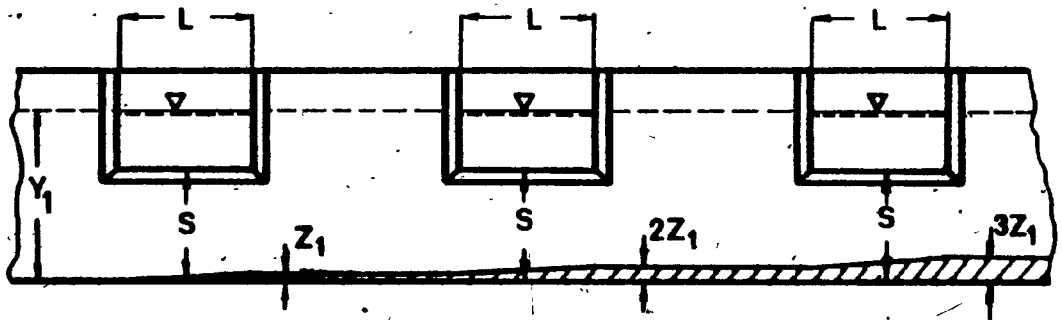

(a) LONGITUDINAL SECTION

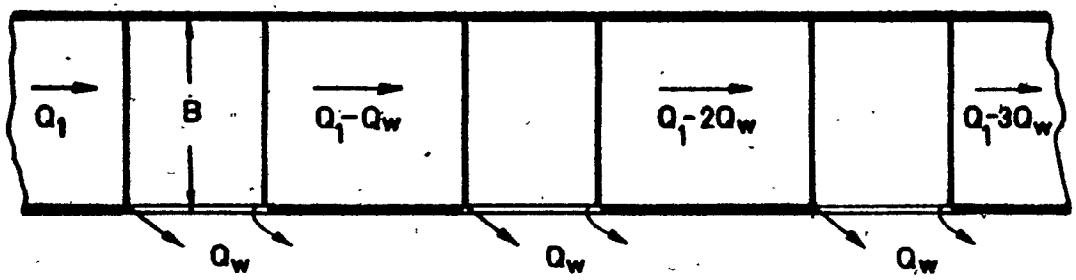

(b) PLAN VIEW

FIG. 41 TYPICAL WEIR ASSEMBLY FOR BED CONTOURING (HUMP)

TABLES

TABLE 1 PHYSICAL MODELS AND SOLUTION TYPES

Model No.	K	$\frac{\pi}{K}$	C	α	Fig. No.	Solution Type	Remarks
1	1.058	170°	∞	170°	11	Numerical	Present Study
2	1.2	150°	∞	150°	12	Numerical	Present Study
3	1.33	135°	∞	130°	13	Numerical	Present Study
4	1.5	120°	∞	120°	14	Numerical	Present Study
5	1.8	100°	∞	100°	15	Numerical	Present Study
6	2.0	90°	Variable		20	Closed Form Solution	Present Study McNown[17]
7	2.0	90°	∞	90°	16	Closed Form Solution	Present Study McNown[17]
8	1.0	180°	0	Variable	21	Closed Form Solution	Present Study Mitchell[18] McNown[17] Gurevich[14]

(continued)

Model No.	K	$\frac{\pi}{K}$	C	α	Fig. No.	Solution Type	Remarks
9	∞	0	Physical Model Same as Case 8				
10	$2 < K < \infty$		If $\alpha > (\pi/K)$, the solution is exact - Same as Case 8. If $\alpha < (\pi/K)$, the solution is numerical - (Present Method)				

TABLE 2 LATERAL WEIR FLOW ANALYSIS (TYPICAL STUDIES)

Reference (1)	Assumptions (2)	Velocity Effect of the Main Channel (3)	Nature of Flow (4)	Type of Solution (5)	Remarks (6)
Engels,H. [9]	Experimental Study	Not Included	Supercritical	Empirical	Low range of velocities in the main channel
Babbit,H.E.[4]	Experimental Study	Not Included	Supercritical	Empirical	Test data is related to weirs set in pipes
Coleman and Smith,D. [5]	Experimental Study	Not Included	Supercritical	Empirical	Proposes three Formulas
Nimo,W.M.R.[19]	Theoretical Approach Momentum Balance	Not Included	Supercritical and Subcritical	Analytical	Valid for any channel shape,no value given for coefficient of discharge
Favre,H. [10]	Friction Considered in the Weir Reach	Not Included	Subcritical and Supercritical	Analytical	Gives surface profiles for gradually varied flow taking friction into account

(Continued)

Reference (1)	Assumptions (2)	Velocity Effect of the Main Channel (3)	Nature of Flow (4)	Type of Solution (5)	Remarks (6)
Collinge,V.K[6]	Related to De Marchi theory	Considered	Subcritical and Supercritical	Analytical	Comments on the influence of the main channel velocity on C_d
Subramanya,K. and Awarthy,S.C.[23]	De Marchi theory and critical conditions at brink of the weir	Considered	Subcritical and Supercritical	Analytical	Obtains a relationship between weir discharge coefficient and channel Froude number
Smith,V.H. [22]	Energy Constant	Considered	Subcritical and Supercritical	Numerical Step-by-Step	Step-by-step computation procedure to obtain weir outflow
El-Khashab,A. and Smith,V.H. [8]	Momentum Balance	Considered	Subcritical and Supercritical	Numerical	Complete experimental investigation of velocity distribution in weir's vicinity

(Continued)

Reference (1)	Assumptions (2)	Velocity Effect of the Main Channel (3)	Nature of Flow (4)	Type of Solution (5)	Remarks (6)
De Marchi,G.[7]	Energy Constant	Not Included	Subcritical and Supercritical	Analytical	More restricted than Nimo's study
Gentilini,B.[13]	Energy Constant	Not Included	Subcritical and Supercritical	Analytical	Experimental verification of De Marchi theory for tranquil flow
Ackers,P.. [1]	Standard Weir Formula	Not Included	Subcritical and Supercritical	Analytical	Considers modification in the main channel geometry
Allen,J.W. [2]	No Theory	Not Included	Supercritical	Empirical	Lateral weirs housed in round pipes
Fraser,W. [11]	Energy Constant	----	Subcritical Supercritical and Critical	Analytical	Weir with a hydraulic pump in the main channel in the reach spanned by the weir

(Continued)

Reference (1)	Assumptions (2)	Velocity Effect of the Main Channel (3)	Nature of Flow (4)	Type of Solution (5)	Remarks (6)
Present Study	Hydrodynamic Model of the Weir	Included	Subcritical	Analytical	L/B ratio less than or equal to one. Rectangular channel with theory based on lateral conduit flow

TABLE 3 LATERAL WEIRS AS IRRIGATION STRUCTURES

Reference (1)	Relevant Aspects (2)	Remarks (3)
Acke[illegible]P. [1]	Effect of a tapered channel in the water surface profile in the weir span is considered	Lateral weirs on round pipes, experimental verification is provided
Garton,J.E.[12]	Automatic cutback irrigation system. Field tests, trapezoidal channel	Level hooded inlet tubes set along a concrete channel to form a series of distribution bays
Humphey,A.S.[16]	Proposed mechanical devices to solve the problem of automated irrigation	States the problem and the importance of automation in irrigation
Sweeten,J.H.and Garton,J.E. [24]	Uniformly discharging irrigation outlet systems in open channels	The system is composed of a battery of siphons fed from the channel
Sweeten,J.H.and Garton,J.E. [25]	Lateral weir batter proposed as an irrigation distribution system	Empirical formula for weir discharge solution is not general enough
Ramamurthy,A.S., Subramanya,K.and Carballada,L.[20]	Channel modification to get uniform outflow through the weir battery by three means (a) bed contouring; (b) side contouring; (c) sill contouring	Limited experimental verification for the bed contouring case is provided
Present Study	Covers the bed and side contouring cases specified in the above reference	Data includes tests on both bed and side contouring of rectangular channels

TABLE 3(a) SUCCESSIVE TRANSFORMATIONS

Point	Transformation Plane			
	Z	$\xi=[V]e^{i\gamma}$	$\xi'=\ell n(\frac{1}{V})+i\gamma$	$t=\cos[\frac{2\xi'_i-\pi}{(2/K)}]$
(1)	(2)	(3)	(4)	(5)
B	$\gamma = -\frac{\pi}{2}$ $V = V_1$	$V_1[e^{-i\frac{\pi}{2}}]$	$\ell n(\frac{1}{V_1})-i\frac{\pi}{2}$	$\cosh \ell n(\frac{1}{V_1^K})$
A	$\gamma = -\frac{\pi}{2}$ $V = 1$	$e^{-i\frac{\pi}{2}}$	$0 - i(\frac{\pi}{2})$	1
F	$\gamma = \alpha-\frac{\pi}{K}$ $V = 1$	$e^{-i(\alpha-\frac{\pi}{K})}$	$0 - i(\alpha-\frac{\pi}{K})$	$\cos(K\alpha)$
E	$\gamma = \frac{\pi}{K}-\frac{\pi}{2}$ $V = 1$	$e^{i(\frac{\pi}{K}-\frac{\pi}{2})}$	$0 + i(\frac{\pi}{K}-\frac{\pi}{2})$	-1
D_1 D^*	$\gamma = \frac{\pi}{K}-\frac{\pi}{2}$ $V = 0$	$0e^{i(\frac{\pi}{K}-\frac{\pi}{2})}$	$\infty + i(\frac{\pi}{K}-\frac{\pi}{2})$	$-\infty$
D_2	$\gamma = -\frac{\pi}{2}$ $V = 0$	$0e^{-i\frac{\pi}{2}}$	$\infty - i\frac{\pi}{2}$	$+\infty$
C	$\gamma = -\frac{\pi}{2}$ $V = V_2$	$V_2e^{-i\frac{\pi}{2}}$	$\ell n(\frac{1}{V_2})-i\frac{\pi}{2}$	$\cosh \ell n(\frac{1}{V_2^K})$
*	$D^* \rightarrow D_1$ denotes the location of D approached from E $D^* \rightarrow D_2$ denotes the location of D approached from C			

TABLE 4 RANGE OF GEOMETRIC VARIABLES - LATERAL WEIR TESTS

Series Number (1)	Sill Height S in Inches (2)	Weir Length L in Inches (3)	Ratio of Weir Length to Channel Width (L/B) (4)	Flume Width B, in Inches (5)
1	2	10.0	1.0	10
2	2	5.0	0.5	10
3	4	10.0	1.0	10
4	4	5.0	0.5	10
5	6*	10.0	1.0	10
6	6	5.0	0.5	10
7	3.86	18.0	1.0	18

* Actual size = 6.07"; Note: 1 inch = 25.4 mm

TABLE 5(a) MAIN VARIABLES OF BED CONTOURING TESTS

Ratio Between Theoretical and Actual Weir Discharge: Qt/Qw	Hump Height Z_1 at End of Weir in Inches	Height of Sill S in Inches	Inlet Froude Number: F_1	Inlet Weir Parameter: F_o	Water Profile Indicator: R_H
(1)	(2)	(3)	(4)	(5)	(6)
0.96	1.0	4.5	.40	.84	0 98
0.99	1.0	5.0	.40	.85	1.03
0.97	1.0	6.25	.35	.84	0.96
1.00	1.0	6.25	.40	.92	0.95
0.96	1.0	7.25	.35	.88	0.95
1.03	1.0	7.25	.40	.93	1.04
1.05	1.5	6.25	.40	.78	1.05
1.04	1.5	7.25	.35	.75	1.02
1.01	2.0	2.75	.40	.60	1.05
1.06	2.0	5.00	.40	.69	1.03
1.06	2.0	6.25	.40	.73	1.03
1.02	2.0	7.25	.35	.70	0.98

Note: 1 inch = 25.4 mm.

TABLE 5(b) MAIN VARIABLES OF LATERAL CONTOURING TESTS

Ratio Between Theoretical and Actual Weir Discharge: Qt/Qw	Side Contraction b_1 in Inches	Height of Sill S in Inches	Inlet Froude Number: F_1	Inlet Weir Parameter: F_o	Water Profile Indicator: R_b
(1)	(2)	(3)	(4)	(5)	(6)
1.02	2.0	4.50	.40	.93	1.06
1.01	2.0	5.00	.40	.92	1.1
1.10	2.0	6.25	.40	.89	1.08
1.04	2.0	6.25	.35	.85	1.04
1.04	3.0	5.00	.40	.80	1.08
1.09	3.0	7.25	.35	.73	1.02

Note: 1 inch = 25.4 mm.

TABLE 6 UPPER RANGE OF WEIR PARAMETER FOR SOME SELECTED SILL HEIGHT RATIOS

Inlet Froude Number: F_1 (1)	Sill Height Ratio: S_{y_1} (2)	Upper Range of Weir Parameter F_o (3)
1.0	.01	10.0
1.0	.25	2.0
1.0	.5	1.41
1.0	.75	1.15
1.0	1.0	1.0